Journal of Computational Physics 231 (2012) 4096–4141

Contents lists available at SciVerse ScienceDirect

Journal of Computational Physics

journal homepage: www.elsevier.com/locate/jcp

Runge–Kutta discontinuous Galerkin method for the approximation of Baer and Nunziato type multiphase models

Erwin Franquet [a,b], Vincent Perrier [b,c,*]

[a] LaTEP-ENSGTI, Bâtiment d'Alembert, rue Jules Ferry, 64 075 Pau Cedex, France
[b] INRIA Bordeaux Sud Ouest, Cagire Team, 351 Cours de la Libération, 33 405 Talence Cedex, France
[c] LMA-IPRA, UMR 5142 CNRS-Université de Pau et des Pays de l' Adour, Avenue de l'Université, 64 013 Pau Cedex, France

ARTICLE INFO

Article history:
Received 8 July 2011
Received in revised form 13 January 2012
Accepted 2 February 2012
Available online 16 February 2012

Keywords:
Compressible multiphase flows
Baer and Nunziato system
Nonconservative products
Discontinuous Galerkin methods

ABSTRACT

A high-order numerical method is developed for the computation of compressible multiphase flows. The model we use is based on the Baer and Nunziato type systems [4]. Among all the other available models in the literature, these systems present the advantage to be able to simulate either interface or mixture problems. Nevertheless, they still raise some issues, mainly based on their non-conservative feature. The numerical method we propose is a discontinuous Galerkin type. In this work, the interior side integrals are computed thanks to [2]. Robustness and high order of accuracy of the method are proved on classical interface problems, but also on suitably derived analytical solutions.

1. Introduction

Multiphase and/or multifluid problems, encountered for example in bubbly flows or instabilities fronts in flow or gas mixing in reactive flows, are known to be tricky. Indeed, they involve strong density ratios and strongly heterogeneous compressibility effects, which induce real modeling issues. Multifluid flows can be divided into two classes of flows: either the modeling scale is at the interface scale, i.e. all the interfaces are tracked and resolved, or the modeling scale is wider than the typical size of the bubbles/droplets, and they are resolved only as average.

For the first kind of flows, a wide range of methods has been developed: the front-tracking methods [23], the half-Lagrangian methods [50,27], the Level-Set methods [31,42,30] or the cut-cell methods [33]. We do not develop these methods in detail, but will focus on their disadvantages. Front-tracking methods are difficult to develop in multi-dimensions. Half-Lagrangian methods often result in strong distorted meshes, which require Arbitrary Lagrange–Euler (ALE) schemes and/or remapping. Level-Set methods are not conservative and correction terms must be added. Finally, the mesh must be able to capture all inclusions, which may be very costly if these ones are small (e.g. mixture flows). For the second kind of flows, an average procedure is performed on the one-fluid Euler or Navier–Stokes system, and only one set of equations is considered for the whole flow. At any point, existence of a fluid is characterized through its volume fraction. Thus, interface problems correspond to solutions for which the volume fraction is either equal to 0 or 1. In the numerical method, a smearing of the interface is allowed. Moreover, mixture problems may also be taken into account provided a suitable modeling is adopted for the small size effects. These flows involve specific difficulties, such as hyperbolicity and non conservative products and interface variables modeling, which will be detailed further. To circumvent these difficulties, many strategies have been adopted [4,37,38,28,2].

* Corresponding author at: INRIA Bordeaux Sud Ouest, Cagire Team, 351 Cours de la Libération, 33 405 Talence Cedex, France.
E-mail addresses: erwin.franquet@univ-pau.fr (E. Franquet), vincent.perrier@inria.fr (V. Perrier).

0021-9991/$ - see front matter © 2012 Elsevier Inc. All rights reserved.
doi:10.1016/j.jcp.2012.02.002

Fatherhood of discontinuous Galerkin methods is usually attributed to Reed and Hill [35]. These methods being Finite Element Methods, their main benefits are their potentially high order accuracy feature and their possible use on unstructured and possibly hybrid meshes. The discontinuous nature of the finite element space allows to use upwind fluxes, which are well suited for convection dominated flows. Moreover, the high order accuracy can be reached by keeping the compactness (which is a benefit for the efficiency in a parallel environment). Last, in the discontinuous Galerkin methods, the boundary conditions are imposed weakly, which for example makes easier to take into account a corner of wall boundaries. Here again, we will not make a review of the huge amount of papers dedicated to discontinuous Galerkin methods. Concerning compressible flows, the main contribution was made in the 90s by Cockburn, Shu and coworkers, see [11] for a review. Recently, some authors have proposed discontinuous Galerkin schemes for multiphase flows [51,45]. Both of these references are based on the Level-Set method, which couples a discretization of an Hamilton–Jacobi equation describing the interface and a Ghost-Fluid [51] or a Cut Cell Method [45]. Our approach is very different, because our discretization is led in one step, by using an hyperbolic system. $P_N P_M$ framework, which includes discontinuous Galerkin methods if $N = M$, have been developed for a very similar system in [18,19]. The difference with our model will be discussed in Section 2.

The paper is organized as follows. In Section 2, we recall how to express the governing equations for a compressible multiphase flow [4]. Then, in Section 3, we show how to derive a discontinuous Galerkin method for the system shown in Section 2. The interior side integrals discretization is based on [2], which is revisited by mean of a stochastic process. This allows to find the same finite volume discretization, but also to compute cell integrals that are consistent with the boundary integrals, which appear in the discontinuous Galerkin formulation as derived in [36]. Finally, Section 4 is devoted to especially dedicated numerical tests, in order to prove robustness and accuracy of the method.

2. Model

2.1. General expression

Among the Eulerian models that aim at modeling the multiphase feature of the flow, most are based on the model developed by Baer and Nunziato [4]. They usually may be written in the following general form:

$$\begin{aligned}
&\frac{\partial \alpha_k}{\partial t} + \mathbf{u}_I \cdot \nabla \alpha_k = \mu (P_k - P_{\bar{k}}) \\
&\frac{\partial (\alpha_k \rho_k)}{\partial t} + \operatorname{div}(\alpha_k \rho_k \mathbf{u}_k) = 0 \\
&\frac{\partial (\alpha_k \rho_k \mathbf{u}_k)}{\partial t} + \operatorname{div}(\alpha_k \rho_k \mathbf{u}_k \otimes \mathbf{u}_k) + \nabla (\alpha_k P_k) = P_I \nabla \alpha_k + \lambda (\mathbf{u}_{\bar{k}} - \mathbf{u}_k) \\
&\frac{\partial (\alpha_k \rho_k E_k)}{\partial t} + \operatorname{div}(\alpha_k (\rho_k E_k + P_k) \mathbf{u}_k) = P_I \mathbf{u}_I \cdot \nabla \alpha_k - \mu P_I (P_k - P_{\bar{k}}) + \lambda \mathbf{u}_I \cdot (\mathbf{u}_{\bar{k}} - \mathbf{u}_k)
\end{aligned} \tag{1}$$

Here, α_k, ρ_k, $\mathbf{u}_k$, P_k, E_k denote volume fraction, density, velocity, static pressure, and total energy of the phase k. The total energy is equal to

$$E_k = \varepsilon_k + \frac{\mathbf{u}_k \cdot \mathbf{u}_k}{2}$$

where ε_k is the internal energy. The thermodynamic parameters of each phase are linked by an equation of state $\varepsilon_k = \varepsilon_k(P_k, \rho_k)$, where ε_k is a concave function of its arguments.

Concerning $\mathbf{u}_I$ and P_I, they stand for the interfacial velocity and pressure. Then, μ and λ are relaxation coefficients that account for the relaxation effects, i.e. pressures work (pressures relaxation) and drag force (velocities relaxation). Finally, we define $\bar{k} = 1$ (resp. $\bar{k} = 2$) when $k = 2$ (resp. $k = 1$).

2.2. Closure of the mathematical model

The partial differential equations composing system (1) may be solved only if the corresponding model is closed and mathematically well-posed.

To close the system, we first need to model the interfacial variables. This point is still in debate and many authors have proposed different formulations. Indeed, there is currently no "better" formulations, since these choices often depend on the physical problems involved. Yet, among all the available relations, only a few may ensure the hyperbolicity of the system, which is fundamental. Therefore, we will only restrict ourselves to these kinds of closure.

So, Baer and Nunziato [4] propose to take:

$$\begin{cases} \mathbf{u}_I = \mathbf{u}_{\text{solid}} \\ P_I = P_{\text{gas}} \end{cases} \tag{2}$$

This closure was obtained for detonation problems, where one of the phase (the heaviest, i.e. liquid phase in our case) is not compressible, contrarily to the other (the lighter, i.e. the gas phase). More recently the inverse choice was proposed [22].

For multiphase problems in pressure equilibrium, it was usual to take an unique pressure for the two phases and the interfacial variables [16,49]. Yet, this choice does not ensure the hyperbolicity and [37] thus proposes the following modification:

$$\begin{cases} \mathbf{u}_I = \mathbf{u}_{\text{solid}} \\ P_I = P_{\text{gas}} + 10^4(1-\alpha_{\text{gas}})^{4/3} \end{cases} \tag{3}$$

The new term is a pressure correction term which guarantees the hyperbolicity.

When both phases are compressible, an other option, fully symmetric, is proposed by [38]:

$$\begin{cases} \mathbf{u}_I = \frac{\sum_k \alpha_k \rho_k \mathbf{u}_k}{\sum_k \alpha_k \rho_k} \\ P_I = \sum_k \alpha_k P_k \end{cases} \tag{4}$$

Thanks to a new averaging procedure obtained in one dimension, a new form is proposed by [39]:

$$\begin{cases} P_I = \frac{Z_1 P_2 + Z_2 P_1}{Z_1 + Z_2} + \text{sgn}\left(\frac{\partial \alpha_1}{\partial x}\right) \frac{Z_1 Z_2 (u_2 - u_1)}{Z_1 + Z_2} \\ u_I = \frac{Z_1 u_1 + Z_2 u_2}{Z_1 + Z_2} + \text{sgn}\left(\frac{\partial \alpha_1}{\partial x}\right) \frac{P_2 - P_1}{Z_1 + Z_2} \end{cases} \tag{5}$$

In a general way, Coquel et al. [12] has shown how these different formulations may modify the mathematical structure of the problem. In this paper, instead of using one of these models or developing a new one, we will directly define the nonconservative terms of (1) which include the interfacial variables. With such an approach, we do not have to worry about the limitations of this modeling anymore. Part of our scheme will be based on [2], for which the continuous system solved for regular flows, and therefore its link with the seven equations model, was left unclear. We will give an expression of this continuous system as a model of type (1) (namely, the expression of $\mathbf{u}_I$ and P_I) in Section 3.4.3. This closure is fully nonlinear, and different from the previous closures that have been proposed until now. Moreover, we will propose a test-case giving evidence of this limit model.

3. Numerical scheme

The discretization of (1) is usually led by splitting the equations into two parts: the hyperbolic operator, in which we have all the derivatives with respect to the spatial variables, and the relaxation operator, which involves all the terms with λ and μ. In this section, we are interested only in the derivation of a numerical scheme for the hyperbolic operator of (1). A strong literature already exists on the discretization of (1) with the closure of Baer and Nunziato (2). In this case, the interfacial velocity is the velocity of the solid and the interfacial pressure is the one of the gas. In one dimension, the system has one double eigenvalue u_S, and five distinct eigenvalues $u_s \pm c_s$, u_g, and $u_g \pm c_g$, where c_i denotes the sound velocity of the phase i. The first step, when deriving a finite volume method consists in solving the Riemann problem. Using the closure (2) simplifies also the solution of the Riemann problem, as it is very well explained in [3,15,47], because

- All solid phase variables remain constant across the three gaseous characteristic fields, while the solid contact changes all gaseous variables.
- The left and right solid nonlinear waves do not affect the gaseous-phase variables.
- Therefore the only difficulty is to find the jump relations across the solid contact.

This problem has first been addressed in [3], which developed an *inverse* method for solving the Riemann problem: their solution consists in first prescribing the states on both sides of the solid contact with the jump relations of [20], and then to search for the associated wave patterns, which allows to find the left and right states of the Riemann problem. The first *direct* method (i.e. with given left and right states) for solving the Riemann problem of (1) with closure (2) was proposed in [41]: jump relations across the solid contact are treated with a vanishingly small thickness method. An iterative method is then developed to obtain the wave structure and the intermediate states of the Riemann problem for given left and right states. The same type of method was developed in [15], but with the jump relations of [20], as [3].

Once the Riemann problem has been solved, the nonconservative nature of the system induces also problems in deriving a Godunov' type numerical scheme. Up to our knowledge, the only systematic way to derive such a scheme is the so-called path conservative scheme of [32].

Last, we mention [46], in which a finite volume numerical scheme was derived for the isentropic version of (1) with closure (2). This method is based on a separation into subsystems: the first one corresponds to the gas phase, the second, expressing the conservation of mass of the solid and momentum of the mixture is conservative, and the third is a compaction dynamic equation. Then the numerical method consists in a well balanced scheme based on the stationary waves for the first subsystem, in a classical conservative scheme for the second subsystem, and in a Engquist–Osher scheme for the third subsystem. The resulting scheme is well balanced, i.e. it is able to capture exactly equilibrium states.

As far as high order methods are concerned, the only works we heard about are [18,19]. In these references, a $P_N P_M$ framework is developed for non-conservative schemes. This framework includes the *DG* framework for $N = M$. These works are

concerned with (1) with closure (2), for which the continuous system is known. Part of their scheme is derived using [36], whose method will be detailed later in this article, where the main remaining difficulty is to find a suitable approximation of the fluxes on the boundaries of the cells. This is achieved by a centered flux in [18] and with a Osher–Solomon type flux in [19]. In both of these works, the fluxes are derived so as to ensure the path conservativity described in [32].

Nevertheless, contrarily to the above cited works, we do not want to prescribe the interfacial pressure and the interfacial velocity. Then we have to deal with the full system (1). From a numerical point of view, this model raises two problems:

1. The interfacial pressure and velocity are not known.
2. The system is not conservative and therefore it is not easy to derive a finite volume method. Logically, the derivation of a discontinuous Galerkin method is even more complicated, because this method basically consists in using finite volume fluxes on the boundaries, and continuous integrals inside the cells.

As explained in [17], the derivation of the system is based on the averaging of the Euler equations, and we will recall in Section 3.1 how the model (1) can be obtained by combining the Euler equations with a simple interface model. Then in Section 3.2, we recall the derivation of a discontinuous Galerkin formulation for nonconservative hyperbolic systems made in [36]. In Section 3.3, we compare the finite volume scheme obtained by Abgrall and Saurel [2] with the scheme obtained by Rhebergen et al. [36] in the case of finite volumes (i.e. approximation and test functions are piecewise constants). From this comparison, we deduce a discontinuous Galerkin formulation of the finite volume scheme derived in [2]. This formulation depends on averaged terms that we compute in Section 3.4 by giving a suitable stochastic model of the multiphase mixture.

3.1. Derivation of the model (1)

In this section, following [17], we briefly explain how the system (1) can be obtained.

The aim is to derive a system which describes the behavior of two fluids that cannot be mixed. The modeling scale is wider than the typical size of the droplets/bubbles (see Fig. 1). The aim of the modeling is not to describe exactly the topology of the flow, but to derive equations for ensemble average, given a set of realizations.

For one realization ω, we denote by $\chi_k(\mathbf{x},\omega)$ ($k = 1$ or 2) the characteristic function of the fluid k: it is equal to 1 if $\mathbf{x}$ is inside the fluid k, and equal to 0 otherwise. As the fluids are not miscible, only one fluid can be present in $\mathbf{x}$, so that $\chi_1(\mathbf{x},\omega) + \chi_2(\mathbf{x},\omega) = 1$. Then the following model holds

$$\chi_k\left(\frac{\partial \mathbf{U}_k}{\partial t} + \operatorname{div}\mathbf{F}_k(\mathbf{U}_k)\right) = 0 \tag{6a}$$

where $\mathbf{U}_k$ is the vector of the Euler system unknowns of the phase k:

$$\mathbf{U}_k = (\rho_k, \rho_k \mathbf{u}_k, \rho_k E_k)$$

and $\mathbf{F}_k$ is the associated flux. This model means that:

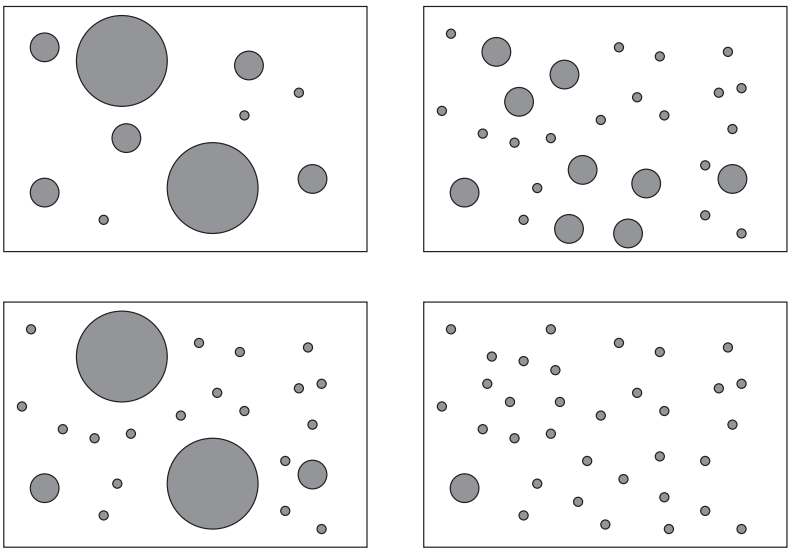

Fig. 1. Different kinds of modeling for the small size effects in the multiphase model. For one realization, the topology of the flow is known. Each time, bubble/droplets are smaller than the modeling scale, represented by the surrounding box. The aim is to derive equations for an average of these different realizations.

- either $\chi_k(\mathbf{x},\omega) = 1$, then the Euler system of the phase k holds,
- or $\chi_k(\mathbf{x},\omega) = 0$.

For closing the system, an equation on χ_k is necessary. This equation is

$$\partial_t \chi_k + \sigma \cdot \nabla \chi_k = 0 \tag{6b}$$

in the sense of distributions. The velocity σ is given by solving a local Riemann problem as described in Fig. 2: if the set $\chi_k = 1$ has a regular boundary, the normal of this surface can be defined. Then the local interface velocity σ is defined as the contact surface velocity of the Riemann problem between the two phases in the direction of the normal (see Fig. 2). The second step of the derivation consists in combining (6a) and (6b) for finding

$$\partial_t(\chi_k \mathbf{U}_k) + \mathrm{div}_{\mathbf{x}}(\chi_k \mathbf{U}_k) - (\mathbf{F}(\mathbf{U}) - \sigma \mathbf{U}) \cdot \nabla \chi_k = 0 \tag{7}$$

Then, still following [17], an ensemble average $\mathbb{E}()$ is performed.

$$\mathbb{E}(\partial_t(\chi_k \mathbf{U}_k)) + \mathbb{E}(\mathrm{div}_{\mathbf{x}}(\chi_k \mathbf{U}_k)) - \mathbb{E}((\mathbf{F}(\mathbf{U}) - \sigma \mathbf{U}) \cdot \nabla \chi_k) = 0 \tag{8}$$

If the operator commutes with the space and time derivation, we have

$$\partial_t \mathbb{E}(\chi_k \mathbf{U}_k) + \mathrm{div}_{\mathbf{x}} \mathbb{E}(\chi_k \mathbf{F}(\mathbf{U}_k)) - \mathbb{E}((\mathbf{F}(\mathbf{U}) - \sigma \mathbf{U}) \cdot \nabla \chi_k) = 0 \tag{9}$$

In this last equation, we see that only a part of the spatial operator can be put into a divergence form, $\mathrm{div}_{\mathbf{x}} \mathbb{E}(\chi_k \mathbf{F}(\mathbf{U}_k))$, whereas the other part $\mathbb{E}((\mathbf{F}(\mathbf{U}) - \sigma \mathbf{U}) \cdot \nabla \chi_k)$ cannot. If we define the averaged conservative variables by Favre average:

$$\begin{cases} \alpha_k = \mathbb{E}(\chi_k) \\ \alpha_k \bar{\rho}_k = \mathbb{E}(\chi_k \rho_k) \\ \alpha_k \bar{\mathbf{u}}_k = \mathbb{E}(\chi_k \mathbf{u}_k) \\ \alpha_k \bar{E}_k = \mathbb{E}(\chi_k E_k) \end{cases}$$

the following system can be obtained (omitting the superscript):

$$\begin{cases} \frac{\partial \alpha_k}{\partial t} + \mathbb{E}(\sigma \cdot \nabla \chi_k) = 0 \\ \frac{\partial \alpha_k \rho_k}{\partial t} + \nabla \cdot (\alpha_k \rho_k \mathbf{u}_k) = \mathbb{E}(\rho_k (\mathbf{u}_k - \sigma) \cdot \nabla \chi_k) \\ \frac{\partial \alpha_k \rho_k \mathbf{u}_k}{\partial t} + \nabla \cdot (\alpha_k \rho_k \mathbf{u}_k \otimes \mathbf{u}_k + \alpha_k P_k) = \mathbb{E}((\rho_k \mathbf{u}_k (\mathbf{u}_k - \sigma) + P_k) \cdot \nabla \chi_k) \\ \frac{\partial \alpha_k \rho_k E_k}{\partial t} + \nabla \cdot (\alpha_k \rho_k E_k \mathbf{u}_k + \alpha_k P_k \mathbf{u}_k) = \mathbb{E}((\rho_k E_k (\mathbf{u}_k - \sigma) + P_k \mathbf{u}_k) \cdot \nabla \chi_k) \end{cases} \tag{10}$$

Last, a modeling step is done, which consists in

- modeling zeroth order terms by the terms of (1) involving nonconservative products,
- modeling the first order fluctuations (i.e. involving a difference of velocity $\mathbf{u}_k - \sigma$) by relaxation terms.

As was previously done in [2], the numerical scheme is directly derived from (6), and not from (1). The idea is that for a given realization, the system (6) can be easier discretized than (1), because it is easier to deal with a known χ_k than with its average.

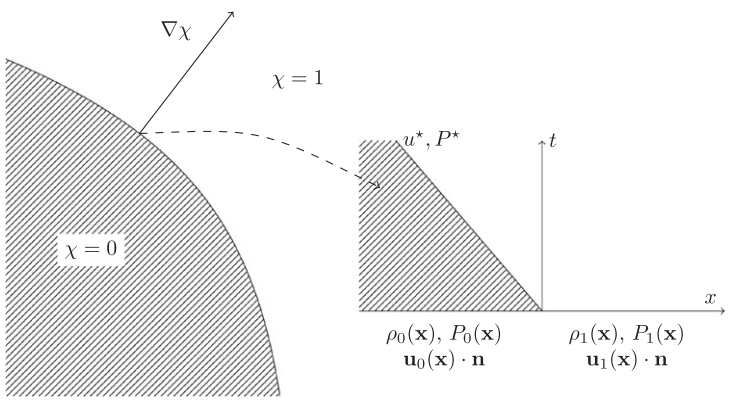

Fig. 2. Local interface variables. If the boundary between the two phases is $\mathcal{C}^1$, then we may define the interfacial velocity and pressure by solving a local Riemann problem. We define by $\mathbf{n}$ the unit vector that has the same direction and sense as $\nabla\chi$. Then we can define the interfacial pressure and velocity as $P_I = P^\star$ and $\mathbf{u}_I = u^\star \mathbf{n}$.

3.2. Discontinuous Galerkin formulation for nonconservative hyperbolic systems

In this Section, following [36], we derive a discontinuous Galerkin formulation for a general non conservative system. We begin by doing the derivation for a conservative system.

For simplifying, we suppose that we are working on an open set Ω with polygonal boundary. This set is meshed by a conforming mesh $\mathcal{T}_h$. We denote by S_t the set of all the sides of the mesh, by S_i the set of the interior sides, and S_b the set of the boundary sides. For all the sides S of S_t, we choose one unitary normal $\mathbf{n}^S$. This normal is supposed to be outward for the sides of S_b. Last, for a given side of a given cell of the mesh, we denote by $\mathbf{n}^{\text{out}}$ the normal going outward of the cell.

The approximation space is composed of functions that are piecewise polynomials: polynomials inside the cells of the mesh $\mathcal{T}_h$, and maybe discontinuous across the sides of $\mathcal{T}_h$. The approximation space is denoted by V_h. For all functions φ of V_h, and all sides S of S_i, we denote:

$$\forall \mathbf{x} \in S \quad \begin{cases} \varphi^R(\mathbf{x}) \lim\limits_{\varepsilon \to 0, \varepsilon > 0} \varphi(\mathbf{x} + \varepsilon \mathbf{n}^S) \\ \varphi^L(\mathbf{x}) \lim\limits_{\varepsilon \to 0, \varepsilon > 0} \varphi(\mathbf{x} - \varepsilon \mathbf{n}^S) \end{cases}$$

and for all $\mathbf{x}$ in an interior side S, we denote by:

$$[\![\varphi]\!](\mathbf{x}) = \varphi^R(\mathbf{x}) - \varphi^L(\mathbf{x}) \quad \text{and} \quad \{\!\{\varphi\}\!\}(\mathbf{x}) = \frac{\varphi^R(\mathbf{x}) + \varphi^L(\mathbf{x})}{2}$$

For the sake of simplicity, we suppose that we are dealing with a conservative equation (and not a system):

$$\forall x \in \Omega \quad \text{div}_{\mathbf{x}} \mathbf{f}(u) = 0 \tag{11}$$

The discontinuous Galerkin method consists in approximating the solution of the weak formulation of (11) by elements of V_h. The test functions of the weak formulation of (11) are also supposed to be in V_h. If u is supposed to be piecewise polynomial, then the derivative in the sense of distributions of $\text{div}_{\mathbf{x}} \mathbf{f}(u)$ is composed of the derivatives in the classical sense inside the cells, and directional Dirac distributions concentrated on the sides of the mesh. Therefore, the integral of the product of φ by $\text{div}_{\mathbf{x}} \mathbf{f}(u)$ is equal to:

$$\int_\Omega \varphi \, \text{div}_{\mathbf{x}} \mathbf{f}(u) = \sum_{T \in \mathcal{T}_h} \int_T \varphi \, \text{div}_{\mathbf{x}} \mathbf{f}(u) + \sum_{S \in S_i} \int_S \hat{\varphi} [\![\mathbf{f}(u)]\!] \cdot \mathbf{n}^S \tag{12a}$$

where $\hat{\varphi}$ is the numerical flux of the test functions. This one is required because there appears a product of distributions, basically an Heaviside (the test functions) by a Dirac (the divergence of $\mathbf{f}(u)$), on each side.

Then an integration by part is performed on each element T of $\mathcal{T}_h$:

$$\begin{aligned} &\int_T \varphi \, \text{div}_{\mathbf{x}} \mathbf{f}(u) \int_T \text{div}_{\mathbf{x}}(\varphi \mathbf{f}(u)) - \int_T \mathbf{f}(u) \nabla \varphi = \int_{\partial T} \varphi \mathbf{f}(u) \cdot \mathbf{n}^{\text{out}} - \int_T \mathbf{f}(u) \nabla \varphi \\ &\int_T \varphi \, \text{div}_{\mathbf{x}} \mathbf{f}(u) \sum_{S \in \partial T} \int_S \varphi \mathbf{f}(u) \cdot \mathbf{n}^{\text{out}} - \int_T \mathbf{f}(u) \nabla \varphi \end{aligned} \tag{12b}$$

If we sum this last equality over $\mathcal{T}_h$, a given interior side, appears twice, with opposite normals. This induces that

$$\sum_{T \in \mathcal{T}_h} \sum_{S \in \partial T} \int_S \varphi \mathbf{f}(u) \cdot \mathbf{n}^{\text{out}} = -\sum_{S \in S_i} \int_S [\![\varphi \mathbf{f}(u)]\!] \cdot \mathbf{n}^S + \sum_{S \in S_b} \int_S \varphi \mathbf{f}(u) \cdot \mathbf{n}^{\text{out}} \tag{12c}$$

Last, applying the formula

$$[\![ab]\!] = \{\!\{a\}\!\}[\![b]\!] + [\![a]\!]\{\!\{b\}\!\}$$

leads to:

$$\int_\Omega \varphi \, \text{div}_{\mathbf{x}} \mathbf{f}(u) = -\sum_{T \in \mathcal{T}_h} \int_T \mathbf{f}(u) \nabla \varphi - \sum_{S \in S_i} \int_S [\![\varphi]\!] \{\!\{\mathbf{f}(u)\}\!\} \cdot \mathbf{n}^S - \sum_{S \in S_i} \int_S \{\!\{\varphi\}\!\} [\![\mathbf{f}(u)]\!] \cdot \mathbf{n}^S + \sum_{S \in S_b} \int_S \varphi \mathbf{f}(u) \cdot \mathbf{n}^{\text{out}} + \sum_{S \in S_i} \int_S \hat{\varphi} [\![\mathbf{f}(u)]\!] \cdot \mathbf{n}^S$$

As remarked in [36], a natural choice of the test function numerical flux for ensuring conservativity is: $\hat{\varphi} = \{\!\{\varphi\}\!\}$. With this choice, the discontinuous Galerkin formulation of (11) is

$$\int_\Omega \varphi \text{div}_{\mathbf{x}} \mathbf{f}(u) = -\sum_{T \in \mathcal{T}_h} \int_T \mathbf{f}(u) \nabla \varphi - \sum_{S \in S_i} \int_S [\![\varphi]\!] \{\!\{\mathbf{f}(u)\}\!\} \cdot \mathbf{n}^S + \sum_{S \in S_b} \int_S \varphi \mathbf{f}(u) \cdot \mathbf{n}^{\text{out}}$$

The implementation may thus be divided into four steps:

1. **Approximate the interior sides integrals**: this is done by a classical finite volume flux.
2. **Compute the internal integrals**: this step is straightforward because the function $\mathbf{f}(\mathbf{u}) \cdot \nabla \varphi$ is continuous inside all the cells. If it is nonlinear, a quadrature method is used.

3. **Integrate in time**: For a k^{th} order scheme, an explicit integration can be led with a Strong Stability Preserving scheme [24], and the scheme is stable with a CFL that does not depend on the space discretization [9].
4. **Stabilize the method for non regular solutions**: the aim is to avoid spurious oscillations. This can be done by adapting slope limiting to the discontinuous Galerkin method [8,7,6,10].

In the non-conservative case, we keep unchanged steps 3 and 4. The terms computed during steps 1 and 2 being strongly linked to the conservative nature, the formulation is quite different:

1. First, the jump across an interface is not defined in general, so that the side integral of (12a) is not defined;.
2. Second, the integration by part of (12b), and the computations that follows in (12c) cannot be made.

Following [36], we propose to keep the formulation (12a), and to define the jumps, thanks to the DalMaso–LeFloch–Murat [13] theory, which we briefly recall.

The definition of nonconservative products developed in [13] consists in first defining a family of path Φ that connect two states u^L and u^R that are on both side of a discontinuity. For a nonconservative product $g(u)\frac{\partial u}{\partial x}$, a family of path is defined as having the following properties:

- **Jump property**

$$\forall u^L, u^R \in \mathbb{R}^p \qquad \Phi(0;u^L,u^R) = u^L \quad \text{and} \quad \Phi(1;u^L,u^R) = u^R$$

- **Consistency**

$$\forall u \in \mathbb{R}^p \quad \forall s \in]0;1[\quad \Phi(s;u,u) = u$$

- **Lipschitz regularity:** For any bounded set $\mathcal{U}$ of $\mathbb{R}^p$, there exists a constant $k > 0$ such that:

$$\left|\frac{\partial \Phi}{\partial s}(s;u^L,u^R) - \frac{\partial \Phi}{\partial s}(s;v^L,v^R)\right| \leqslant k|(u^L - v^L) - (u^R - v^R)|$$

with all these hypothesis, it is proved in [13] that the nonconservative product can be defined as a Borel measure μ. When u is smooth, this measure corresponds to a classical integration. When u is discontinuous at a point $\{x_0\}$, it is equal to:

$$\mu(\{x_0\}) = \int_0^1 g(\Phi(s,u^L(x_0),u^R(x_0)),x_0)\frac{\partial \Phi}{\partial s}(s,u^L(x_0),u^R(x_0))\mathrm{d}s$$

This definition allows to define the second integral of (12a). If the same numerical flux for the test functions is used, then for the problem:

$$\mathrm{div}_x \mathbf{f}(u) + \sum_{i=1}^{3} a_i(u)\frac{\partial u}{\partial x_i} = 0$$

the following discontinuous Galerkin formulation is found:

$$\begin{aligned}\int_\Omega \varphi \mathrm{div}_{\mathbf{x}}\mathbf{f}(u) = &-\sum_{T\in\mathcal{T}_h}\int_T \mathbf{f}(u)\nabla\varphi + \sum_{T\in\mathcal{T}_h}\int_T \varphi\sum_{i=1}^{3}a_i(u)\frac{\partial u}{\partial x_i} - \sum_{S\in S_i}\int_S [\![\varphi]\!]\{\!\{\mathbf{f}(u)\}\!\}\cdot\mathbf{n}^S \\ &+ \sum_{S\in S_i}\int_S \{\!\{\varphi\}\!\}\int_0^1 \frac{\partial \Phi}{\partial s}(s,u^L,u^R)\mathbf{a}(\Phi(s,u^L,u^R),.)\cdot\mathbf{n}^S + \sum_{S\in S_b}\int_S \varphi\mathbf{f}(u)\cdot\mathbf{n}^{\text{out}}\end{aligned} \tag{13}$$

where $\mathbf{a}$ denotes the vector (a_1,a_2,a_3).

For stabilizing the method, the integration on the interior sides are replaced by numerical fluxes. Finding these numerical flux are not an easy task for general hyperbolic nonconservative systems. In the next Section, we derive these fluxes for the multiphase system.

3.3. Numerical fluxes

In this Section, we compare the discontinuous Galerkin formulation of [36] that was recalled in the previous subsection, with the finite volume formulation of [2]. The aim is to define the numerical fluxes of the discontinuous Galerkin formulation of (13).

As in the previous Section, the space Ω has been divided into cells. At time $t^{(n)}$, we suppose that all the variables of the mean flow are known: the volume fraction of each fluid $\alpha_i^{(n)}$, and the density, pressure, and velocity $\rho_i^{(n)}$, $P_i^{(n)}$, $\mathbf{u}_i^{(n)}$.

From the knowledge of $\alpha_1^{(n)}(\mathbf{x})$, we rebuild a stochastic process $\chi_1(\mathbf{x},\omega)$ which has the following properties:

- for all $\mathbf{x}$, ω, $\chi_1 = 1$ or $\chi_1 = 0$,
- for all $\mathbf{x}$ in which the variables are continuous, $\mathbb{E}(\chi_1(\mathbf{x})) = \alpha_1(\mathbf{x})$.

For one given realization ω, $\chi_1(\mathbf{x},\omega) = 1$ if the fluid 1 lies in $\mathbf{x}$, and $\chi_1(\mathbf{x},\omega) = 0$ otherwise.

Our aim in this section is to derive the normal numerical fluxes on the sides of the mesh. For a given interior side S, we still denote by $\mathbf{n}^S$ the normal of this side. Given two states on the left and on the right of the side, we use the Godunov method: we first solve the Riemann problem in the direction of the normal, and then integrate the equation, see Fig. 3. Depending on whether $\chi_1^L(\mathbf{x},\omega) = 0$ or 1, and whether $\chi_1^R(\mathbf{x},\omega) = 0$ or 1, four cases shall be investigated.

$\chi_1^L(\mathbf{x}) = 0$ and $\chi_1^R(\mathbf{x}) = 0$ In this case, an example of the solution of the Riemann problem is shown on Fig. 4. The integration is led as for a classical finite volume method [48]: the intermediate U^{int} state at $x = 0$ is computed, and then the flux $\mathbf{F}_2(U^{\text{int}})$ is added on the left side, and withdrawn from the right cell. We denote this flux by $\mathbf{F}_2^{\text{eul}}\left(\mathbf{U}_1^L, \mathbf{U}_1^R, \mathbf{n}^S\right)$, and more generally, if we denote by $\mathcal{F}_{ij}^{k,+}$ what is added for the fluid k on the right cell, from the integration of the Riemann problem between the phase i and j, and by $\mathcal{F}_{ij}^{k,-}$ what is added on the left cell, we find

$$\begin{cases} \mathcal{F}_{22}^{1,+} = 0 \\ \mathcal{F}_{22}^{1,-} = 0 \\ \mathcal{F}_{22}^{2,+} = \mathbf{F}_2^{\text{eul}}\left(\mathbf{U}_1^L, \mathbf{U}_1^R, \mathbf{n}^S\right) \\ \mathcal{F}_{22}^{2,-} = -\mathbf{F}_2^{\text{eul}}\left(\mathbf{U}_1^L, \mathbf{U}_1^R, \mathbf{n}^S\right) \end{cases}$$

$\chi_1^L(\mathbf{x}) = 1$ and $\chi_1^R(\mathbf{x}) = 0$ This case is more difficult than the previous one, because the discontinuity of χ_1 has to be taken into account in the integration. The position of this discontinuity leads to two cases which are shown in Fig. 5, depending on the sign of the contact surface $u^\star$.

1. If $u^\star$ **is negative** then on the right cell, the integration is led classically, as there is no discontinuity of χ_1 inside the right cell: the flux $\mathbf{F}_2\left(U_{12}^{\text{int}}\right)$ is withdrawn from the right cell. We denote this flux by $\mathbf{F}_2^{\text{eul}}\left(\mathbf{U}_1^L, \mathbf{U}_2^R, \mathbf{n}^S\right)$. On the left cell, this same flux has to be added, but the discontinuity on χ_1 has also to be taken into account. We denote by $\mathbf{U}_L^\star$ the state on the left of the surface contact. Then the integration on the left leads to a flux

$$\mathbf{F}_1(\mathbf{U}_L^\star)\cdot\mathbf{n}^S - u^\star\mathbf{U}_L^\star = \begin{pmatrix} 0 \\ P^\star\mathbf{n}_x^S \\ P^\star\mathbf{n}_y^S \\ P^\star\mathbf{n}_z^S \\ P^\star u^\star \end{pmatrix}$$

Note that this flux does not depend on the equation of state. Note also that we find the same result by computing $\mathbf{F}_2(\mathbf{U}_R^\star)\cdot\mathbf{n}^S - u^\star\mathbf{U}_R^\star$, thanks to conservativity. From now on, we denote this flux by $\mathbf{F}^{\text{lag}}\left(\mathbf{U}_1^L, \mathbf{U}_2^R, \mathbf{n}^S\right)$. To summarize, the integration of this Riemann problem gives:

- On the phase 2, in the right cell: the Eulerian flux $\mathbf{F}_2^{\text{eul}}\left(\mathbf{U}_1^L, \mathbf{U}_2^R, \mathbf{n}^S\right)$ is withdrawn.
- On the phase 1, in the right cell: nothing is added nor withdrawn.
- On the phase 2, in the left cell: the Eulerian flux $\mathbf{F}_2^{\text{eul}}\left(\mathbf{U}_1^L, \mathbf{U}_2^R, \mathbf{n}^S\right)$ is added, and the Lagrangian flux $\mathbf{F}^{\text{lag}}\left(\mathbf{U}_1^L, \mathbf{U}_2^R, \mathbf{n}^S\right)$ is withdrawn.
- On the phase 1, in the left cell: the Lagrangian flux $\mathbf{F}^{\text{lag}}\left(\mathbf{U}_1^L, \mathbf{U}_2^R, \mathbf{n}^S\right)$ is added.

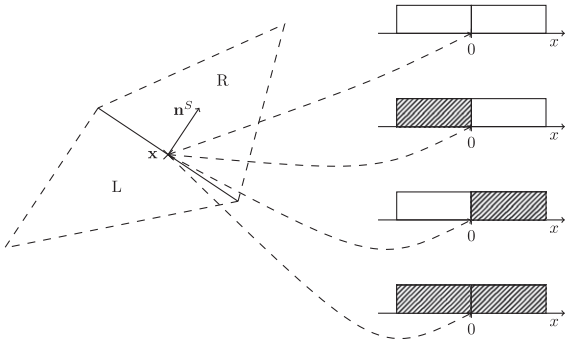

Fig. 3. Decomposition of the side integral into four Riemann problems. The side S has a normal $\mathbf{n}^S$ and two adjacent cells, which we denote by L (where $\mathbf{n}^S$ is outward) and R (where $\mathbf{n}^S$ is inward). At the point $\mathbf{x}$, there might be four possible Riemann problems, which initial conditions are shown on the right of the figure. The first phase is in white whereas the second phase is shaded.

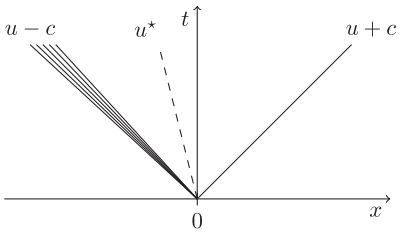

Fig. 4. Example of solution of a Riemann problem involving a pure phase. In case shown on the picture, the left wave is a rarefaction wave and the right wave is a shock. The integration is led classically by computing the flux at $x = 0$, and by adding this flux on the left and withdrawing it on the right.

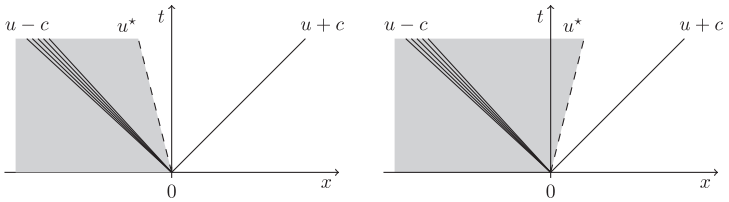

Fig. 5. Example of solution of a Riemann problem involving two different phases. The first phase is in white whereas the second phase is shaded. The flux integration strongly depends on whether the velocity of the surface contact $u^\star$ is positive or negative. This contact surface correspond to a jump in $\nabla\chi$, which integration raises a Lagrangian flux.

2. If $u^\star$ **is positive** the integration on the left cell is straightforward: it consists only in one Eulerian flux $\mathbf{F}_1^{\text{eul}}\left(\mathbf{U}_1^L, \mathbf{U}_2^R, \mathbf{n}^S\right)$ which is added on the fluid 1, and nothing on the fluid 2. On the left cell, the integration leads to withdrawing the Eulerian flux $\mathbf{F}_1^{\text{eul}}\left(\mathbf{U}_1^L, \mathbf{U}_2^R, \mathbf{n}^S\right)$ on the phase 1, and adding the Lagrangian flux, whereas only a Lagrangian flux is withdrawn from phase 2.

To summarize the paragraph, the total flux added on the right cell, on the phase 1, that comes from the integration of the Riemann problem with phase 1 on the left and phase 2 on the right is

$$\mathcal{F}_{12}^{1,+} = -\mathcal{H}(u_{12}^\star(\mathbf{n}^S))\left(\mathbf{F}_1^{\text{eul}}\left(\mathbf{U}_1^L, \mathbf{U}_2^R, \mathbf{n}^S\right) - \mathbf{F}^{\text{lag}}\left(\mathbf{U}_1^L, \mathbf{U}_2^R, \mathbf{n}^S\right)\right)$$

where $\mathcal{H}$ denotes the Heaviside function, i.e. $\mathcal{H}(x) = 1$ if $x > 0$, and $\mathcal{H}(x) = 0$ otherwise. On the phase 2, the flux for the right cell is equal to

$$\mathcal{F}_{12}^{2,+} = -\mathcal{H}(-u_{12}^\star(\mathbf{n}^S))\mathbf{F}_2^{\text{eul}}\left(\mathbf{U}_1^L, \mathbf{U}_2^R, \mathbf{n}^S\right) - \mathcal{H}(u_{12}^\star(\mathbf{n}^S))\mathbf{F}^{\text{lag}}\left(\mathbf{U}_1^L, \mathbf{U}_2^R, \mathbf{n}^S\right)$$

The flux on the left cell for the phase 1 is equal to

$$\mathcal{F}_{12}^{1,-} = \mathcal{H}(u_{12}^\star(\mathbf{n}^S))\mathbf{F}_1^{\text{eul}}(\mathbf{U}_1^L, \mathbf{U}_2^R, \mathbf{n}^S) + \mathcal{H}(-u_{12}^\star(\mathbf{n}^S))\mathbf{F}^{\text{lag}}\left(\mathbf{U}_1^L, \mathbf{U}_2^R, \mathbf{n}^S\right)$$

and for the phase 2, it can be written as

$$\mathcal{F}_{12}^{2,-} = \mathcal{H}(-u_{12}^\star(\mathbf{n}^S))\left(\mathbf{F}_2^{\text{eul}}\left(\mathbf{U}_1^L, \mathbf{U}_2^R, \mathbf{n}^S\right) - \mathbf{F}^{\text{lag}}\left(\mathbf{U}_1^L, \mathbf{U}_2^R, \mathbf{n}^S\right)\right)$$

$\chi_1^L(\mathbf{x}) = 0$ and $\chi_1^R(\mathbf{x}) = 1$ Reasoning as for the case $\chi_1^L(\mathbf{x}) = 1$ and $\chi_1^R(\mathbf{x}) = 0$, we find that the total flux added on the right cell, on the phase 2, that comes from the integration of the Riemann problem with phase 2 on the left and phase 1 on the right is

$$\mathcal{F}_{21}^{2,+} = -\mathcal{H}(u_{21}^\star(\mathbf{n}^S))\left(\mathbf{F}_2^{\text{eul}}\left(\mathbf{U}_2^L, \mathbf{U}_1^R, \mathbf{n}^S\right) - \mathbf{F}^{\text{lag}}\left(\mathbf{U}_2^L, \mathbf{U}_1^R, \mathbf{n}^S\right)\right)$$

On the phase 1, the flux for the right cell is equal to

$$\mathcal{F}_{21}^{1,+} = -\mathcal{H}(-u_{21}^\star(\mathbf{n}^S))\mathbf{F}_1^{\text{eul}}\left(\mathbf{U}_2^L, \mathbf{U}_1^R, \mathbf{n}^S\right) - \mathcal{H}(u_{21}^\star(\mathbf{n}^S))\mathbf{F}^{\text{lag}}\left(\mathbf{U}_2^L, \mathbf{U}_1^R, \mathbf{n}^S\right)$$

The flux on the left cell for the phase 2 is equal to

$$\mathcal{F}_{21}^{2,-} = \mathcal{H}(u_{21}^\star(\mathbf{n}^S))\mathbf{F}_2^{\text{eul}}\left(\mathbf{U}_2^L, \mathbf{U}_1^R, \mathbf{n}^S\right) + \mathcal{H}(-u_{21}^\star(\mathbf{n}^S))\mathbf{F}^{\text{lag}}\left(\mathbf{U}_2^L, \mathbf{U}_1^R, \mathbf{n}^S\right)$$

and for the phase 1, it can be written as

$$\mathcal{F}_{21}^{1,-} = \mathcal{H}\left(-u_{21}^{\star}(\mathbf{n}^S)\right)\left(\mathbf{F}_1^{\text{eul}}\left(\mathbf{U}_2^L, \mathbf{U}_1^R, \mathbf{n}^S\right) - \mathbf{F}^{\text{lag}}\left(\mathbf{U}_2^L, \mathbf{U}_1^R, \mathbf{n}^S\right)\right)$$

$\chi_1^L(\mathbf{x}) = 1$ and $\chi_1^R(\mathbf{x}) = 1$ This case is integrated as for the case with $\chi_1^L(\mathbf{x}) = 0$ and $\chi_1^R(\mathbf{x}) = 0$, and we find

$$\begin{cases} \mathcal{F}_{11}^{1,+} = \mathbf{F}_1^{\text{eul}}\left(\mathbf{U}_1^L, \mathbf{U}_1^R, \mathbf{n}^S\right) \\ \mathcal{F}_{11}^{1,-} = -\mathbf{F}_1^{\text{eul}}\left(\mathbf{U}_1^L, \mathbf{U}_1^R, \mathbf{n}^S\right) \\ \mathcal{F}_{11}^{2,+} = 0 \\ \mathcal{F}_{11}^{2,-} = 0 \end{cases}$$

Averaging The last step for obtaining the multiphase system in Section 3.1 was to perform an average. This is also the way that is followed for obtaining the total flux for the average system. Let us denote by $\mathbb{P}(i,j)$ the probability to have a Riemann problem between phase i on the left and phase j on the right. Then the total flux on a given point $\mathbf{x}$ of a given side S is equal to

$$\widetilde{F}^{k,+} = \sum_{i,j} \mathbb{P}(i,j)\mathcal{F}_{ij}^{k,+} \quad \text{and} \quad \widetilde{F}^{k,-} = \sum_{i,j} \mathbb{P}(i,j)\mathcal{F}_{ij}^{k,-} \tag{14}$$

Computing the weights $\mathbb{P}(i,j)$ is out of the scope of this Section, this will be done in Section 3.4, by stating precisely how χ_1 can be chosen. Here, we are concentrated on finding an expression for the conservative numerical flux and the nonconservative numerical flux for the formulation (13).

Expression for the conservative and nonconservative flux. The total flux $\mathcal{F}^{k,\pm}$ is split into two types of flux:

- $\mathcal{F}^{k,\text{eul},\pm}$: the sum of the fluxes that are of Eulerian type
- $\mathcal{F}^{k,\text{lag},\pm}$: the sum of the fluxes that are of a Lagrangian type.

We remark that $\mathcal{F}^{k,\text{eul},+} = -\mathcal{F}^{k,\text{eul},-}$, which is a property of conservation. The Lagrangian fluxes never match this property, because they are put only on one of the neighboring cells. We can therefore identify in the discretization the conservative part and the nonconservative part. Consequently we propose to approximate the conservative flux of (13) as follows:

$$\int_S [\![\varphi]\!]\{\!\{\mathbb{E}(\chi_k \mathbf{F}(\mathbf{U}))\}\!\} \cdot \mathbf{n}^S \approx \int_S [\![\varphi]\!]\mathcal{F}^{k,\text{eul},+}$$

and the nonconservative flux as

$$\int_S \{\!\{\varphi\}\!\} \int_0^1 \frac{\partial \Phi}{\partial s}(s, u^L, u^R)\mathbb{E}((\mathbf{F}(\mathbf{U}) - \sigma\mathbf{U})\nabla\chi_k) \cdot \mathbf{n}^S \approx \int_S \varphi^L \mathcal{F}^{k,\text{lag},-} + \int_S \varphi^R \mathcal{F}^{k,\text{lag},+}$$

Equation for the volume fraction. Following [2], the volume fraction equation is discretized by adding a first component to $\mathbf{U}$, which is the volume fraction, and by adding a first component to the conservative flux $\mathbf{F}$ which is 0. Thus, the only fluxes that appear in the volume fraction discretization are the Lagrangian fluxes.

3.4. Discrete modeling of two phase flows

The aim of this section is to compute all the probabilities and mathematical expectancies that still appear in the numerical scheme. They both appear:

- in the fluxes, through $\mathbb{P}(i,j)$;
- in the internal integrals, especially in the integral of $\mathbb{E}((\mathbf{F}(\mathbf{U}) - \sigma\mathbf{U})\nabla\chi_k)$ inside the cells.

As far as we are concerned, the simplest model consists in taking the image of a Gaussian stochastic process:

$$\chi_1 = \frac{1 + \text{sgn}(g_{\mathbf{x}})}{2}$$

For the sake of simplicity, we suppose that $\text{Var}(g_x) = 1$ for all $\mathbf{x}$. We denote by $m(\mathbf{x})$ its mean. The constraint $\mathbb{E}(\chi_1) = \alpha_1$ induces:

$$\mathbb{E}(\chi_1) = \frac{1}{\sqrt{2\pi}} \int_{\mathbb{R}} \frac{1 + \text{sgn}(g)}{2} \mathrm{e}^{-(g - m(\mathbf{x}))^2/2}\, \mathrm{d}g = \frac{1}{\sqrt{2\pi}} \int_{\mathbb{R}} \frac{1 + \text{sgn}(u + m(\mathbf{x}))}{2} \mathrm{e}^{-g^2/2}\, \mathrm{d}g$$

which leads to

$$\alpha_1(\mathbf{x}) = \frac{1}{\sqrt{2\pi}} \int_{-m(\mathbf{x})}^{\infty} \mathrm{e}^{-g^2/2}\, \mathrm{d}g \tag{15}$$

As the function erf is $\mathcal{C}^\infty$ with nonnegative derivative, this means that m has at least the same regularity as α_1.

We denote by $\widetilde{R}$ the autocorrelation function:

$$\widetilde{R}(\mathbf{x},\mathbf{y}) = \mathbb{E}((g_{\mathbf{x}} - m(\mathbf{x}))(g_{\mathbf{y}} - m(\mathbf{y})))$$

We suppose that the centered process $g_{\mathbf{x}} - m(\mathbf{x})$ is stationary and isotropic, i.e. a function R exists such that:

$$\widetilde{R}(\mathbf{x},\mathbf{y}) = R(\|\mathbf{x}-\mathbf{y}\|)$$

3.4.1. Computation of the weights at the boundaries

In Section 3.3, we defined the integrals at the sides as averages of simple Riemann problems, see (14). These fluxes depend on $\mathbb{P}(i,j)$, which is the probability of having a contact between the fluid i and the fluid j at a given point on the side.

On a side, and with a given normal $\mathbf{n}$ and a given function u, we denote by $u^L(\mathbf{x})$ the value of u on the left and by $u^R(\mathbf{x})$ the value on the right. We remark that a contact exists between the phase i and the phase j provided $\chi_i^L(\mathbf{x}) = 1$ and $\chi_j^R(\mathbf{x}) = 1$, so that

$$\mathbb{P}(i,j) = \mathbb{E}\left(\chi_i^L(\mathbf{x})\chi_j^R(\mathbf{x})\right)$$

The following proposition gives the value of this probability for $i = j$.

Proposition 1. *If $g_{\mathbf{x}}$ is a Gaussian process such that for all $\mathbf{x}$ where α_1 is continuous,*

$$\mathbb{E}\left(\frac{1+\operatorname{sgn}(g_{\mathbf{x}})}{2}\right) = \alpha_1(\mathbf{x})$$

with variance 1. α is continuous inside the cells of a mesh, and might be discontinuous on a side, then on a point of discontinuity of $\alpha_1(\mathbf{x})$

$$\mathbb{E}(\chi_1^L(\mathbf{x})\chi_1^R(\mathbf{x})) = \min\left(\alpha_1^L(\mathbf{x}), \alpha_1^R(\mathbf{x})\right)$$

Proof. This proof consists in giving an expression of $\mathbb{E}(\chi_1^L(\mathbf{x})\chi_1(\mathbf{x}+\tau\mathbf{n}))$ where $\tau > 0$, and then to compute the limit when $\tau \to 0$. The vector $(g_{\mathbf{x}}, g_{\mathbf{x}+\tau\mathbf{n}})$ is a Gaussian vector with mean $(m(\mathbf{x}), m(\mathbf{x}+\tau\mathbf{n}))$, and with autocorrelation matrix

$$C = \begin{pmatrix} 1 & R(\tau) \\ R(\tau) & 1 \end{pmatrix}$$

where $R(\tau)$ is the cross correlation function of $g_{\mathbf{x}}$. Then the cross correlation of the process $\chi_1^L(\mathbf{x})\chi_1(\mathbf{x}+\tau\mathbf{n})$ is

$$\mathbb{E}(\chi_1^L(\mathbf{x})\chi_1(\mathbf{x}+\tau\mathbf{n})) = \frac{1}{2\pi\sqrt{\det C}} \int_{\mathbb{R}}\int_{\mathbb{R}} \frac{1+\operatorname{sgn}(g_1)}{2}\,\frac{1+\operatorname{sgn}(g_2)}{2} \exp\left(-\frac{u^T C^{-1} u}{2}\right) \mathrm{d}g_1\,\mathrm{d}g_2$$

with $u = (g_1 - m^L(\mathbf{x}), g_2 - m(\mathbf{x}+\tau\mathbf{n}))^T$, with $\det C = 1 - R^2(\tau)$. We remark that the expression when $\tau \to 0$, $\det C \to 0$, so that $\mathbb{E}(\chi_1^L(\mathbf{x})\chi_1(\mathbf{x}+\tau\mathbf{n}))$ seems to be singular. Therefore, we are looking for a suitable variable change for removing this singularity. The matrix C^{-1} can be transformed as

$$C^{-1} = \frac{1}{1-R(\tau)^2}\begin{pmatrix} 1 & -R(\tau) \\ -R(\tau) & 1 \end{pmatrix} = \frac{1}{2(1-R(\tau)^2)} P^T \begin{pmatrix} 1+R(\tau) & 0 \\ 0 & 1-R(\tau) \end{pmatrix} P$$

with

$$P = \begin{pmatrix} -1 & 1 \\ 1 & 1 \end{pmatrix}$$

In the integral, we change the variable g such that $v = Pu$. Then the integral becomes (note that $\det P = 2$)

$$\mathbb{E}(\chi_1^L(\mathbf{x})\chi_1(\mathbf{x}+\tau\mathbf{n})) = \frac{1}{4\pi\sqrt{\det C}} \int\int_{\mathbb{R}^2} \frac{1+\operatorname{sgn}(g_1)}{2}\,\frac{1+\operatorname{sgn}(g_2)}{2}\, \mathrm{e}^{-\frac{v_1^2}{4(1-R(\tau))}} \mathrm{e}^{-\frac{v_2^2}{4(1+R(\tau))}} \mathrm{d}v_1\,\mathrm{d}v_2$$

with

$$\begin{cases} g_1 = m^L(\mathbf{x}) + \frac{v_2 - v_1}{2} \\ g_2 = m(\mathbf{x}+\tau\mathbf{n}) + \frac{v_1+v_2}{2} \end{cases}$$

Moreover, $\det C = 1 - R(\tau)^2$. By doing the variable change

$$\begin{cases} w_1 = \frac{v_1}{\sqrt{2(1-R(\tau))}} \\ w_2 = \frac{v_2}{\sqrt{2(1+R(\tau))}} \end{cases}$$

we find

$$\mathbb{E}\left(\chi_1^L(\mathbf{x})\chi_1(\mathbf{x}+\tau\mathbf{n})\right) = \frac{1}{2\pi}\int_{\mathbb{R}}\int_{\mathbb{R}} \frac{1+\mathrm{sgn}(g_1)}{2}\frac{1+\mathrm{sgn}(g_2)}{2} e^{-w_1^2/2} e^{-w_2^2/2}\, dw_1\, dw_2$$

with

$$\begin{cases} g_1 = m^L(\mathbf{x}) + \frac{1}{2}\left(w_2\sqrt{2(1+R(\tau))} - w_1\sqrt{2(1-R(\tau))}\right) \\ g_2 = m(\mathbf{x}+\tau\mathbf{n}) + \frac{1}{2}\left(w_2\sqrt{2(1+R(\tau))} + w_1\sqrt{2(1-R(\tau))}\right) \end{cases}$$

Therefore the cross correlation can be put into the following form

$$\frac{1}{2\pi}\int\int_{D_\tau} \frac{1+\mathrm{sgn}(g_1)}{2}\frac{1+\mathrm{sgn}(g_2)}{2} e^{-w_1^2/2} e^{-w_2^2/2}\, dw_1\, dw_2$$

with the domain D_τ defined by

$$\begin{cases} w_2 \geqslant \sqrt{\frac{1-R(\tau)}{1+R(\tau)}}\, w_1 - \frac{2}{\sqrt{2(1+R(\tau))}} m^L(\mathbf{x}) \\ w_2 \geqslant -\sqrt{\frac{1-R(\tau)}{1+R(\tau)}}\, w_1 - \frac{2}{\sqrt{2(1+R(\tau))}} m(\mathbf{x}+\tau\mathbf{n}) \end{cases}$$

When $R(\tau) \to 1$, the limit integration domain is defined as

$$w_2 \geqslant \max(-m^L(\mathbf{x}), -m^R(\mathbf{x}))$$

Therefore the limit cross correlation is equal to

$$\frac{1}{2\pi}\int_{\mathbb{R}} e^{-w_1^2/2} dw_1 \int_{w_2 \geqslant \max(-m^L(\mathbf{x}), -m^R(\mathbf{x}))} e^{-w_2^2/2} dw_2 = \min(\alpha^L(\mathbf{x}), \alpha^R(\mathbf{x})) \qquad \square$$

Proposition 1 emphasizes the strength of the modeling of the flow topology by a stochastic process. Actually, what was missing in [2] was to give a spatial correlation of the flow topology. Therefore the weights were only *assumed* (see [2, p.376]), whereas in our case, the expression of the weights are a direct consequence of the modeling.

Knowing the weights $\mathbb{P}(i,i)$ for $i = 1, 2$, we can compute all the other weights, as indicated in the following proposition.

Proposition 2. *The weights are given by*

$$\begin{aligned} \mathbb{P}(1,1) &= \min\left(\alpha_1^L(\mathbf{x}), \alpha_1^R(\mathbf{x})\right) \\ \mathbb{P}(1,2) &= \max\left(\alpha_1^L(\mathbf{x}) - \alpha_1^R(\mathbf{x}), 0\right) \\ \mathbb{P}(2,2) &= \min\left(\alpha_2^L(\mathbf{x}), \alpha_2^R(\mathbf{x})\right) \\ \mathbb{P}(2,1) &= \max\left(\alpha_2^L(\mathbf{x}) - \alpha_2^R(\mathbf{x}), 0\right) \end{aligned}$$

Proof. Using the fact that $\chi_1 + \chi_2 = 1$,

$$\begin{aligned} \alpha_1^L(\mathbf{x}^-) &= \mathbb{E}\left(\chi_1^L(\mathbf{x})\right) \\ &= \mathbb{E}\left(\chi_1^L(\mathbf{x})\left(\chi_1^R(\mathbf{x}) + \chi_2^R(\mathbf{x})\right)\right) \\ &= \mathbb{E}\left(\chi_1^L(\mathbf{x})\chi_1^R(\mathbf{x})\right) + \mathbb{E}\left(\chi_1^L(\mathbf{x})\chi_2^R(\mathbf{x})\right) \\ \alpha_1^L(\mathbf{x}^-) &= \mathbb{P}(1,1) + \mathbb{P}(1,2) \end{aligned}$$

so that, using Proposition 1

$$\mathbb{P}(1,2) = \alpha_1^L(\mathbf{x}) - \min\left(\alpha_1^L(\mathbf{x}), \alpha_1^R(\mathbf{x})\right)$$

This means that either $\min\left(\alpha_1^L(\mathbf{x}), \alpha_1^R(\mathbf{x})\right) = \alpha_1^L(\mathbf{x})$, and $\mathbb{P}(1,2) = 0$, or $\min(\alpha_1^L(\mathbf{x}), \alpha_1^R(\mathbf{x})) = \alpha_1^R(\mathbf{x})$, and $\mathbb{P}(1,2) = \alpha_1^L(\mathbf{x}) - \alpha_1^R(\mathbf{x})$. The computation of the other $\mathbb{P}(i,j)$ with $i \neq j$ can be proved in the same manner. $\square$

3.4.2. Internal integral

In this section, we are interested in finding an expression for

$$\mathbb{E}((\mathbf{F}(\mathbf{U}) - \sigma\mathbf{U}) \cdot \nabla\chi_1)$$

which must then be integrated inside the cells. Suppose that the boundary of the set Γ defined by

$$\Gamma = \{\mathbf{x} \in \mathbb{R}^2 \ \chi_1(\mathbf{x}) = 1\}$$

is continuous. Then $(\mathbf{F}(\mathbf{U}) - \sigma\mathbf{U})$ is defined by solving a one dimensional Riemann problem, where the direction is defined by the normal of the boundary of Γ (see Fig. 2).

For a given realization, the value of $(\mathbf{F}(\mathbf{U}) - \sigma\mathbf{U}) \cdot \nabla\chi_1$ strongly depends on the value of $\nabla\chi_1$:

1. if $\nabla\chi_1 = \delta$, then we have an interface between phase 2 and phase 1. Then for computing $(\mathbf{F}(\mathbf{U}) - \sigma\mathbf{U})$ at the interface, we solve the Riemann problem in the direction $\mathbf{n}$ given by the gradient of χ.
2. If $\nabla\chi_1 = 0$, then we do not care about the value of $(\mathbf{F}(\mathbf{U}) - \sigma\mathbf{U})$.

A first step for studying the gradient of χ consists in studying its directional derivative. For a given direction $\mathbf{n}$ and a given $\mathbf{x}$, we are interested in the behavior of

$$T_\chi(\tau) = \frac{\chi_1(\mathbf{x} + \tau\mathbf{n}) - \chi_1(\mathbf{x})}{\tau}$$

when $\tau \to 0$. $T_\chi(\tau)$ can have three values: $-1/\tau$, 0, $1/\tau$, depending on the values of χ_1

$\chi_1(\mathbf{x} + \tau\mathbf{n})$	$\chi_1(\mathbf{x})$	$T_\chi(\tau)$
0	0	0
0	1	$-\frac{1}{\tau}$
1	0	$\frac{1}{\tau}$
1	1	0

Given a direction $\mathbf{n}$, $(\mathbf{F}(\mathbf{U}) - \sigma\mathbf{U})$ can take two different values, depending on whether $\nabla\chi_1$ is the same or opposite to $\mathbf{n}$. Therefore, what we want to compute is the probability of having $T_\chi > 0$ and the probability of having $T_\chi < 0$. These events can be recast as follows:

$$T_\chi > 0 \iff \chi_1(\mathbf{x} + \tau\mathbf{n})(1 - \chi_1(\mathbf{x})) = 1$$
$$T_\chi < 0 \iff \chi_1(\mathbf{x})(1 - \chi_1(\mathbf{x} + \tau\mathbf{n})) = 1$$

Thus, computing the probability of having $\nabla\chi_1$ in one given direction $\mathbf{n}$ is equivalent to finding the limit of

$$\mathbb{E}\left(\frac{\chi_1(\mathbf{x} + \tau\mathbf{n})(1 - \chi_1(\mathbf{x}))}{\tau}\right) \quad \text{and} \quad \mathbb{E}\left(\frac{\chi_1(\mathbf{x})(1 - \chi_1(\mathbf{x} + \tau\mathbf{n}))}{\tau}\right).$$

The behavior of these expectancies is given in the following proposition

Proposition 3. *We suppose that the autocorrelation function R is regular near 0. If α_1 can be derived in a given point $\mathbf{x}$, and for a given direction $\mathbf{n}$, the behavior of*

$$\frac{\mathbb{E}(\chi_1(\mathbf{x})\chi_1(\mathbf{x} + \tau\mathbf{n})) - \alpha_1(\mathbf{x})}{\tau}$$

when the nonnegative real number τ tends to 0, depends on the behavior of the autocorrelation function R near 0:

- *If $R'(0) \neq 0$ then $\mathbb{E}(\chi_1(\mathbf{x})\chi_1(\mathbf{x} + \tau\mathbf{n})) - \alpha_1(\mathbf{x})$ behaves as $\sqrt{\tau}$, and the ratio has an infinite limit.*
- *If $R'(0) = 0$ and $R''(0) \neq 0$, then the ratio has a limit that depends on $R''(0)$.*
- *If $R'(0) = 0$ and $R''(0) = 0$, then the ratio has a limit which depends only on the derivative of the first moment:*

$$\frac{\mathbb{E}(\chi_1(\mathbf{x})\chi_1(\mathbf{x} + \tau\mathbf{n})) - \alpha_1(\mathbf{x})}{\tau} \to \begin{cases} 0 & \text{if } \nabla\alpha_1(\mathbf{x}) \cdot \mathbf{n} > 0 \\ \nabla\alpha_1(\mathbf{x}) \cdot \mathbf{n} & \text{if } \nabla\alpha_1(\mathbf{x}) \cdot \mathbf{n} < 0 \end{cases}$$

The proof of this proposition is too long for being exposed here, and is detailed in Appendix A.

We want that the result does not depend on the values of $R''(0)$, because this is a modeling parameter. Therefore, from now on, we suppose that we are in the third case of Proposition 3, i.e. $R'(0) = R''(0) = 0$. With this choice, $g_{\mathbf{x}}$ can be derived, and its derivative is a Dirac mass concentrated on $\nabla\alpha_1(\mathbf{x})$. Consequently, $\nabla\chi_1$ is also a Dirac mass concentrated on the direction of $\nabla\ \alpha_1$. From the direction $\nabla\alpha_1$, we define the associated unitary vector $\mathbf{n}(\nabla\alpha_1)$. The interfacial velocity and pressure are defined by solving a local Riemann problem which initial condition is given by (see Fig. 2)

$$\begin{cases} \mathbf{U}(\xi, 0) = \mathbf{U}_2(\mathbf{x}) \cdot \mathbf{n}(\nabla\alpha_1) & \text{if} \quad \xi < 0 \\ \mathbf{U}(\xi, 0) = \mathbf{U}_1(\mathbf{x}) \cdot \mathbf{n}(\nabla\alpha_1) & \text{if} \quad \xi > 0 \end{cases}$$

and we denote by $u^\star(\nabla\alpha_1)$ and $P^\star(\nabla\alpha_1)$ the velocity and pressure of the surface contact. With these notations, we finally find

$$\mathbb{E}((\mathbf{F}(\mathbf{U})-\sigma\mathbf{U})\cdot\nabla\chi_1) = \begin{pmatrix} 0 \\ -P^\star(\nabla\alpha_1)n_x(\nabla\alpha_1)\|\nabla\alpha_1\| \\ -P^\star(\nabla\alpha_1)n_y(\nabla\alpha_1)\|\nabla\alpha_1\| \\ -P^\star(\nabla\alpha_1)n_z(\nabla\alpha_1)\|\nabla\alpha_1\| \\ -u^\star(\nabla\alpha_1)P^\star(\nabla\alpha_1)\|\nabla\alpha_1\| \end{pmatrix}$$

3.4.3. Some remarks on the internal terms found

With the notations of the previous section, setting

$$\begin{cases} \mathbf{u}_I = u^\star(\nabla\alpha_1)\mathbf{n}(\nabla\alpha_1) \\ P_I = P^\star(\nabla\alpha_1) \end{cases}$$

then the integration of the internal term can be written as it appears in the model (1), with $\mathbf{u}_I\cdot\nabla\alpha_1$ in the volume fraction equation, $P_I\nabla\alpha_1$ in the momentum, and $P_I\mathbf{u}_I\cdot\nabla\alpha_1$ in the energy equation.

Behavior when one of the phase is incompressible. The solution of the Riemann problem is computed by intersecting the wave curves from the left and right state, projected in the plane (u,P) (see [48]). If the phase 1 is considered as incompressible, then its associated wave curve is vertical, as shown on Fig. 6. Consequently, the interfacial velocity is equal to the velocity of the incompressible phase, as was supposed in [4]. Yet, the interfacial pressure is not equal to the pressure of the compressible phase, as was supposed in [4].

Expression in the acoustic approximation. If the acoustic approximation holds, the pressure and velocity at the contact surface read

$$\begin{cases} P_I = \frac{Z_2P_1+Z_1P_2}{Z_1+Z_2} + \frac{Z_1Z_2(\mathbf{u}_2-\mathbf{u}_1)\cdot\mathbf{n}(\nabla\alpha_1)}{Z_1+Z_2} \\ \mathbf{u}_I = \frac{Z_1\mathbf{u}_1\cdot\mathbf{n}(\nabla\alpha_1)+Z_2\mathbf{u}_2\cdot\mathbf{n}(\nabla\alpha_1)+P_2-P_1}{Z_1+Z_2}\mathbf{n}(\nabla\alpha_1) \end{cases} \tag{16}$$

where Z_i denotes the acoustic impedance of the fluid i for $i = 1, 2$. In one dimension, this expression is the same as [5, p. 510], but is slightly different in two dimensions. Note in particular that this expression is invariant by a Galilean frame change, which is not the case of [5].

3.5. Exact preservation of contact discontinuity

As stated in [1], preserving exactly the contact discontinuities is necessary for avoiding spurious pressure oscillations in contact discontinuities. The scheme we developed ensure this condition, mainly because this condition was already ensured in [2]. More precisely, the following proposition is proved.

Proposition 4. *If both of the fluids follow a stiffened gas equation of state, and if they both have an equal uniform velocity* $\mathbf{u}_0$ *and pressure* P_0*, then the uniform pressure and velocity are preserved by the scheme.*

Proof. This property is ensured by the finite volume approximation [2, pp. 383–384]. Following their proof, the solution of all the single phase Riemann problems is straightforward: all the acoustic waves are evanescent, and the only variation of the variables is on the contact discontinuities of heterogeneous Riemann problems. For a given cell K, and for one of its side S, we denote by $\mathbf{n}^S$ the normal of S, outward with respect to K. The neighbor of the cell K with respect to S is denoted by $\overline{K}$. Then two situations may occur

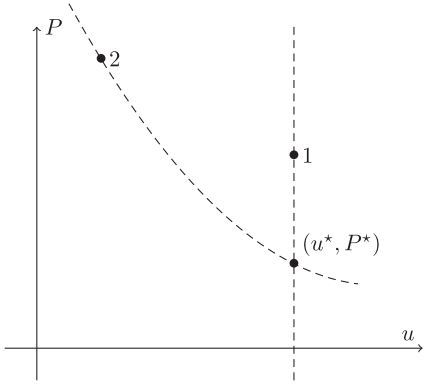

Fig. 6. Riemann problem in the plane (u,P) when one phase is incompressible. The phase 2 is on the left, and the phase 1 on the right. The phase 1 is supposed to be incompressible. Therefore, its wave curve is a straight vertical line, and the velocity of the intersection is equal to the velocity of the incompressible phase, as in [4]. Note that the pressure at the intersection is not equal to the pressure of the compressible phase.

- If $\mathbf{u}_0 \cdot \mathbf{n}^S > 0$: the sum of the fluxes does not make appear any Lagrangian flux. The total flux is composed of the Eulerian flux from the homogeneous Riemann problem, whose weight is $\min\left(\alpha_K^{(i)}(\mathbf{x}^-), \alpha_{\overline{K}}^{(i)}(\mathbf{x}^+)\right)$, and of the Eulerian flux from the heterogeneous Riemann problem if it exists, whose weight is $\max\left(\alpha_K^{(i)}(\mathbf{x}^-) - \alpha_{\overline{K}}^{(i)}(\mathbf{x}^+), 0\right)$. In any case

  $$\min\left(\alpha_K^{(i)}(\mathbf{x}^-), \alpha_{\overline{K}}^{(i)}(\mathbf{x}^+)\right) + \max\left(\alpha_K^{(i)}(\mathbf{x}^-) - \alpha_{\overline{K}}^{(i)}(\mathbf{x}^+), 0\right) = \alpha_K^{(i)}(\mathbf{x}^-)$$

  so that the total flux is equal to $\alpha_K^{(i)}(\mathbf{x}^-)\mathbf{F}^{(i)}\left(\mathbf{U}_K^{(i)}(\mathbf{x}^-)\right) \cdot \mathbf{n}^S$.
- If $\mathbf{u}_0 \cdot \mathbf{n}^S < 0$: the total flux is composed of a Lagrangian flux coming from the heterogeneous Riemann problem. Up to a sign, its expression does not depend whether this heterogeneous Riemann problem is a $0-1$ or a $1-0$ Riemann problem: it is always equal to $\mathcal{F}^{\text{lag}}\mathbf{n}^S = (0, P_0\mathbf{n}^S, P_0\mathbf{u}_0 \cdot \mathbf{n}^S)$. It is multiplied by a plus sign if $\alpha_K^{(i)}(\mathbf{x}^-) > \alpha_{\overline{K}}^{(i)}(\mathbf{x}^-)$, and a minus otherwise. It is moreover weighted by the probability $\alpha_K^{(i)}(\mathbf{x}^-) - \alpha_{\overline{K}}^{(i)}(\mathbf{x}^-)$ if $\alpha_K^{(i)}(\mathbf{x}^-) > \alpha_{\overline{K}}^{(i)}(\mathbf{x}^-)$, and $\alpha_{\overline{K}}^{(i)}(\mathbf{x}^+) - \alpha_K^{(i)}(\mathbf{x}^-)$ otherwise. Therefore the contribution of the Lagrangian fluxes is always equal to

  $$\left(\alpha_K^{(i)}(\mathbf{x}^-) - \alpha_{\overline{K}}^{(i)}(\mathbf{x}^+)\right)\mathcal{F}^{\text{lag}}\mathbf{n}^S$$

Using the same argument as for the previous case, the total Eulerian contribution is $\alpha_{\overline{K}}^{(i)}(\mathbf{x}^+)\mathbf{F}^{(i)}\left(\mathbf{U}_{\overline{K}}^{(i)}(\mathbf{x}^+)\right) \cdot \mathbf{n}^S$.

Still following [2], Eulerian fluxes can be rewritten as

$$\mathbf{F}^{(i)}\left(\mathbf{U}_K^{(i)}(\mathbf{x})\right) \cdot \mathbf{n}^S = \mathcal{F}^{\text{lag}}\mathbf{n}^S + \mathbf{u}_0 \cdot \mathbf{n}^S\mathbf{U}_K^{(i)}(\mathbf{x})$$

and the total flux on a point of a side can be rewritten as

$$\alpha_K^{(i)}(\mathbf{x}^-)\mathcal{F}^{\text{lag}}\mathbf{n}^S + \alpha_K^{(i)}(\mathbf{x}^{-\text{sgn}(\mathbf{u}_0\cdot\mathbf{n}^S)})\mathbf{u}_0 \cdot \mathbf{n}^S\mathbf{U}_K^{(i)}(\mathbf{x}^{-\text{sgn}(\mathbf{u}_0\cdot\mathbf{n}^S)})$$

Thus, the scheme can be rewritten as

$$\int_K \varphi(\mathbf{x})\frac{(\alpha\mathbf{U}_K)^{n+1} - (\alpha\mathbf{U}_K)^n}{\delta t} - \int_K \alpha_K^{(i)}(\mathbf{x})F_K^{(i)} \cdot \nabla\varphi(\mathbf{x}) - \int_K \varphi(\mathbf{x})\mathcal{F}^{\text{lag}} \cdot \nabla\alpha_K^{(i)}(\mathbf{x}) + \sum_S \int_S \varphi(\mathbf{x})\alpha_K^{(i)}(\mathbf{x})\mathcal{F}^{\text{lag}} \cdot \mathbf{n}^S + \sum_S \int_S \varphi(\mathbf{x})\alpha_K^{(i)}(\mathbf{x}^{-\text{sgn}(\mathbf{u}_0\cdot\mathbf{n}^S)})\mathbf{U}_K^{(i)}(\mathbf{x}^{-\text{sgn}(\mathbf{u}_0\cdot\mathbf{n}^S)})\mathbf{u}_0 \cdot \mathbf{n}^S = 0$$

The conservative flux which is integrated in the cell can be rewritten as a sum of a Lagrangian contribution and the conservative vector

$$\int_K \alpha_K^{(i)}(\mathbf{x})F_K^{(i)} \cdot \nabla\varphi(\mathbf{x}) = \int_K \alpha_K^{(i)}(\mathbf{x})\mathcal{F}^{\text{lag}} \cdot \nabla\varphi(\mathbf{x}) + \int_K \alpha_K^{(i)}(\mathbf{x})\mathbf{U}_K^{(i)}\mathbf{u}_0 \cdot \nabla\varphi(\mathbf{x})$$

The cell integrals with Lagrangian flux can be added to give

$$-\int_K \text{div}\left(\alpha_K^{(i)}(\mathbf{x})\mathcal{F}^{\text{lag}}\right)$$

which vanishes when added to the boundary integral with a Lagrangian flux, by using the Greene formula. Consequently, the scheme has been simplified as

$$\int_K \varphi(\mathbf{x})\frac{(\alpha\mathbf{U}_K)^{n+1} - (\alpha\mathbf{U}_K)^n}{\delta t} - \int_K \alpha_K^{(i)}(\mathbf{x})\mathbf{U}_K^{(i)}\mathbf{u}_0 \cdot \nabla\varphi(\mathbf{x}) + \sum_S \int_S \varphi(\mathbf{x})\alpha_K^{(i)}(\mathbf{x}^{-\text{sgn}(\mathbf{u}_0\cdot\mathbf{n}^S)})\mathbf{U}_K^{(i)}(\mathbf{x}^{-\text{sgn}(\mathbf{u}_0\cdot\mathbf{n}^S)})\mathbf{u}_0 \cdot \mathbf{n}^S = 0$$

Four equations are obtained by writing each component of the previous system, with

$$\mathbf{U}_K^{(i)}(\mathbf{x}) = \left(1, \rho_K^{(i)}, \rho_K^{(i)}\mathbf{u}_0^x, \rho_K^{(i)}\mathbf{u}_0^y, \rho_K^{(i)}E_K^{(i)}\right)$$

The equation obtained for the components of the velocity are obviously proportional to the one obtained for the density (by multiplying it by $\mathbf{u}_0^x$ and $\mathbf{u}_0^y$), so that on each point of the cell K, the velocity is constant at time $n+1$. Then, the kinetic part of the energy equation vanishes, thanks to the equation on $\rho_K^{(i)}$ and to the uniformity of $\mathbf{u}$. The following equation holds for the internal energy

$$\int_K \varphi(\mathbf{x})\frac{\left(\alpha_K^{(i)}(\rho\varepsilon)_K^{(i)}\right)^{n+1} - (\alpha_K^{(i)}(\rho\varepsilon)_K^{(i)})^n}{\delta t} - \int_K \alpha_K^{(i)}(\mathbf{x})(\rho\varepsilon)_K^{(i)}\mathbf{u}_0 \cdot \nabla\varphi(\mathbf{x}) + \sum_S \int_S \varphi(\mathbf{x})\alpha_K^{(i)}(\mathbf{x}^{-\text{sgn}(\mathbf{u}_0\cdot\mathbf{n}^S)})(\rho\varepsilon)_K^{(i)}(\mathbf{x}^{-\text{sgn}(\mathbf{u}_0\cdot\mathbf{n}^S)})\mathbf{u}_0 \cdot \mathbf{n}^S = 0$$

And finally, using the stiffened gas equation of state $(\rho\varepsilon)^{(i)} = \frac{P+\gamma^{(i)}P^{\infty,i}}{\gamma^{(i)}-1}$, we see that the pressure equation is just the equation on α_K, multiplied by $P_0 + \gamma^{(i)}P^{\infty,i}$, which ends the proof. □

Note that the hypothesis on the equation of state is necessary, because even for *one phase flows* with strongly nonlinear equations, contact surface might not be conserved, which can induce pressure oscillations [40].

4. Numerical tests

Our aim is to demonstrate the capabilities of the RKDG method for multiphase problems. Therefore, all the numerical simulations presented hereafter involve two different fluids. The fluids are supposed to follow either the perfect gas equation of state, i.e.

$$\varepsilon_k = \frac{P_k}{(\gamma_k - 1)\rho_k} \tag{17}$$

where γ_k is the polytropic coefficient, or the stiffened gas equation of state

$$\varepsilon_k = \frac{P_k + \gamma_k P_{\infty,k}}{(\gamma_k - 1)\rho_k} \tag{18}$$

where γ_k and $P_{\infty,k}$ are given coefficients. This equation is such that for $P_k \ll P_{\infty,k}$, the fluid is nearly incompressible whereas when P_k is of the same order as $P_{\infty,k}$, the fluid is compressible.

4.1. Time integration and slope limiting

The time integration is led explicitly by using Strong Stability Preserving schemes [24] corresponding to the spatial order of discretization. The spectral basis of Legendre (in one dimension), and of Dubiner (in two dimensions) are used for having only a diagonal system to solve at each time step.

For interface tests, a slope limiting is necessary, because the volume fraction, which is equal to 1 in one phase, and 0 in the other is not regular. We perform it as follows:

- If the volume fraction is either equal to 1 or equal to 0, then the conservative variables of the phase that exists are limited.
- If the volume fraction is neither equal to 0 nor to 1, then in each cell, the following steps are followed
  1. Compute the average of each of the conservative variables $\alpha_k\rho_k$, $\alpha_k u_k^x$, $\alpha_k u_k^y$ and $\alpha_k\rho_k E_k$. We denote the average by $\langle\alpha_k\rho_k\rangle$, $\langle\alpha_k u_k^x\rangle$, $\langle\alpha_k u_k^y\rangle$ and $\langle\alpha_k\rho_k E_k\rangle$.
  2. Limit the volume fraction. This is done as for example in [8]. The new volume fraction is denoted by $\tilde{\alpha}_k(\mathbf{x})$.
  3. Rebuild the conservative variables as

$$(\alpha_k\rho_k)(\mathbf{x}) = \tilde{\alpha}_k(\mathbf{x})\frac{\langle\alpha_k\rho_k\rangle}{\langle\alpha_k\rangle}$$

$$\left(\alpha_k\rho_k u_k^x\right)(\mathbf{x}) = \tilde{\alpha}_k(\mathbf{x})\frac{\langle\alpha_k\rho_k u_k^x\rangle}{\langle\alpha_k\rangle}$$

$$\left(\alpha_k\rho_k u_k^y\right)(\mathbf{x}) = \tilde{\alpha}_k(\mathbf{x})\frac{\langle\alpha_k\rho_k u_k^y\rangle}{\langle\alpha_k\rangle}$$

$$(\alpha_k\rho_k E_k)(\mathbf{x}) = \tilde{\alpha}_k(\mathbf{x})\frac{\langle\alpha_k\rho_k E_k\rangle}{\langle\alpha_k\rangle}$$

For mixture tests, the slope limiting is performed on the characteristic variables of the system. The computations of the left and right eigenvectors of the full system is described in Appendix D. The left and right eigenvectors depends on the interfacial velocity and pressure. For simplifying this computation, the expression given by (16) is used for the interface variables.

From a practical point of view, the minmod limiter was used in both cases.

4.2. Consistency test of the scheme

In the finite volume scheme proposed in [2], the limit system solved by the discrete equations method was left unclear. Derivation of the limit system was necessary in the discontinuous Galerkin formulation, because of the cell integrals. This limit was derived in Section 3.4.2, and was discussed in Section 3.4.3. The aim of this test is to prove the consistency of the numerical method with the model (1) with the closure explained in Section 3.4.3.

A simple way to derive an analytical solution of a given hyperbolic system consists in computing a self similar solution attached to a characteristic field. Basically, for a given hyperbolic system

$$\partial_t\mathbf{u} + A(\mathbf{u})\partial_x\mathbf{u} = 0,$$

a solution $\mathbf{u}(x,t)$ is searched as a function of the variable x/t, i.e. $\mathbf{u}(x,t) = \mathbf{u}_0\left(\frac{x}{t}\right)$. Then denoting by ξ the variable of $\mathbf{u}_0$,

$$\left(A(\mathbf{u}) - \frac{x}{t}\mathbf{Id}\right)(\mathbf{u}_0)_\xi = 0 \tag{19}$$

For having a non trivial solution of (19), x/t must be equal to an eigenvalue of the matrix A.

In this test, we are interested in self similar solutions associated to the field $\mathbf{u}_I$. In this case, the volume fraction is a free parameter, and the other variables can be computed by solving an ODE system. Computations of the ODE system are detailed in Appendix C. Here, it is worth highlighting that if the closure (2) is considered, one of the phase entropy is constant and the velocity of the other phase is also constant which are not the case here.

We denote by P the function such that $P'(x) = (x-1)^4(x+1)^4$ and $P(0) = 0$. On the boundaries of the domain, α_2 takes the values $\alpha_2^{(L)}$ on the left and $\alpha_2^{(R)}$ on the right, and α_2 is then set to

$$\begin{cases} \alpha_2(x) = \alpha_2^{(L)} & \text{if } x < x_1, \\ \alpha_2(x) = \alpha_2^{(L)} + \frac{\alpha_2^{(R)} - \alpha_2^{(L)}}{P(1)} P\left(\frac{x - \frac{x_1+x_2}{2}}{\frac{x_1-x_2}{2}}\right) & \text{if } x_1 < x < x_2, \\ \alpha_2(x) = \alpha_2^{(R)} & \text{if } x > x_2. \end{cases}$$

With this definition, α_2 is a regular function. The variables are set to

$$\begin{aligned} &\alpha_2^{(L)} = 0.4 \quad \rho_2^{(L)} = 1 \\ &\alpha_2^{(R)} = 0.6 \quad P_1^{(L)} = 10 \quad u_1^{(L)} = 1.0 \\ &\rho_1^{(L)} = 0.1 \quad P_2^{(L)} = 2 \quad u_2^{(L)} = 1.2 \end{aligned}$$

with $x_1 = 0.4$ and $x_2 = 0.6$. Both of the fluids are governed by the perfect gas equation of state with $\gamma_1 = 1.2$ and $\gamma_2 = 1.9$. For keeping a regular wave, we must ensure that the characteristics are not crossing. For checking this, $\mathbf{u}_I$ was drawn on Fig. 7. This proves that $\mathbf{u}_I$ increases through the wave, which means that the characteristics associated to $\mathbf{u}_I$ will never cross. The computation is led until time 0.1 on a [0,1] domain. The interfacial velocity is approximatively equal to 3, so that the non constant part of the initial condition has been transported of approximatively 0.3. The results obtained for a number of cells equal to 100, 200, 400 and 800 cells are shown on Fig. 8, using a magnified view between 0.6 and 1. The exact solution is computed by the method of characteristics, which then allows to compute the L^2 error to check the convergence order. Results are shown in Fig. 9. Both of these figures make evidence that the scheme developed is consistent with the model (1) with the closure explained in Section 3.4.3.

4.3. One dimensional two-phase entropic wave

The aim of this test is to prove the high order accuracy on a regular one dimensional entropic wave. Following [28], the entropic waves of (1) are characterized by an uniform velocity and pressure. Therefore we take a computational domain of [0; 1], where the fluids have the same uniform velocity of 10 m s^{-1} and a pressure of 1 Pa. Associated boundary conditions are periodic. This small value for the pressure is taken so as to reduce the associated sound velocity, which allows to use a larger time step.

The volume fractions are given by:

$$\alpha_1 = \alpha_1^\infty + \begin{cases} 3\exp\left(\frac{1}{10(x-0.3)(x-0.7)}\right) & \text{if } 0.3 < x < 0.7 \\ 0 & \text{else} \end{cases}$$

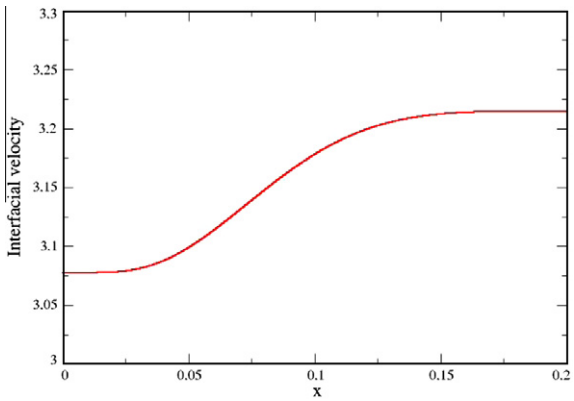

Fig. 7. Interfacial velocity across the self similar associated to the field $\mathbf{u}_I$. The interfacial velocity increases across the wave, so that the characteristics associated to the field $\mathbf{u}_I$ never cross.

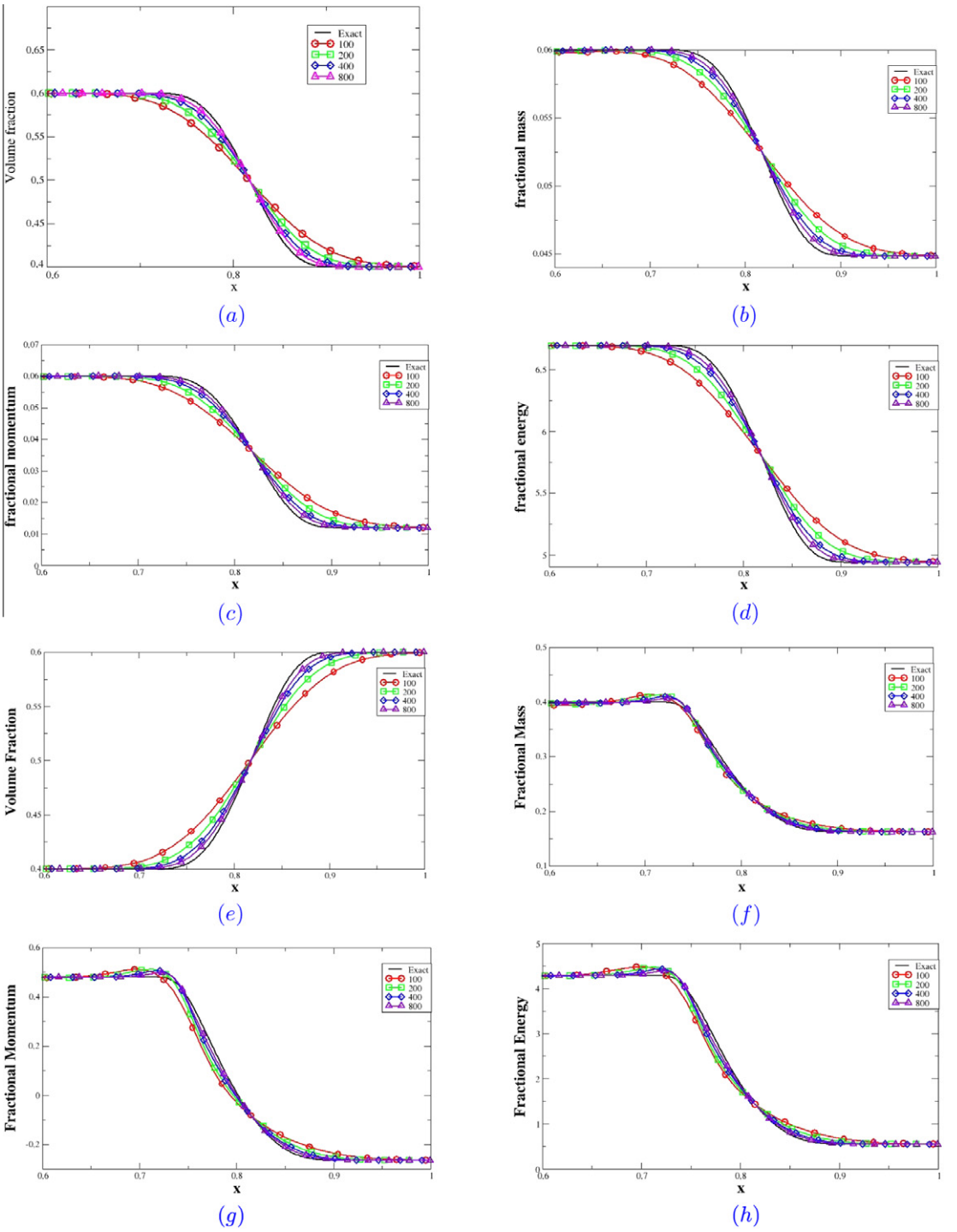

Fig. 8. Results for the consistency test for all the variables. Exact solutions are compared with the solutions computed with 100, 200, 400 800 cells. Convergence to the exact solution is observed for all the variables of fluid 1 ((a), (b), (c), (d)), and of fluid 2 ((e), (f), (g), (h)).

$$\alpha_2 = \alpha_2^\infty - \begin{cases} 3\exp\left(\frac{1}{10(x-0.3)(x-0.7)}\right) & \text{if } 0.3 < x < 0.7 \\ 0 & \text{else} \end{cases}$$

with $\alpha_1^\infty = 0.6$ and $\alpha_2^\infty = 0.4$.

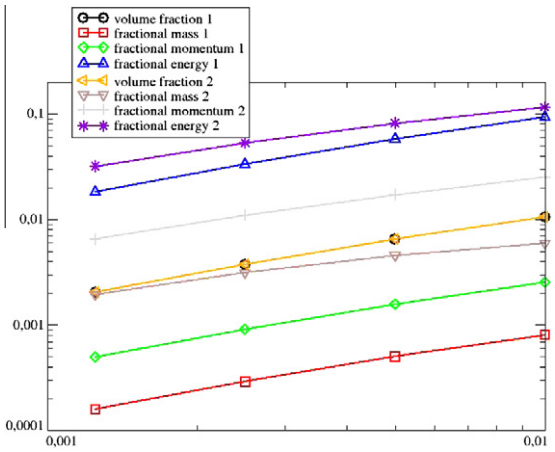

Fig. 9. The convergence order of the consistency test is drawn for all the conservative variables computed: the L^2 error is computed for the mesh with 100, 200, 400 and 800 cells. For all the variables, the convergence is proved to be close to 1.

The densities are defined by:

$$\rho_1 = \rho_1^{\infty} + \rho_1^{\text{amp}} \begin{cases} 10^8 (x-0.3)^4 (x-0.5)^4 & \text{if } 0.3 < x < 0.5 \\ 0 & \text{else} \end{cases}$$

$$\rho_2 = \rho_2^{\infty} + \rho_2^{\text{amp}} \begin{cases} 10^8 (x-0.7)^4 (x-0.5)^4 & \text{if } 0.5 < x < 0.7 \\ 0 & \text{else} \end{cases}$$

with $\rho_1^{\infty} = 1$ kg m^{-3}, $\rho_1^{\text{amp}} = 5$ kg m^{-3}, $\rho_2^{\text{amp}} = 0.003$ kg m^{-3} and $\rho_2^{\infty} = 0.001$ kg m^{-3}. Both fluids follow a perfect gas equation of state, with a polytropic coefficient of 1.4 and 1.648. The functions ρ_1 and ρ_2 are $\mathcal{C}^4$ and α_1 and α_2 are $\mathcal{C}^{\infty}$ functions of x.

The computation is led until $t = 0.15$ s, for finite element discretizations of order 0, 1 and 2. In order to fully see the benefits of high order these tests are done with exactly the same degrees of freedom for each test. Thus, we use a 120 cells mesh in the DG^0 case, a 60 cells mesh in the DG^1 case and a 40 cells mesh in the DG^2 case.

Results are shown in Fig. 10, in comparison with the exact solution. Benefits of high order discretization is clearly visible. The smearing of all variables in the DG^0 case disappears when order increases. We may also see that fluid densities are better described with the DG^2 solutions than with the two others. Finally, we conclude this test by a study of the convergence order, in Fig. 11. For a kth degree of approximation, an order accuracy of $k+1$ is found.

Eventually, we also propose to use this test so as to give a numerical evidence of the Abgrall criterion, theoretically proved in Section 3.5. Indeed, in this test, the pressures and velocities of each phase are uniform in the whole domain and are therefore expected to remain uniform during the computation.

Corresponding results are depicted in Fig. 12, for the DG^0, DG^1 and DG^2 solutions.

4.4. Helium–air shock tube

This test is based on the classical Sod shock tube [44], except that the left side is filled with helium instead of air. The shock tube is 1 m long and the initial discontinuity is located at 0.5 m. Each fluid is described by a perfect gas equation of state (17) $\gamma = 1.648$ for helium and $\gamma = 1.4$ for air.

The mesh used contains 200 nodes and 100 nodes in the DG^0 and DG^1 cases, and the CFL number is set at 0.5 for the DG^0 scheme and at 0.3 for the DG^1 scheme.

Results are shown in Fig. 13, at time $t = 0.2$ s. In Fig. 13(a)–(c) we compare the numerical solutions obtained with the DG^0 scheme (circle) and the DG^1 scheme (square) for the total density, the velocity and the pressure. We also show on these figures the analytical solution (line) so as to compare the benefits of using high order scheme. Thus, we may clearly see that there is a good agreement between the DG^1 solution and the exact one, contrary to the DG^0 case. As an example, let us see the total density profiles. The post-shocked state cannot be distinguished from the state behind the contact discontinuity with the DG^0 solutions. In consequence, the shock wave and the contact discontinuity cannot be discriminated. In the same way, we may note that the isentropic wave is very smeared. On the contrary, the DG^1 solution gives a better description of the flow. The different waves (shock, contact discontinuity and isentropic) are sharper and each constant state is well described.

Finally, in Fig. 14, we compare the convergence order of the numerical scheme for the DG^0 and DG^1 approaches. The solution being not regular, we obviously do not recover the convergence order of 1 and 2. Nevertheless, we may clearly see an improvement of the order of the scheme.

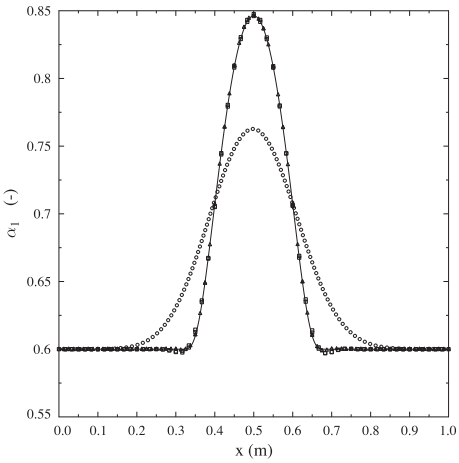

(a) Volume fraction profiles.

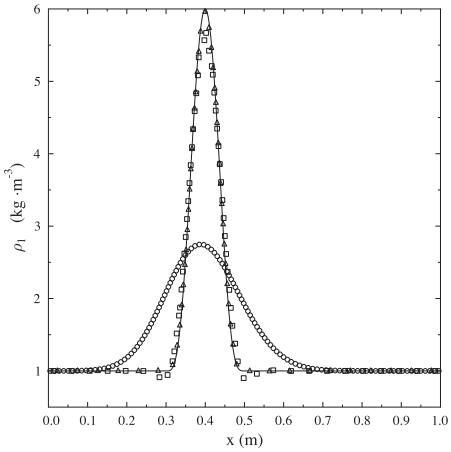

(b) Density of fluid 1 profiles.

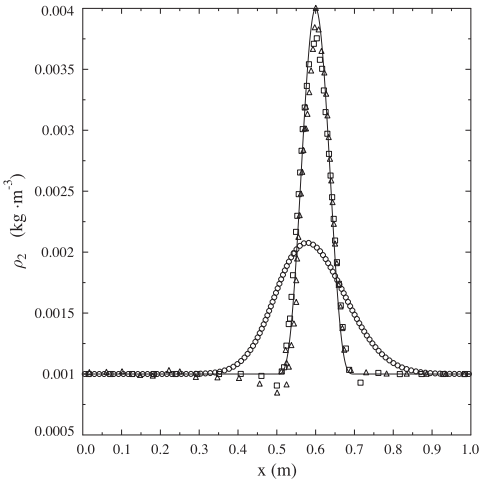

(c) Density of fluid 2 profiles.

Fig. 10. One dimensional two-phase entropic wave. Comparison of the DG^0 (circle) and DG^1 (square) and DG^2 (triangle) solutions with the exact solution (line). The comparisons are made with a constant number of degrees of freedom.

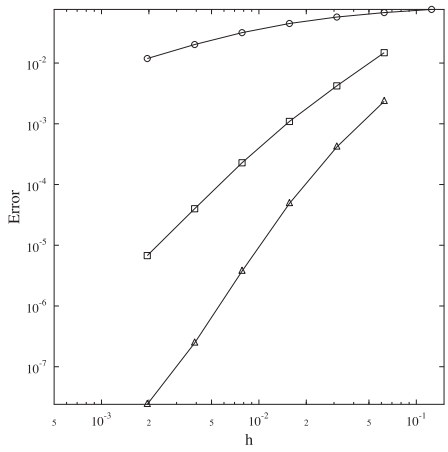

Fig. 11. One dimensional two-phase entropic wave. Convergence order of the DG^0 (circle) and the DG^1 (square) and the DG^2 schemes (triangle). Usual orders of 1, 2 and 3 are found.

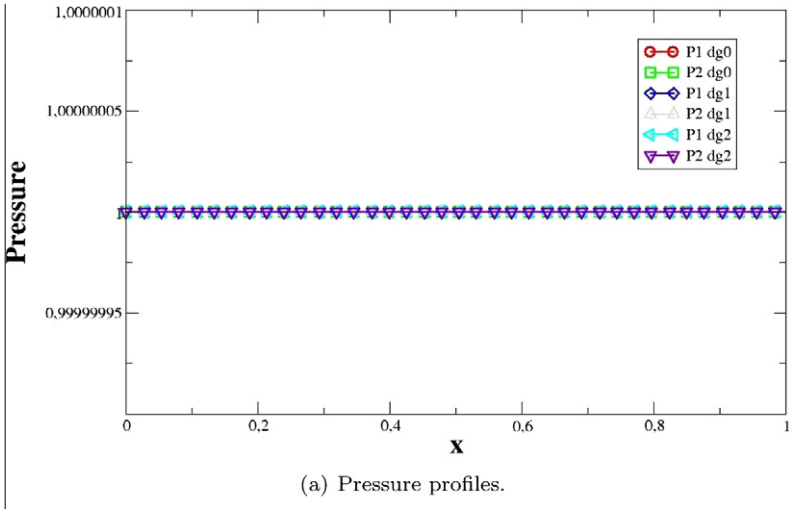

(a) Pressure profiles.

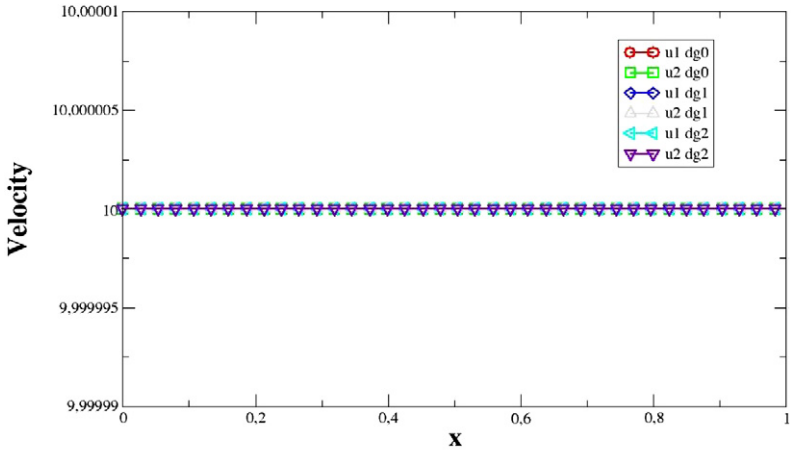

(b) Velocity profiles.

Fig. 12. Numerical evidence of the Abgrall criterion. Comparison of the pressures Fig. 12(a) and velocities Fig. 12(b) of each phase for the DG^0 and DG^1 and DG^2 solutions.

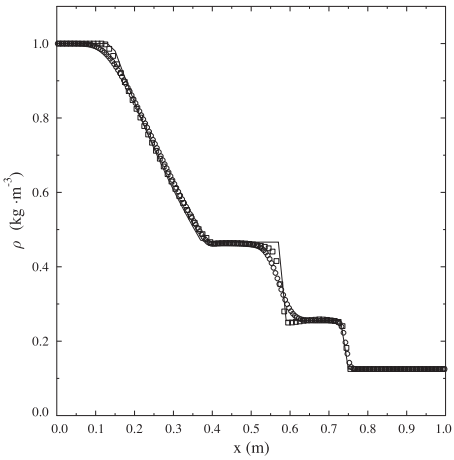

(a) Total density profiles.

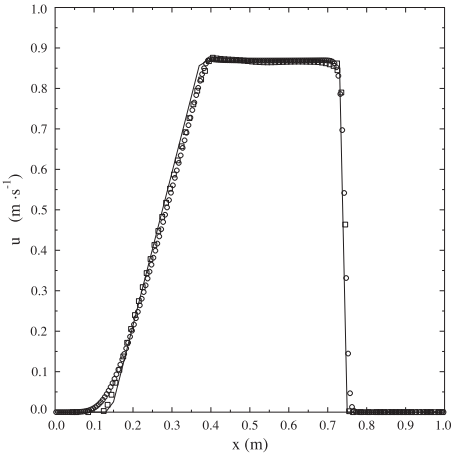

(b) Velocity profiles.

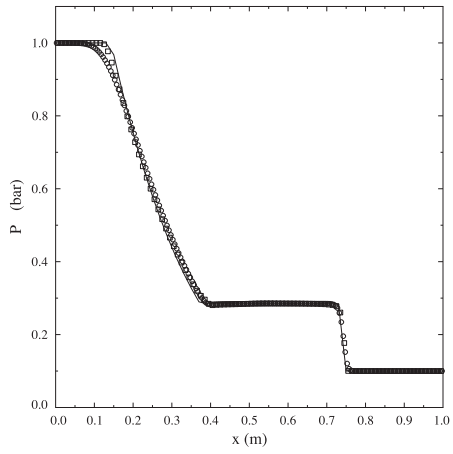

(c) Pressure profiles.

Fig. 13. Multiphase Sod shock tube. Comparison of the DG^0 (circle) and DG^1 (square) solutions with the exact solution (line).

4.5. Water–air shock tube

We now consider a shock tube filled with water under high pressure at the left and with air at low pressure at the right. The shock tube is still 1 m long but the initial discontinuity is now set at 0.7 m. The initial data are: $P_L = 10^9$ Pa,

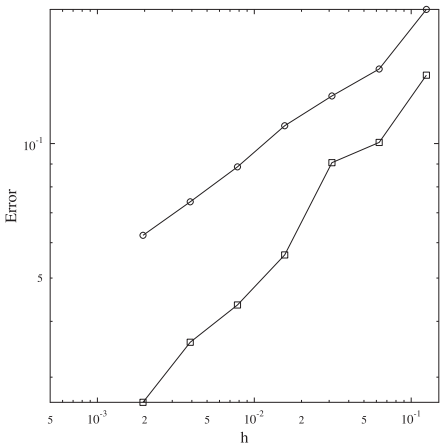

Fig. 14. Multiphase Sod shock tube. Convergence order of the DG^0 (circle) and the DG^1 schemes (square). Since the solution involves discontinuities, the convergence order of 1 and 2 are not recovered. Nevertheless, we may observe a better convergence order with the DG^1 scheme.

$\rho_L = 1000$ kg m^{-3}, $u_L = 0$ m s^{-1} and $P_R = 10^5$ Pa, $\rho_R = 50$ kg m^{-3}, $u_R = 0$ m s^{-1}. Water is governed by the stiffened gas equation of state (18), with $\gamma = 4.4$ and $P_\infty = 6 \cdot 10^8$ Pa, whereas air obeys the perfect gas equation of state, with $\gamma = 1.4$. This test is known to be a particularly tricky one [26,1,43,21,38,2]. Indeed, it involves two pure materials with different equations of state and the interface problem that has to be solved induces an interfacial mixture-due to the smearing of the interface-where the sound velocity is not easily computed. It is then common for many schemes to fail to perform such a test, see [38] for more details.

Here, we use in the present simulation a mesh composed of 60 nodes. The CFL number is still set at 0.5 in the DG^0 case and at 0.3 in the DG^1 case.

Results are shown in Fig. 15, at time $t = 229$ μs. Since each part of the domain is filled with a pure fluid, we may compute an exact solution for this test. Therefore, we compare this analytical solution with the numerical ones, obtained with a DG^0 and DG^1 scheme, in Fig. 15. First of all, we note that the method is still able to perform this test. Then, we may see that the DG^1 scheme improves the quality of the solution: diffusion is drastically reduced and physical variables are better described. For example, the velocity, which is slightly over-estimated with the DG^0 solution, is now well computed.

4.6. Multiphase shock tubes

Eventually, we will deal with some multiphase shock tube problems, where we have mixtures on both chambers, proposed by [3,15]. Let us first recall here that these references deal with the Baer and Nunziato model, that is to say the closure (2) is considered for the model (1). For this reason, and as stated in Section 4.2, our present model has a different mathematical structure and waves' pattern. Therefore, we will not use the exact solutions developed in the references therein.

We first consider the test 1 of [15]. It consists in a 1 m long shock tube with initial discontinuity placed at 0.5 m. For each chamber, we have the following initial data: for the left chamber $P_{L,1} = 1$ Pa and $P_{L,2} = 1$ Pa, $\rho_{L,1} = 1$ kg m^{-3} and $\rho_{L,2} = 0.5$ kg m^{-3}, $u_{L,1} = 0$ m s^{-1} and $u_{L,2} = 0$ m s^{-1}, and finally $\alpha_{L,1} = 0.4$ whereas for the right chamber $P_{R,1} = 2$ Pa and $P_{R,2} = 2$ Pa, $\rho_{R,1} = 2$ kg m^{-3} and $\rho_{R,2} = 1.5$ kg m^{-3}, $u_{R,1} = 0$ m s^{-1} and $u_{R,2} = 0$ m s^{-1}, $\alpha_{R,1} = 0.8$. Each fluid is governed by the perfect gas equation of state with parameter $\gamma_1 = \gamma_2 = 1.4$. In Fig. 16, the solution is presented at time $t = 0.1$ s for a DG^1 solution computed on a 5000 cells mesh. We also show on the same figure the converged solution obtained with the DG^0 solution on a 10,000 cells mesh. We have a good agreement between each solution.

Our second example is the test 3 proposed by [3]. Initially, we thus impose the following conditions: at the left chamber, we have $P_{L,1} = 1.5666$ Pa and $P_{L,2} = 1.5$ Pa, $\rho_{L,1} = 0.9123$ kg m^{-3} and $\rho_{L,2} = 2.6718$ kg m^{-3}, $u_{L,1} = 1.6305$ m s^{-1} and $u_{L,2} = -0.05$ m s^{-1}, $\alpha_{L,1} = 0.1$, in the right chamber we set $P_{R,1} = 1.1675$ Pa and $P_{R,2} = 1.5$ Pa, $\rho_{R,1} = 0.8592$ kg m^{-3} and $\rho_{R,2} = 1.3359$ kg m^{-3}, $u_{R,1} = -0.0129$ m s^{-1} and $u_{R,2} = 0.5438$ m s^{-1}, $\alpha_{R,1} = 0.9$. The perfect gas equation of state is considered for each fluid, with the same parameter $\gamma = 1.4$. The results are presented in Fig. 18, at time $t = 0.1$s, for a 5000 cells mesh in the DG^1 case, which is compared to a converged solution obtained on a 10,000 cells mesh in the DG^0 case. In some part of the domain, we still have a fair matching between each solution. Yet, the computed solution with DG^1 scheme diverges from the attended solution, especially the volume fraction of phase 1 which tends to 1 between $x = 0.5$ and 0.55. Consequently, the other variables could not be well computed anymore in this part of the domain. Moreover, this new wrong state induces new waves that modify the behavior of the solution. To our opinion, there could be at least two explanations for this behavior.

1. First, the system we deal with is non conservative. In the case of a conservative system, it is known that a conservative scheme must be used otherwise the scheme converges to a wrong solution. This means that when dealing with the discontinuous Galerkin method with a conservative system, it is necessary to conserve the average of each conserved

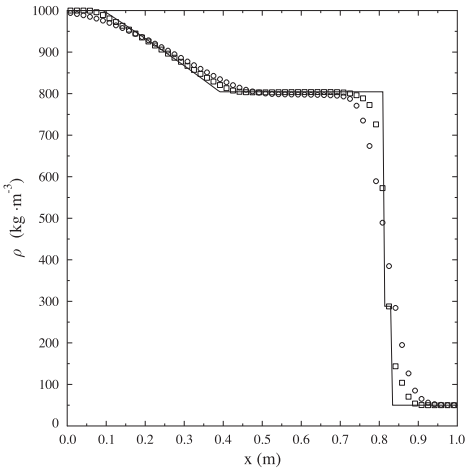

(a) Total density profiles.

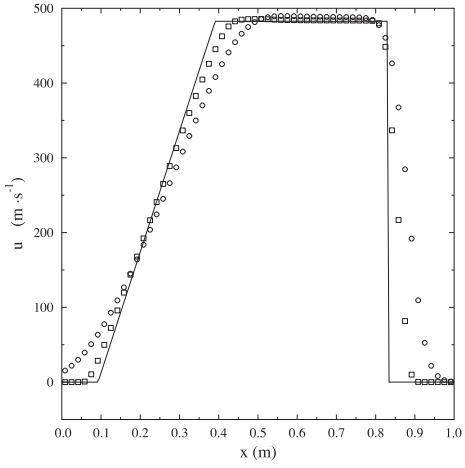

(b) Velocity profiles.

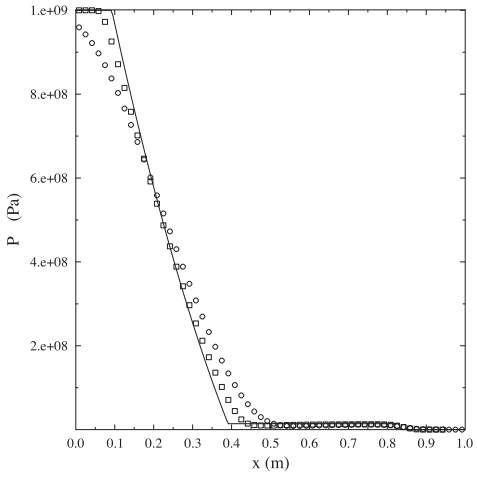

(c) Pressure profiles.

Fig. 15. Liquid–gas shock tube. Comparison of the DG^0 (circle) and DG^1 (square) solutions with the exact solution (line).

variables inside each cell. In the case of a non conservative system, a similar constraint should exist yet the variables in each cell are governed by non conservative equations and it is thus not easy to find which variables should be averagely conserved.

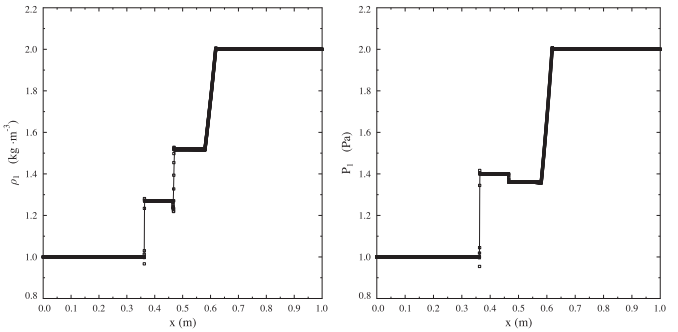

(a) Density profiles of phase 1.

(b) Pressure profiles of phase 1.

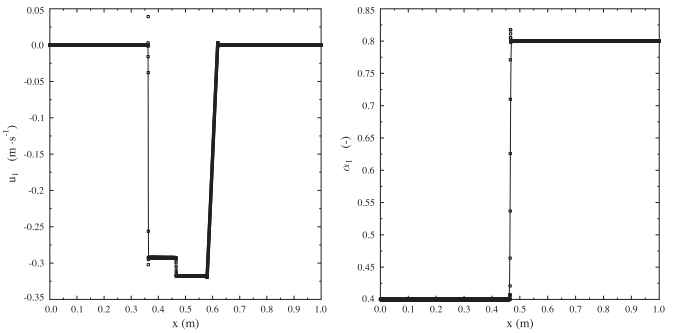

(c) Velocity profiles of phase 1.

(d) Volume fraction profiles of phase 1.

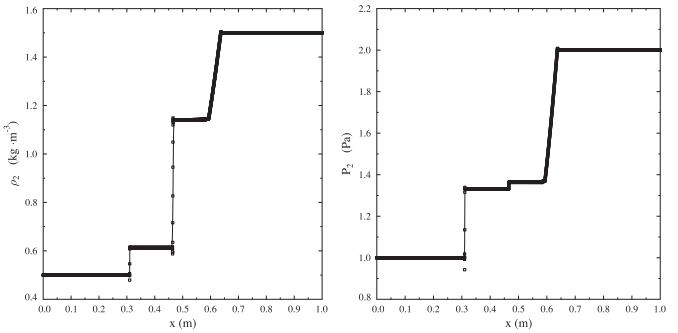

(e) Density profiles of phase 2.

(f) Pressure profiles of phase 2.

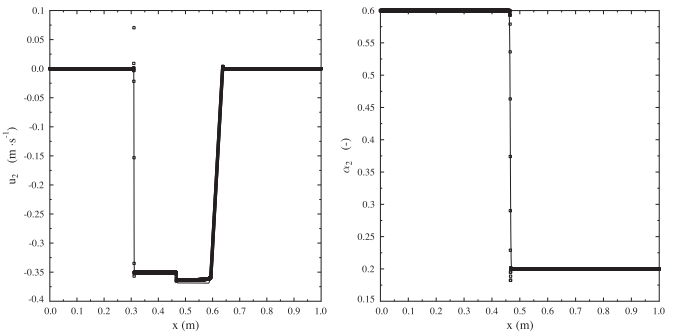

(g) Velocity profiles of phase 2.

(h) Volume fraction profiles of phase 2.

Fig. 16. Multiphase shock tube: Test 1 of [15]. Comparison of the DG^1 (square) solution with the converged DG^0 (line) solution.

2. Secondly, the system may undergo a resonance phenomenon, because the eigenvalues of the system $[u_I, u_1, u_2, u_1 - c_1, u_1 + c_1, u_2 - c_2, u_2 + c_2]$ do not have the same order and may intersect within a wave. In the present test case, we show in Fig. 19 the behavior of some eigenvalues. Contrary to the previous test case, whose eigenvalues are presented in Fig. 17, we may see here that several eigenvalues are intersecting.

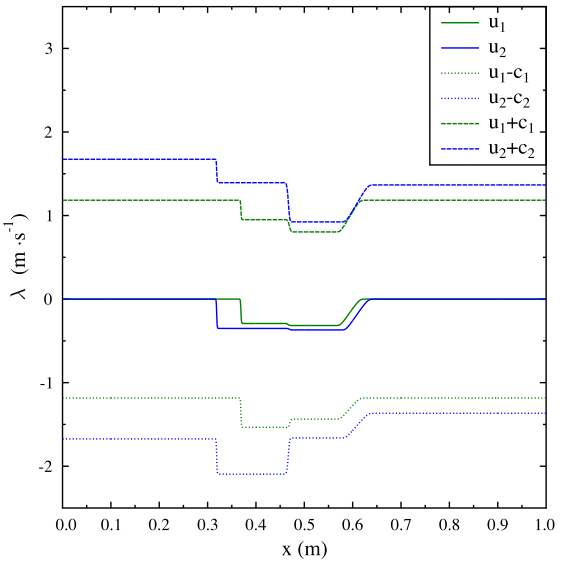

Fig. 17. Multiphase shock tube: Test 1 of [15]. Behavior of some eigenvalues.

So, excepting the part where α_2 vanishes, the results keep acceptable.

Our last example is the test 2 of [15]. The initial data are now: $P_{L,1} = 500$ Pa and $P_{L,2} = 2$ Pa, $\rho_{L,1} = 800$ kg m^{-3} and $\rho_{L,2} = 1.5$ kg m^{-3}, $u_{L,1} = 0$ m s^{-1} and $u_{L,2} = 0$ m s^{-1}, and $\alpha_{L,1} = 0.4$, $P_{R,1} = 600$ Pa and $P_{R,2} = 1$ Pa, $\rho_{R,1} = 1000$ kg m^{-3} and $\rho_{R,2} = 1$ kg m^{-3}, $u_{R,1} = 0$ m s^{-1} and $u_{R,2} = 0$ m s^{-1}, $\alpha_{R,1} = 0.3$. The first fluid now obeys the stiffened gas equation of state with $\gamma_1 = 3.0$ and $P_\infty = 100$ Pa, the other one is not modified. The solution is still presented at time $t = 0.1$ s in Fig. 20 for a 5000 cells mesh in the DG^1 case, with comparison with a converged solution with a 10,000 cells in the DG^0 case. Here again, we note the same behavior as in the previous test case: some area has appeared in the DG^1 case in which the volume fraction of phase 2 vanishes. Once more, we may see in Fig. 21 that we have an intersection of some eigenvalues.

4.7. Two dimensional two-phase entropic wave

In this Section, we test the order of the scheme on a regular two dimensional entropic wave. This test is an adaptation of the test of Section 4.3.

The computational domain is a periodic $[0;1] \times [0;1]$ square. The fluids have the same uniform velocity of $\mathbf{u} = (10,10)$, and a pressure of 1 Pa. For a given point $(x,y) \in [0;1] \times [0;1]$, we define

$$r_\alpha = \sqrt{(x-0.5)^2 + (y-0.5)^2}$$
$$r_{\rho_1} = \sqrt{(x-0.4)^2 + (y-0.5)^2}$$
$$r_{\rho_2} = \sqrt{(x-0.6)^2 + (y-0.5)^2}$$

The volume fractions are given by:

$$\alpha_1 = \alpha_1^\infty + \begin{cases} 3\exp\left(\frac{1}{10(r_\alpha-0.2)(r_\alpha+0.2)}\right) & \text{if } r_\alpha < 0.2 \\ 0 & \text{else} \end{cases}$$

$$\alpha_2 = \alpha_2^\infty - \begin{cases} 3\exp\left(\frac{1}{10(r_\alpha-0.2)(r_\alpha+0.2)}\right) & \text{if } r_\alpha < 0.2 \\ 0 & \text{else} \end{cases}$$

with $\alpha_1^\infty = 0.6$ and $\alpha_2^\infty = 0.4$.

The densities are defined by:

$$\rho_1 = \rho_1^\infty + \rho_1^{\text{amp}} \begin{cases} 10^8 (r_{\rho_1} - 0.1)^4 (r_{\rho_1} + 0.1)^4 & \text{if } r_{\rho_1} < 0.1 \\ 0 & \text{else} \end{cases}$$

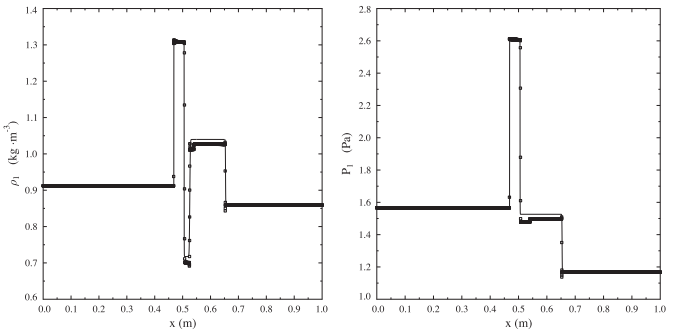

(a) Density profiles of phase 1.

(b) Pressure profiles of phase 1.

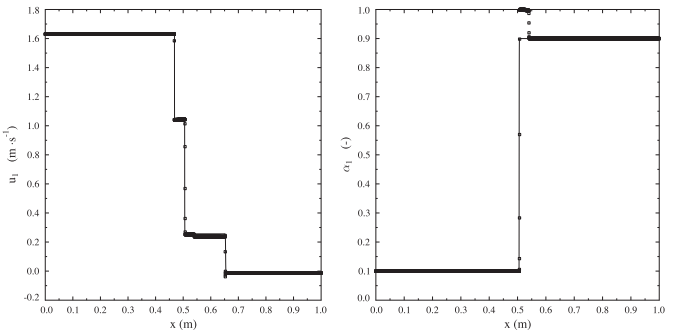

(c) Velocity profiles of phase 1.

(d) Volume fraction profiles of phase 1.

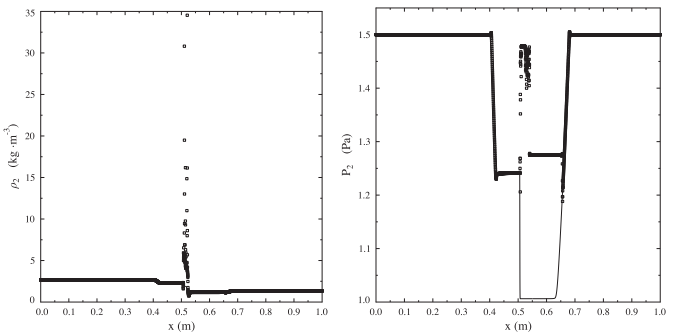

(e) Density profiles of phase 2.

(f) Pressure profiles of phase 2.

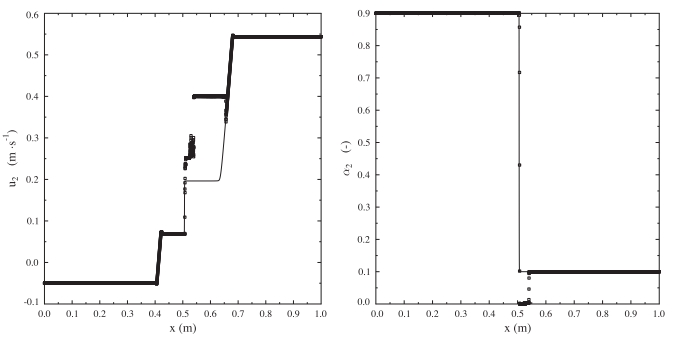

(g) Velocity profiles of phase 2.

(h) Volume fraction profiles of phase 2.

Fig. 18. Multiphase shock tube: Test 3 of [3]. Comparison of the DG^1 (square) solution with the converged DG^0 (line) solution.

$$\rho_2 = \rho_2^{\infty} + \rho_2^{\text{amp}} \begin{cases} 10^8 (r_{\rho_2} - 0.1)^4 (r_{\rho_2} + 0.1)^4 & \text{if } r_{\rho_2} < 0.1 \\ 0 & \text{else} \end{cases}$$

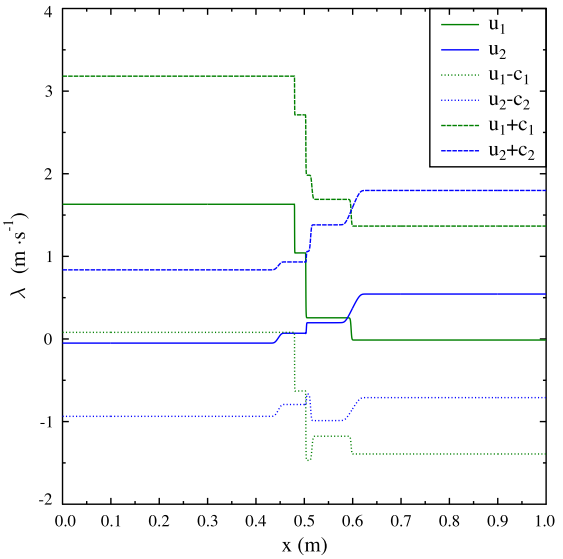

Fig. 19. Multiphase shock tube: Test 3 of [3]. Behavior of some eigenvalues.

with $\rho_1^\infty = 1\text{kg}\cdot\text{m}^{-3}$, $\rho_1^{\text{amp}} = 5\ \text{kg m}^{-3}$, $\rho_2^{\text{amp}} = 0.003\ \text{kg m}^{-3}$ and $\rho_2^\infty = 0.001\ \text{kg m}^{-3}$. Both of the fluids follow a perfect gas equation of state, with a polytropic coefficient equal of 1.4 and to 1.648. The functions ρ_1 and ρ_2 are $\mathcal{C}^4$ and α_1 and α_2 are $\mathcal{C}^\infty$ functions of x.

The computation is led until $t = 0.15$ s, for finite element discretizations of order 0, 1 and 2. Results with the different schemes are obtained with a number of degrees of freedom nearly constant, as shown in the Table 1.

In Fig. 22, we show the results for the DG^0 and the DG^1 scheme. It is clear that the flow variables are better described. To have a better idea of this behavior, we present a slice of the different solutions, between $(0,0)$ and $(1,1)$, in Fig. 23. Benefits of the high order are emphasized. As previously, we finally present the order estimations obtained with the various schemes in Fig. 24.

4.8. Multiphase vortex

Our aim in this test is to deal with a regular solution with a non-uniform pressure for the multiphase model (1). In the single phase case, it is possible to test the advection of an isentropic vortex [14,54,53,52]. Here we want to use a similar test in a multiphase context, with the same pressure and velocity for each phase: $P_1 = P_2$ and $u_1 = u_2$. In that case, the model is equivalent to the Baer and Nunziato model, and the corresponding version for the advection of a multiphase vortex is available in [18]. Derivation of such solution is detailed in Appendix B. The expression of the initial condition is:

$$\begin{cases} P = P^\infty \left(1 - \frac{\gamma_1 - 1}{\gamma_1} \frac{\rho_1^\infty}{P^\infty} \frac{\delta^2}{16\pi^2\phi} \mathrm{e}^{2\phi(1-r^2)}\right)^{\frac{\gamma_1}{\gamma_1 - 1}} \\ u_1^\theta = -\frac{r\delta}{2\pi} \mathrm{e}^{\phi(1-r^2)} \\ u_2^\theta = u_1^\theta \sqrt{\frac{\rho_1^\infty}{\rho_2^\infty}} \left(1 - \frac{\gamma_1 - 1}{\gamma_1} \frac{\rho_1^\infty}{P^\infty} \frac{\delta^2}{16\pi^2\phi} \mathrm{e}^{2\phi(1-r^2)}\right)^{\frac{\gamma_2 - \gamma_1}{2\gamma_2(\gamma_1 - 1)}} \\ \rho_k = \rho_k^\infty \left(\frac{P}{P^\infty}\right)^{\frac{1}{\gamma_k}} \\ \rho = \left(\frac{Y_1^\infty}{\rho_1} + \frac{Y_2^\infty}{\rho_2}\right)^{-1} \\ \alpha_k = \frac{\rho Y_k^\infty}{\rho_k} \end{cases}$$

Corresponding values for these parameters are given in Table 2.

A constant velocity along the x axis is also added in the whole domain, equal to 7 m s^{-1}.

The computational domain is a rectangle delimited by $-3.5 \leqslant y \leqslant 3.5$ and $-7 \leqslant x \leqslant 7$. Periodic boundary conditions are imposed at the left and the right sides of the domain, whereas wall conditions are imposed on the top and the bottom. Here again, we test finite element discretizations of order 0, 1 and 2. Results are presented after 1 s. In Fig. 25, we show the vortex velocity for the DG^2 scheme. Here, the mean velocity of the flow has been withdrawn in the final results so as to see only the vortex. Good accuracy is obtained. In order to have a fair comparison between the different accuracies order, we present in

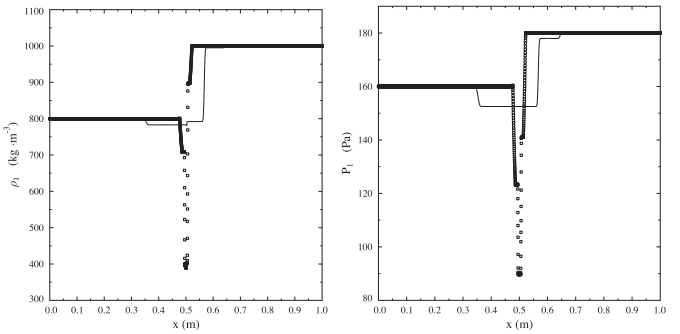

(a) Density profiles of phase 1.

(b) Pressure profiles of phase 1.

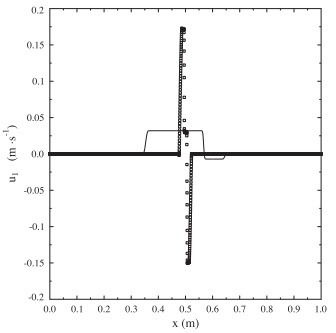

(c) Velocity profiles of phase 1.

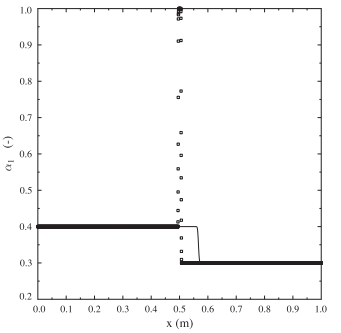

(d) Volume fraction profiles of phase 1.

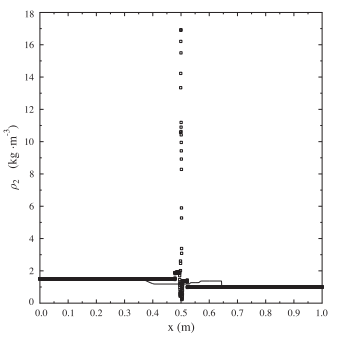

(e) Density profiles of phase 2.

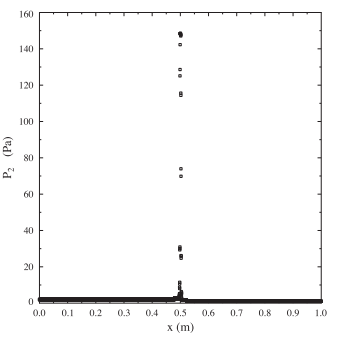

(f) Pressure profiles of phase 2.

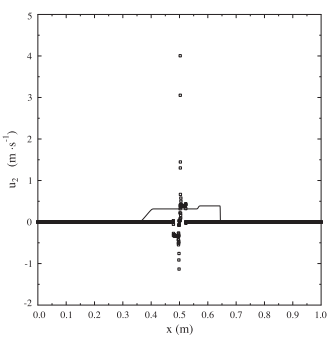

(g) Velocity profiles of phase 2.

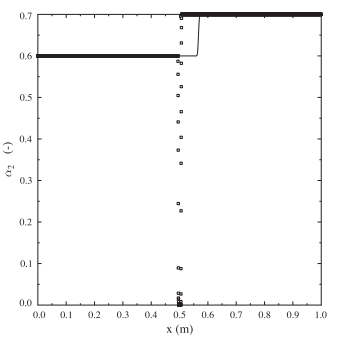

(h) Volume fraction profiles of phase 2.

Fig. 20. Multiphase shock tube: Test 2 of [15]. Comparison of the DG^1 (square) solution with the converged DG^0 (line) solution.

Fig. 26 a slice along $x = 0$. The number of degrees of freedom is still kept nearly constant, as shown in Table 3. We may clearly see the boons of high order.

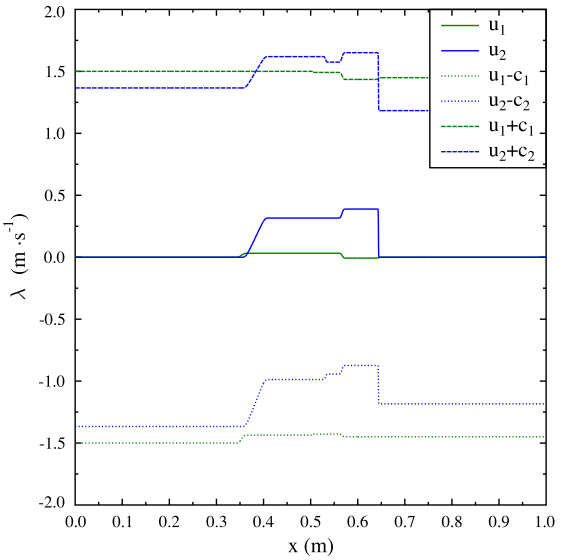

Fig. 21. Multiphase shock tube: Test 2 of [15]. Behavior of some eigenvalues: u_1 and u_2 intersect and also $u_1 + c_1$ and $u_2 + c_2$.

Table 1
Numbers of cells and degrees of freedom for the two dimensional two-phase entropic wave.

Degree	# Cell	# D.o.f.
0	1502	1502
1	506	1518
2	288	1728

4.9. Travelling bubble

For this test and the next one, the domain is a rectangle of 0.325 m long and 0.089 m high. It is filled with air, with a density $\rho = 1.4$ kg m^{-3}, except for a bubble of helium, with a density $\rho = 0.25463$ kg m^{-3}, of 0.05 m of radius. Initially, all the domain is at atmospheric pressure and with an uniform horizontal velocity $u = -100$ m s^{-1}. The two fluids are described by a perfect gas equation of state, as in Section 4.4.

The computational domain is an unstructured triangular conforming mesh, composed of 8932 triangles generated with `emc2`. The CFL number is 0.3.

In Fig. 27, we show the numerical results for the DG^0 and the DG^1 schemes, at time $t = 0.001$ s. In this case, the exact solution is known: the bubble must be translated from -0.1 m. We may observe that the interface is sharper with the second order solution than with the first order one.

4.10. Shock bubble interaction

Our aim here is to compute the test proposed by Quirk and Karni [34], based on the experiments of Haas and Sturtevant [25]. As described in Fig. 28, there is now a shock wave, moving to the left from the right part of the domain, which will interact with the bubble. The Mach number of the shock is 1.22, which implies that behind the shock wave, air has a density of 1.92691 kg m^{-3}, a velocity of -0.33361 m s^{-1}, and a pressure of 1.5698 Pa. The fluids involved are such that the Atwood number is negative, which is referred as the divergent case in the previous publications. It is then known that it will lead to a reversal of the bubble that is penetrated by a jet of surrounding fluid and then gives two vortex downstream of the flow.

In this test, we still use an unstructured triangular conforming mesh, containing 14086 triangles, generated with `Gmsh`.

Numerical results are shown in Fig. 29. Mixture density evolution is shown, with the corresponding isovalues, for the DG^0 and the DG^1 schemes. Here again, this test is well described by both schemes which give qualitatively good results. The reversal of the bubble and the interface is better described with the DG^1 scheme. Finally, we also present isovalues of the volume fraction in Fig. 30 at time $t = 230$ ms. We may clearly see that the interface is more sharpen in the DG^1 case.

4.11. Richtmyer–Meshkov instability

Eventually, we show the capability of the method to compute Richtmyer–Meshkov instability. Therefore, we consider the test proposed by Nourgaliev et al. [29], schematically described in Fig. 31. An interface, separating a light gas (air) from a

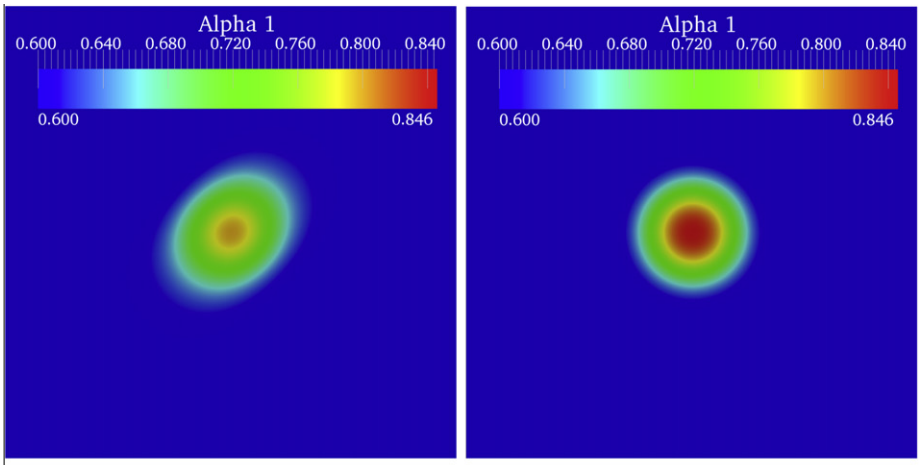

(a) Volume fraction profiles.

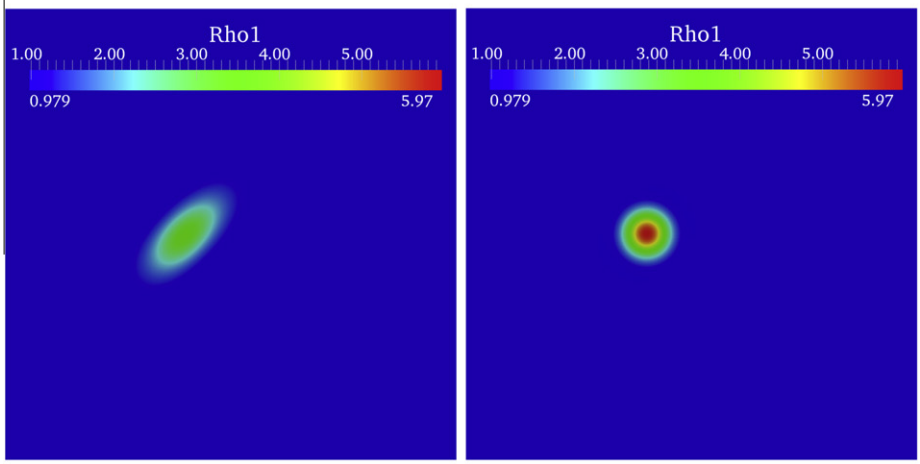

(b) Density of fluid 1 profiles.

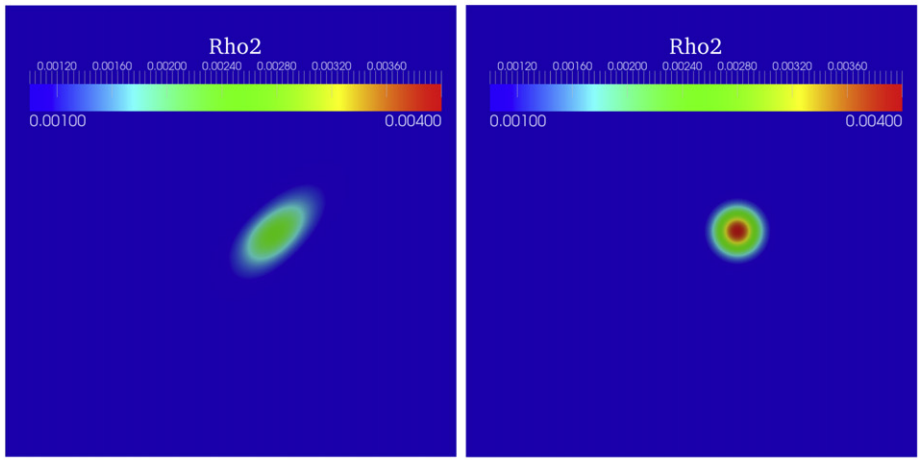

(c) Density of fluid 2 profiles.

Fig. 22. Two dimensional two-phase entropic wave. Comparison of the volume fraction of phase 1 and densities of each phase obtained with a DG^0 scheme (left) and a DG^1 (right) scheme. In this test, the number of degrees of freedom is nearly constant, as detailed in Table 1.

heavy one (SF_6), is attained by a $M = 1.24$ shock wave. Initially, the fluids are at rest and at an uniform pressure of $P = 10^5$ Pa. For the SF_6, we have an initial density of 5.04 kg m^{-3} and a polytropic coefficient $\gamma = 1.093$.

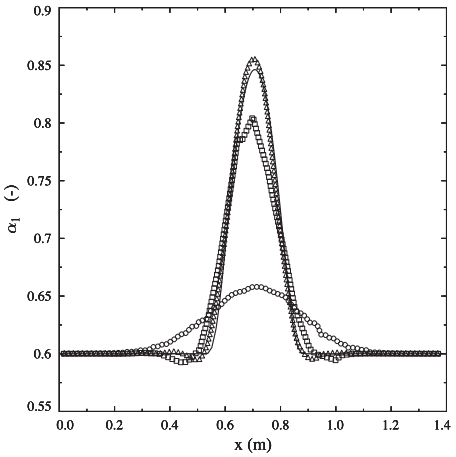

Fig. 23. Slice of the two dimensional two-phase entropic wave along the $y = x$ line. Comparison of the volume fraction for the DG^0 (circle) and DG^1 (square) and DG^2 (triangle) solutions with the exact solution (line). In this test, the number of degrees of freedom is nearly constant, as detailed in Table 1. Note that the DG^2 solution is slightly stronger than the analytical solution, which is unexpected. This is due to the fact that the resolution is very low (about 15 cells in the slice). As a consequence, even if the initial solution is regular, the gradient of the initial solution is strong compared with the resolution, and is therefore seen as a discontinuity, which induces a small oscillation.

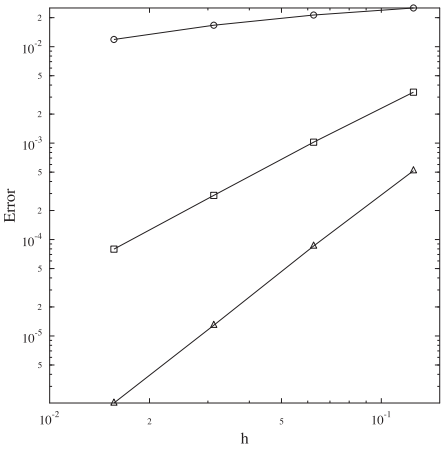

Fig. 24. Convergence order for the two dimensional two-phase entropic wave test. The order accuracy of $k + 1/2$ is found, as usual for the discontinuous Galerkin method.

Table 2
Initial conditions for the multiphase vortex.

P^∞	ρ_1^∞	ρ_2^∞	α_1^∞	α_2^∞	γ_1	γ_2	δ	ϕ
1	1	3	0.4	0.6	1.4	1.8	4	1

The mesh is still unstructured and composed of 11,538 triangles.

In Fig. 32, we show a sequence of the mixture density for the DG^1 solution. The description of the flow is similar to the one obtained by [29]. Finally, in order to prove the relative accuracy of the method, we show a quantitative comparison of the time evolutions of the spike, the edge of the bubble and the thickness of the mixing layer with the corresponding results in [29]. As it may be seen in Fig. 33, the results are relatively good.

5. Conclusion

In this article, we present a Runge–Kutta discontinuous Galerkin method for multiphase compressible flows, involving either interface or mixture problems. The multiphase model is based on a Baer and Nunziato formulation [4], but with a different closure for the interfacial variables. The numerical method is a discontinuous Galerkin method, based on the

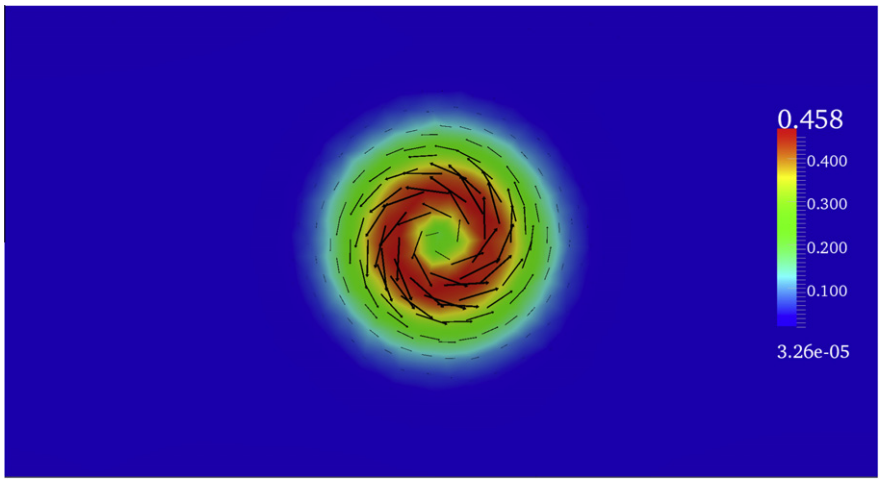

Fig. 25. Multiphase vortex. Vortex velocity minus mean velocity flow contours and vectors obtained with the DG^2 scheme. Meshes are detailed in Table 3.

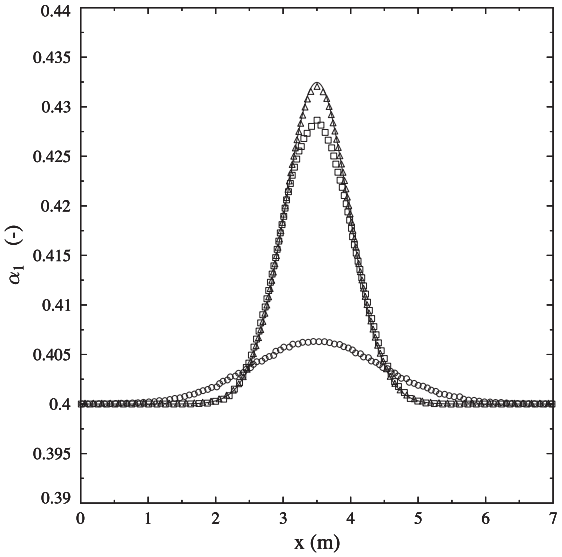

Fig. 26. Slice of the multiphase vortex along the y-axis. Comparison of the volume fraction for the DG^0 (circle) and DG^1 (square) and DG^2 (triangle) solutions with the exact solution (line). In this test, the number of degrees of freedom is nearly constant, as detailed in Table 3.

Table 3
Numbers of cells and degrees of freedom for the multiphase vortex.

Degree	# Cell	# D.o.f.
0	12,314	12,314
1	4092	12,276
2	2112	12,672

formulation of [36] where interior side integrals are determined by revisiting the method proposed by [2] thanks to a stochastic approach. This allows to derive a continuous limit for the numerical scheme developed in [2]. This continuous limit has been validated with a specially dedicated test case. Our discontinuous formulation inherits from the main property of [2], i.e. it is average conservative. Nonconservative products are unambiguously discretized. Analytical solutions for the continuous system are developed, so as to ensure that the scheme is $(k+1)^{\text{th}}$ order in one dimension and $(k+1/2)$th order in two dimensions. Classical shock tubes and interface problems are also tested. A good agreement with the analytical and experimental solutions is observed. These tests also prove the robustness of the method. Three multiphase Riemann problems were also tested. In the first one, a good agreement has been achieved between the DG^0 and DG^1 solution. For the two others,

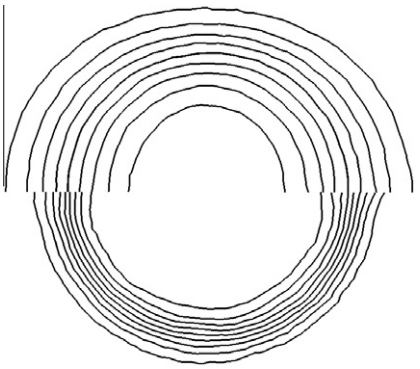

Fig. 27. Travelling bubble. Isolines of the volume fraction ($\alpha = 0.1; 0.2; \ldots; 0.9$) for the DG^0 (top) and the DG^1 (bottom) solutions.

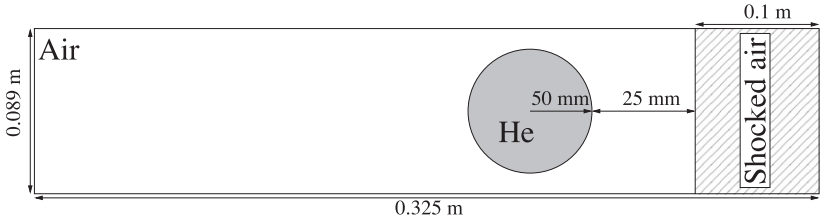

Fig. 28. Computational domain for the shock bubble interaction.

a symptomatic behavior is obtained. In the DG^1 case, the volume fraction of one of the phase vanishes on a part of the domain, leading to wrong computed variables here and to a waves' pattern different from the DG^0 computation. This behavior might be attributed to a resonance phenomenon. Further work on this issue shall be addressed. Current work is devoted to the incorporation of reactive effects, by mean of reactive Riemann solvers.

Appendix A. Proof of Proposition 3

In this appendix, we prove the following proposition.

Proposition 3. *We suppose that R is regular near 0. If α_1 can be derived in a given point* $\mathbf{x}$*, and for a given direction* $\mathbf{n}$*, the behavior of*

$$\frac{\mathbb{E}(\chi_1(\mathbf{x})\chi_1(\mathbf{x}+\tau\mathbf{n})) - \alpha_1(\mathbf{x})}{\tau}$$

when the nonnegative real number τ tends to 0, depends on the behavior of the autocorrelation function R near 0:

- *If $R'(0) \neq 0$ then $\mathbb{E}(\chi_1(\mathbf{x})\chi_1(\mathbf{x}+\tau\mathbf{n})) - \alpha_1(\mathbf{x})$ behaves as $\sqrt{\tau}$, and the ratio has an infinite limit.*
- *If $R'(0) = 0$ and $R''(0) \neq 0$, then the ratio has a limit that depends on $R''(0)$.*
- *If $R'(0) = 0$ and $R''(0) = 0$, then the ratio has a limit which depends only on the derivative of the first moment:*

$$\frac{\mathbb{E}(\chi_1(\mathbf{x})\chi_1(\mathbf{x}+\tau\mathbf{n})) - \alpha_1(\mathbf{x})}{\tau} \to \begin{cases} 0 & \text{if } \nabla\alpha_1(\mathbf{x})\cdot\mathbf{n} > 0 \\ \nabla\alpha_1(\mathbf{x})\cdot\mathbf{n} & \text{if } \nabla\alpha_1(\mathbf{x})\cdot\mathbf{n} < 0 \end{cases}$$

Proof. Using the same computations as for the proof of Proposition 1, what we aim here is to compute the first order development in τ of:

$$\mathbb{E}(\chi_1(\mathbf{x})\chi_1(\mathbf{x}+\tau\mathbf{n})) = \frac{1}{2\pi}\int\int_{D_\tau} \mathrm{e}^{-w_1^2/2}\mathrm{e}^{-w_2^2/2}\,\mathrm{d}w_1\,\mathrm{d}w_2$$

with the domain D_τ defined by:

$$\begin{cases} w_2 \geqslant \sqrt{\frac{1-R(\tau)}{1+R(\tau)}}w_1 - \frac{2}{\sqrt{2(1+R(\tau))}}m(\mathbf{x}) \\ w_2 \geqslant -\sqrt{\frac{1-R(\tau)}{1+R(\tau)}}w_1 - \frac{2}{\sqrt{2(1+R(\tau))}}m(\mathbf{x}+\tau\mathbf{n}) \end{cases}$$

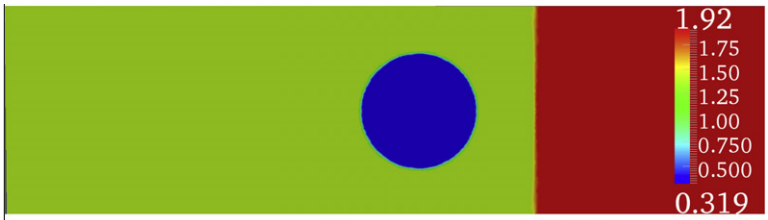

(a) $t = 0\,\text{ms}$.

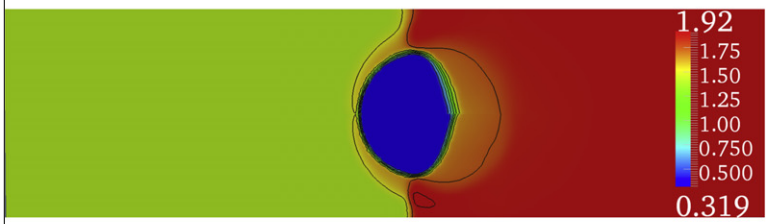

(b) $t = 43.954\,\text{ms}$.

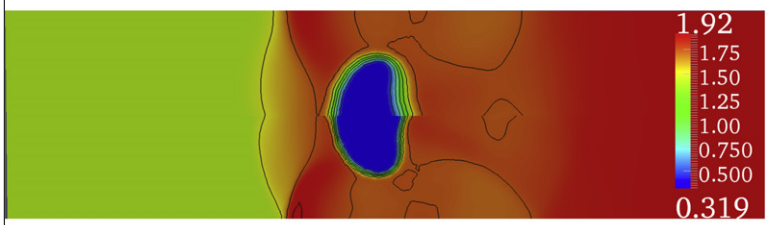

(c) $t = 82.923\,\text{ms}$.

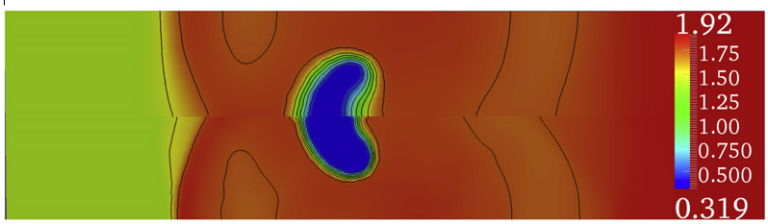

(d) $t = 121.507\,\text{ms}$.

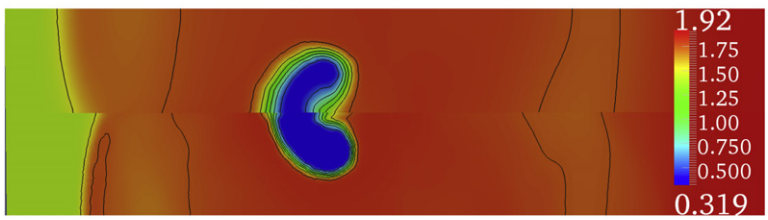

(e) $t = 158.71\,\text{ms}$.

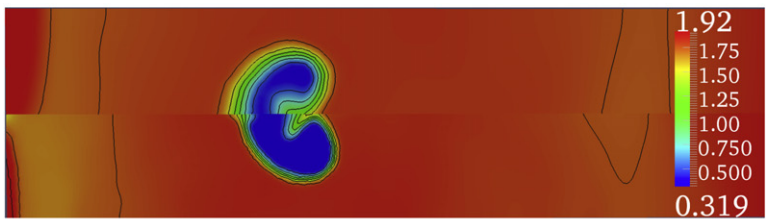

(f) $t = 195.029\,\text{ms}$.

Fig. 29. Interaction of a shock wave with an helium bubble in air. Contours of the mixture density for the DG^0 (top) and the DG^1 (bottom) schemes. Isovalues are also represented in black lines.

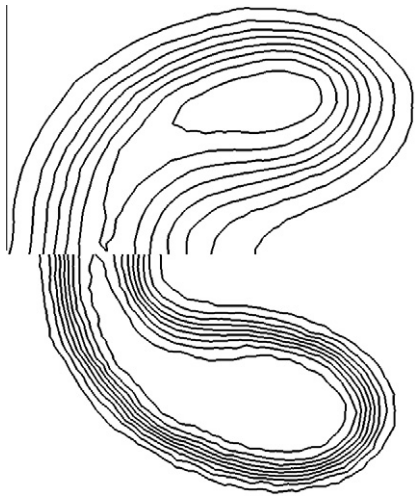

Fig. 30. Interaction of a shock wave with an helium bubble in air. Isovalues of the volume fraction for the DG^0 (top) and the DG^1 (bottom) solutions.

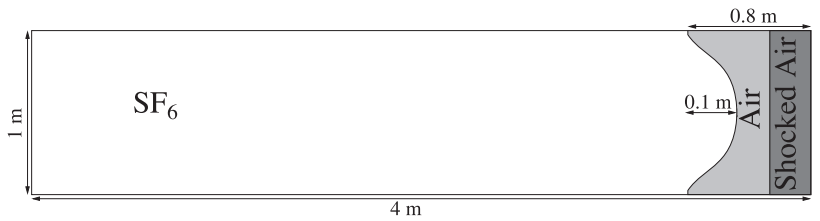

Fig. 31. Computational domain for the Richtmyer–Meshkov instability.

The intersection of the straight lines defining the domain D_τ is such that

$$\begin{cases} w_2^0(\tau) = \sqrt{\frac{1-R(\tau)}{1+R(\tau)}} w_1^0(\tau) - \frac{2}{\sqrt{2(1+R(\tau))}} m(\mathbf{x}) \\ w_2^0(\tau) = -\sqrt{\frac{1-R(\tau)}{1+R(\tau)}} w_1^0(\tau) - \frac{2}{\sqrt{2(1+R(\tau))}} m(\mathbf{x}+\tau\mathbf{n}) \end{cases}$$

for which the solution is:

$$w_1^0(\tau) = \frac{m(\mathbf{x}) - m(\mathbf{x}+\tau\mathbf{n})}{\sqrt{2(1-R(\tau))}}$$

and

$$w_2^0(\tau) = -\frac{m(\mathbf{x}) + m(\mathbf{x}+\tau\mathbf{n})}{\sqrt{2(1+R(\tau))}}$$

We denote by $b^-(\tau)$ and $b^+(\tau)$ the functions:

$$\begin{cases} b^+(w_1,\tau) = \sqrt{\frac{1-R(\tau)}{1+R(\tau)}} w_1 - \frac{2}{\sqrt{2(1+R(\tau))}} m(\mathbf{x}) \\ b^-(w_1,\tau) = -\sqrt{\frac{1-R(\tau)}{1+R(\tau)}} w_1 - \frac{2}{\sqrt{2(1+R(\tau))}} m(\mathbf{x}+\tau\mathbf{n}) \end{cases}$$

The cross correlation $\mathbb{E}(\chi_k(\mathbf{x})\chi_k(\mathbf{x}+\tau\mathbf{n}))$ is equal to the integral above the straight lines defined by b^- and b^+. In this equality, it appears the integral which will be equal to $\alpha_1(\mathbf{x})$ when $\tau \to 0$ (which is the integral above the line $w_2 = -m(\mathbf{x})$) and the integral between this straight line and the straight line $w_2 = w_2^0(\tau)$:

$$\mathbb{E}(\chi_k(\mathbf{x})\chi_k(\mathbf{x}+\tau\mathbf{n})) = \frac{1}{2\pi}\int_{w_2 \geqslant -m(\mathbf{x})}\int_{-\infty}^{\infty} e^{-w_1^2/2} e^{-w_2^2/2}\, dw_1\, dw_2 - \frac{1}{2\pi}\int_{-m(\mathbf{x})}^{w_2^{(0)}(\tau)}\int_{-\infty}^{\infty} e^{-w_1^2/2} e^{-w_2^2/2}\, dw_1\, dw_2 - \frac{1}{2\pi} \times \int_{\tilde{D}_\tau} e^{-w_1^2/2} e^{-w_2^2/2}\, dw_1\, dw_2 \tag{20}$$

(a) $t = 0\,\mathrm{s}$.

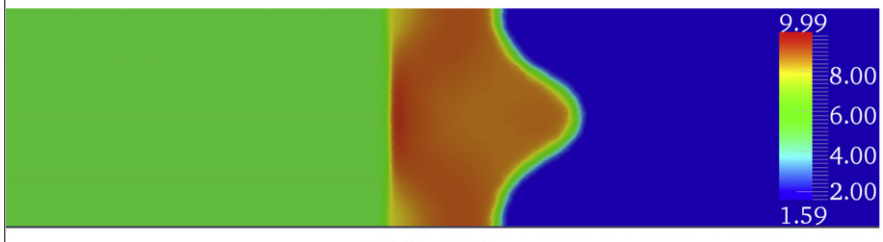

(b) $t = 1.229\,\mathrm{s}$.

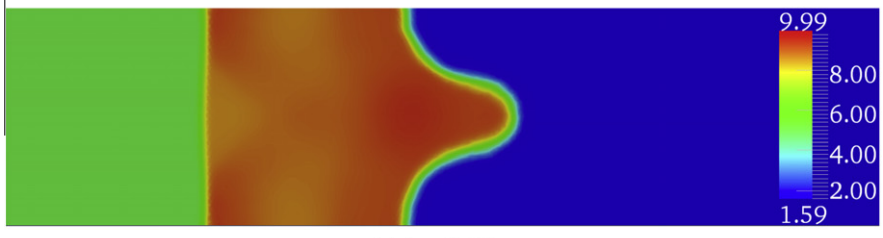

(c) $t = 3.355\,\mathrm{s}$.

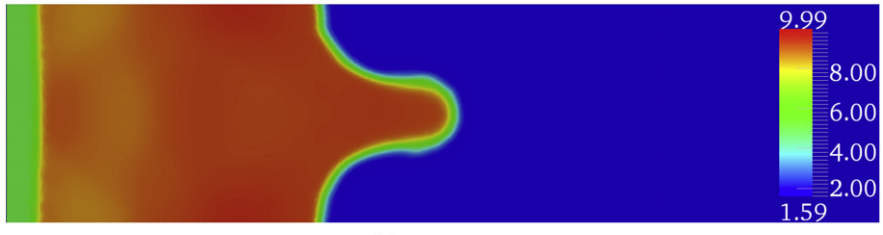

(d) $t = 4.566\,\mathrm{s}$.

(e) $t = 8.277\,\mathrm{s}$.

Fig. 32. Richtmyer–Meshkov instability. Contours of the mixture density obtained with the DG^1 scheme.

where $\widetilde{D}_\tau$ is defined by:

$$\begin{cases} w_2 \leqslant \sqrt{\frac{1-R(\tau)}{1+R(\tau)}} w_1 - \frac{2}{\sqrt{2(1+R(\tau))}} m(\mathbf{x}) \\ w_2 \leqslant -\sqrt{\frac{1-R(\tau)}{1+R(\tau)}} w_1 - \frac{2}{\sqrt{2(1+R(\tau))}} m(\mathbf{x}+\tau\mathbf{n}) \\ w_2 \geqslant w_2^{(0)}(\tau) \end{cases}$$

The first integral of (20) is equal to $\alpha_1(\mathbf{x})$.

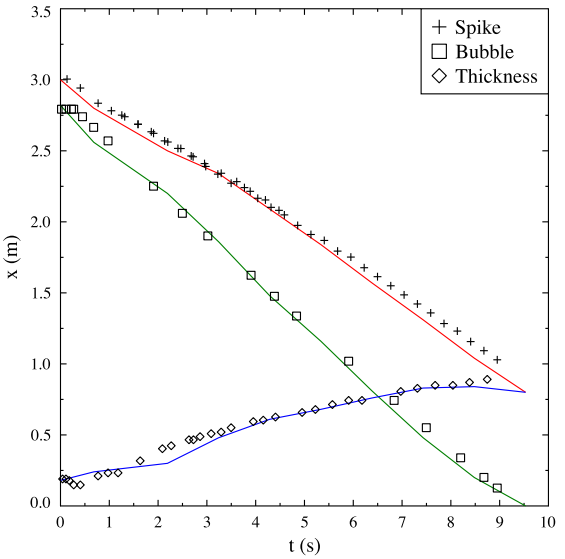

Fig. 33. Richtmyer–Meshkov instability. Comparison of the time evolutions of characteristic positions for the DG^1 scheme (lines) and the results of [29] (symbols).

Second integral of (20). In this paragraph, we want to perform a first order approximation of:

$$I_2 = \frac{1}{2\pi}\int_{-m(\mathbf{x})}^{w_2^{(0)}(\tau)}\int_{-\infty}^{\infty} e^{-w_1^2/2}e^{-w_2^2/2}dw_1dw_2$$

We remark that this integral can be integrated in w_1:

$$I_2 = \frac{1}{\sqrt{2\pi}}\int_{-m(\mathbf{x})}^{w_2^{(0)}(\tau)} e^{-w_2^2/2}dw_2$$

and we thus have:

$$w_2^{(0)}(\tau) = -\frac{m(\mathbf{x})+m(\mathbf{x}+\tau\mathbf{n})}{\sqrt{2(1+R(\tau))}} = -\frac{m(\mathbf{x})+m(\mathbf{x})+\tau\nabla m(\mathbf{x})\cdot\mathbf{n}+o(\tau)}{\sqrt{4+2\tau R'(0)+o(\tau)}} = -\frac{m(\mathbf{x})+m(\mathbf{x})+\tau\nabla m(\mathbf{x})\cdot\mathbf{n}+o(\tau)}{2\sqrt{1+\frac{\tau R'(0)}{2}+o(\tau)}}$$

$$= -\left(m(\mathbf{x})+\frac{\nabla m(\mathbf{x})\cdot\mathbf{n}}{2}\tau+o(\tau)\right)\left(1+\frac{R'(0)}{2}\tau+o(\tau)\right)^{-1/2} = -\left(m(\mathbf{x})+\frac{\nabla m(\mathbf{x})\cdot\mathbf{n}}{2}\tau+o(\tau)\right)\left(1-\frac{R'(0)}{4}\tau+o(\tau)\right)$$

$$w_2^{(0)}(\tau) = -m(\mathbf{x}) - \left(\frac{\nabla m(\mathbf{x})\cdot\mathbf{n}}{2} - \frac{R'(0)m(\mathbf{x})}{4}\right)\tau + o(\tau)$$

which leads to:

$$I_2 = -\frac{1}{\sqrt{2\pi}}\left(\frac{\nabla m(\mathbf{x})\cdot\mathbf{n}}{2} - \frac{R'(0)m(\mathbf{x})}{4}\right)e^{-m^2(\mathbf{x})/2}\tau + o(\tau)$$

By computing the derivative of relation (15), we have:

$$\nabla\alpha_1(\mathbf{x})\cdot\mathbf{n} = \frac{e^{-m^2(\mathbf{x})/2}\nabla m(\mathbf{x})\cdot\mathbf{n}}{\sqrt{2\pi}}$$

so that we can rewrite I_2 as follows:

$$I_2 = \left(-\frac{\nabla\alpha_1(\mathbf{x})\cdot\mathbf{n}}{2} + \frac{R'(0)m(\mathbf{x})e^{-m^2(\mathbf{x})/2}}{4\sqrt{2\pi}}\right)\tau + o(\tau)$$

Third integral of (20). In this paragraph, we are interested in the behavior of the integral:

$$2\pi I_3 = \int_{-\infty}^{w_1^{(0)}(\tau)} \int_{w_2^{(0)}(\tau)}^{b^-(w_1,\tau)} e^{-w_2^2/2} e^{-w_1^2/2} dw_2 dw_1 + \int_{w_1^{(0)}(\tau)}^{\infty} \int_{w_2^{(0)}(\tau)}^{b^+(w_1,\tau)} e^{-w_2^2/2} e^{-w_1^2/2} dw_2 dw_1$$

In the integrals with respect to w_2, we change w_2 to $z_2 + w_2^{(0)}$, to find:

$$2\pi I_3 = \int_{-\infty}^{w_1^{(0)}(\tau)} \int_{0}^{b^-(w_1,\tau)-w_2^{(0)}(\tau)} e^{-(z_2+w_2^{(0)})^2/2} e^{-w_1^2/2} dz_2 dw_1 + \int_{w_1^{(0)}(\tau)}^{\infty} \int_{0}^{b^+(w_1,\tau)-w_2^{(0)}(\tau)} e^{-\left(z_2+w_2^{(0)}\right)^2/2} e^{-w_1^2/2} dz_2 dw_1$$

The behavior of I_3 depends on the behavior of $w_1^{(0)}$ and of $b^-(w_1,\tau) - w_2^{(0)}(\tau)$ and $b^+(w_1,\tau) - w_2^{(0)}(\tau)$:

$$b^-(w_1,\tau) - w_2^{(0)}(\tau) = -\sqrt{\frac{1-R(\tau)}{1+R(\tau)}} w_1 + \frac{m(\mathbf{x}) - m(\mathbf{x}+\tau\mathbf{n})}{\sqrt{1+R(\tau)}}$$

$$b^+(w_1,\tau) - w_2^{(0)}(\tau) = \sqrt{\frac{1-R(\tau)}{1+R(\tau)}} w_1 - \frac{m(\mathbf{x}) - m(\mathbf{x}+\tau\mathbf{n})}{\sqrt{1+R(\tau)}}$$

$$w_1^{(0)}(\tau) = \frac{m(\mathbf{x}) - m(\mathbf{x}+\tau\mathbf{n})}{\sqrt{1-R(\tau)}}$$

If we suppose that R is smooth near 0, then:

$$R(\tau) = 1 + R'(0)\tau + \frac{R''(0)}{2}\tau^2 + o(\tau^2)$$

Case 1: $R'(0) \neq 0$. In this case, we have:

$$b^-(w_1,\tau) - w_2^{(0)}(\tau) = -\sqrt{-\tfrac{R'(0)}{2}}\sqrt{\tau} + o(\sqrt{\tau})$$

$$b^+(w_1,\tau) - w_2^{(0)}(\tau) = \sqrt{-\tfrac{R'(0)}{2}}\sqrt{\tau} + o(\sqrt{\tau})$$

$$w_1^{(0)}(\tau) = o(\sqrt{\tau})$$

Therefore in I_3, in the integral with respect to z_2, we change z_2 to $\tilde{z}_2\sqrt{\tau}$, and we find

$$4\pi I_3 = \int_{-\infty}^{w_1^{(0)}(\tau)} \int_{0}^{\frac{b^-(w_1,\tau)-w_2^{(0)}(\tau)}{\sqrt{\tau}}} e^{-(\tilde{z}_2\sqrt{\tau}+w_2^{(0)})^2/2} e^{-w_1^2/2} \sqrt{\tau}\, d\tilde{z}_2\, dw_1 + \int_{w_1^{(0)}(\tau)}^{\infty} \int_{0}^{\frac{b^+(w_1,\tau)-w_2^{(0)}(\tau)}{\sqrt{\tau}}} e^{-(\tilde{z}_2\sqrt{\tau}+w_2^{(0)})^2/2} e^{-w_1^2/2} \sqrt{\tau}\, d\tilde{z}_2\, dw_1$$

We then can find the limit of $2\pi I_3/\sqrt{\tau}$, which is equal to:

$$\frac{2\pi I_3}{\sqrt{\tau}} = \int_{-\infty}^{0} e^{-w_1^2/2} e^{-m^2(x)} \left(-\sqrt{-\frac{R'(0)}{2}} w_1\right) dw_1 + \int_{0}^{\infty} e^{-w_1^2/2} e^{-m^2(x)} \left(\sqrt{-\frac{R'(0)}{2}} w_1\right) dw_1 + o(1)$$

$$= 2e^{-m^2(x)/2} \sqrt{-\frac{R'(0)}{2}} \int_{0}^{\infty} w_1 e^{-w_1^2/2} + o(1) = 2e^{-m^2(x)/2} \sqrt{-\frac{R'(0)}{2}} + o(1)$$

Thus, in this case, we have:

$$I_3 \sim \frac{e^{-m^2(x)/2}}{\pi} \sqrt{-\frac{R'(0)}{2}}\sqrt{\tau}$$

Case 2: $R'(0) = 0$ and $R''(0) \neq 0$. In this case, we have:

$$b^-(w_1,\tau) - w_2^{(0)}(\tau) = -\left(\sqrt{-\frac{R''(0)}{2}} w_1 + \frac{\nabla m(\mathbf{x})\cdot\mathbf{n}}{2}\right)\tau + o(\tau)$$

$$b^+(w_1,\tau) - w_2^{(0)}(\tau) = \left(\sqrt{-\frac{R''(0)}{2}} w_1 + \frac{\nabla m(\mathbf{x})\cdot\mathbf{n}}{2}\right)\tau + o(\tau)$$

$$w_1^{(0)}(\tau) = \frac{m(\mathbf{x}) - (m(\mathbf{x}) + \tau\nabla m(\mathbf{x})\cdot\mathbf{n} + o(\tau))}{\sqrt{-R''(0)\tau^2}} = -\frac{\nabla m(\mathbf{x})\cdot\mathbf{n}}{\sqrt{-R''(0)}} + o(1)$$

Therefore in the integrals with respect to z_2, we change z_2 to $\tilde{z}_2\tau$, and we find:

$$2\pi I_3 = \int_{-\infty}^{w_1^{(0)}(\tau)} \int_{0}^{\frac{b^-(w_1,\tau)-w_2^{(0)}(\tau)}{\tau}} e^{-(\tilde{z}_2\tau+w_2^{(0)})^2/2} e^{-w_1^2/2} \tau d\tilde{z}_2 dw_1 + \int_{w_1^{(0)}(\tau)}^{\infty} \int_{0}^{\frac{b^+(w_1,\tau)-w_2^{(0)}(\tau)}{\tau}} e^{-(\tilde{z}_2\tau+w_2^{(0)})^2/2} e^{-w_1^2/2} \tau d\tilde{z}_2 dw_1$$

We then can find the limit of $2\pi I_3/\tau$, for which we have:

$$\begin{aligned}\frac{2\pi I_3}{\tau} &= -\int_{-\infty}^{-\frac{\nabla m(\mathbf{x})\cdot\mathbf{n}}{\sqrt{-R''(0)}}} e^{-w_1^2/2} e^{-m^2(\mathbf{x})/2}\left(\sqrt{-\frac{R''(0)}{2}}w_1 + \frac{\nabla m(\mathbf{x})\cdot\mathbf{n}}{2}\right)dw_1 \\ &\quad + \int_{-\frac{\nabla m(\mathbf{x})\cdot\mathbf{n}}{\sqrt{-R''(0)}}}^{\infty} e^{-w_1^2/2} e^{-m^2(\mathbf{x})/2}\left(\sqrt{-\frac{R''(0)}{2}}w_1 + \frac{\nabla m(\mathbf{x})\cdot\mathbf{n}}{2}\right)dw_1 + o(1) \\ &= e^{-m^2(x)/2}\sqrt{-\frac{R''(0)}{2}}\left\{-\int_{-\infty}^{-\frac{\nabla m(\mathbf{x})\cdot\mathbf{n}}{\sqrt{-R''(0)}}} w_1 e^{w_1^2/2}dw_1 + \int_{-\frac{\nabla m(\mathbf{x})\cdot\mathbf{n}}{\sqrt{-R''(0)}}}^{\infty} w_1 e^{w_1^2/2}dw_1\right\} \\ &\quad + \frac{\nabla m(\mathbf{x})\cdot\mathbf{n} e^{-m^2(\mathbf{x})/2}}{2}\left\{-\int_{-\infty}^{-\frac{\nabla m(\mathbf{x})\cdot\mathbf{n}}{\sqrt{-R''(0)}}} e^{w_1^2/2}dw_1 + \int_{-\frac{\nabla m(\mathbf{x})\cdot\mathbf{n}}{\sqrt{-R''(0)}}}^{\infty} e^{w_1^2/2}dw_1\right\}\end{aligned}$$

Finally, we get:

$$\frac{2\pi I_3}{\tau} = 2e^{-m^2(\mathbf{x})/2}\sqrt{-\frac{R''(0)}{2}}\exp\left(\frac{(\nabla m(\mathbf{x})\cdot\mathbf{n})^2}{2R''(0)}\right) - \nabla m(\mathbf{x})\cdot\mathbf{n} e^{-m^2(\mathbf{x})/2}\int_{-\frac{\nabla m(\mathbf{x})\cdot\mathbf{n}}{\sqrt{-R''(0)}}}^{\frac{\nabla m(\mathbf{x})\cdot\mathbf{n}}{\sqrt{-R''(0)}}} e^{w_1^2/2}dw_1$$

Case 3: $R'(0) = R''(0) = 0$. In this case we have:

$$\begin{aligned}b^-(w_1,\tau) - w_2^{(0)}(\tau) &= -\frac{\nabla m(\mathbf{x})\cdot\mathbf{n}}{2}\tau + o(\tau) \\ b^+(w_1,\tau) - w_2^{(0)}(\tau) &= \frac{\nabla m(\mathbf{x})\cdot\mathbf{n}}{2}\tau + o(\tau) \\ w_1^{(0)}(\tau) &= \frac{m(\mathbf{x}) - (m(\mathbf{x}) + \tau\nabla m(\mathbf{x})\cdot\mathbf{n} + o(\tau))}{\sqrt{-\frac{R^{(3)}(0)}{3}\tau^3}} = -\frac{\nabla m(\mathbf{x})\cdot\mathbf{n}}{\sqrt{-\frac{R^{(3)}(0)}{3}}}\frac{1}{\sqrt{\tau}} + o\left(\frac{1}{\sqrt{\tau}}\right)\end{aligned}$$

This means that:

- either $\nabla m(\mathbf{x})\cdot\mathbf{n} > 0$, then $w_1^{(0)}(\tau) \to -\infty$
- or $\nabla m(\mathbf{x})\cdot\mathbf{n} < 0$, then $w_1^{(0)}(\tau) \to \infty$

Doing the same variable change as in the previous case leads to:

$$2\pi I_3 = \int_{-\infty}^{w_1^{(0)}(\tau)}\int_0^{\frac{b^-(w_1,\tau)-w_2^{(0)}(\tau)}{\tau}} e^{-(\tilde{z}_2\tau + w_2^{(0)})^2/2} e^{-w_1^2/2}\tau d\tilde{z}_2 dw_1 + \int_{w_1^{(0)}(\tau)}^{\infty}\int_0^{\frac{b^+(w_1,\tau)-w_2^{(0)}(\tau)}{\tau}} e^{-(\tilde{z}_2\tau + w_2^{(0)})^2/2} e^{-w_1^2/2}\tau d\tilde{z}_2 dw_1$$

We then can find the limit of $2\pi I_3/\tau$, which is equal to

- If $\nabla m(\mathbf{x})\cdot\mathbf{n} > 0$, then

$$\frac{2\pi I_3}{\tau} = \frac{(\nabla m(\mathbf{x})\cdot\mathbf{n})e^{-m^2(x)/2}}{2}\int_{-\infty}^{\infty} e^{-w_1^2/2}dw_1 = \frac{(\nabla m(\mathbf{x})\cdot\mathbf{n})e^{-m^2(x)/2}}{2}\sqrt{2\pi}$$

- If $\nabla m(\mathbf{x})\cdot\mathbf{n} < 0$, then

$$\frac{2\pi I_3}{\tau} = -\frac{(\nabla m(\mathbf{x})\cdot\mathbf{n})e^{-m^2(x)/2}}{2}\int_{-\infty}^{\infty} e^{-w_1^2/2}dw_1 = -\frac{(\nabla m(\mathbf{x})\cdot\mathbf{n})e^{-m^2(x)/2}}{2}\sqrt{2\pi}$$

Consequently, we have:

$$I_3 = \frac{|\nabla\alpha_1(\mathbf{x})\cdot\mathbf{n}|}{2} + o(\tau)$$

Conclusion on the behavior of $\mathbb{E}(\chi_1(\mathbf{x})\chi_1(\mathbf{x}+\tau\mathbf{n}))$. Three cases are obtained:

- If $R'(0) \neq 0$ then I_3 behaves as $\sqrt{\tau}$, and I_2 as τ, so that $\mathbb{E}(\chi_1(\mathbf{x})\chi_1(\mathbf{x}+\tau\mathbf{n})) - \alpha(\mathbf{x})$ behaves as $\sqrt{\tau}$, and the ratio with τ has an infinite limit.
- If $R'(0) = 0$ and $R''(0) \neq 0$, then the ratio has a limit that depends on $R''(0)$.
- If $R'(0) = 0$ and $R''(0) = 0$, then the ratio has a limit which depends only on the derivative of the first moment:

$$\frac{\mathbb{E}(\chi_1(\mathbf{x})\chi_1(\mathbf{x}+\tau\mathbf{n}))-\alpha(\mathbf{x})}{\tau} \to \begin{cases} 0 & \text{if } \nabla\alpha(\mathbf{x})\cdot\mathbf{n} > 0 \\ \nabla\alpha(\mathbf{x})\cdot\mathbf{n} & \text{if } \nabla\alpha(\mathbf{x})\cdot\mathbf{n} < 0 \end{cases} \quad \square$$

Appendix B. Derivation of an isentropic vortex solution for the seven equations model

In this appendix, we are looking for a two dimensional, polar-symmetric, steady solution with divergence free velocities for the seven equations model (1).

Following [28, pp. 668–669], the system in entropic variables (without relaxation terms) is:

$$\begin{cases} \alpha_k\rho_k T_k\left(\frac{\partial s_k}{\partial t}+\mathbf{u}_k\cdot\nabla s_k\right) = (P_I-P_k)(\mathbf{u}_I-\mathbf{u}_k)\cdot\nabla\alpha_k \\ \alpha_k\rho_k\left(\frac{\partial \mathbf{u}_k}{\partial t}+(\mathbf{u}_k\cdot\nabla)\mathbf{u}_k\right)+\nabla(\alpha_k P_k) = P_I\nabla\alpha_k \\ \alpha_k\left(\frac{\partial P_k}{\partial t}+\mathbf{u}_k\cdot\nabla P_k\right)+\alpha_1\rho_1 a_k^2 \mathrm{div}\mathbf{u}_k = \rho_k a_{k,I}^2(\mathbf{u}_I-\mathbf{u}_k)\cdot\nabla\alpha_k \\ \frac{\partial\alpha_k}{\partial t}+\mathbf{u}_I\cdot\nabla\alpha_k = 0 \end{cases} \tag{21}$$

The classical vortex solution derivation is based on the following assumptions:

1. All the variables depend only on the radius r.
2. The velocity is divergence free, which, with the previous assumption, induces that the velocity is orthoradial.

In the case of a two fluid vortex, we choose to search a solution such that all the velocities are divergence free, and such that all the thermodynamic variables are polar symmetric. For simplifying the system (21), we search solutions such that all the terms with a gradient of α_k vanish. This is possible provided we have $\mathbf{u}_I\cdot\nabla\alpha_k = 0$, and $(\mathbf{u}_k-\mathbf{u}_I)\cdot\nabla\alpha_k = 0$. If α_k is polar-symmetric and $\mathbf{u}_k$ is divergence free and depends only on r, then $\mathbf{u}_k\cdot\nabla\alpha_k = 0$. Moreover, as seen in Section 3.4, the product of the gradient of α by the interfacial velocity is computed by solving a one dimensional problem such that:

- A unitary direction $\mathbf{n}$ is defined as having the same direction as $\nabla\alpha_1$.
- The left state is a phase 2, with a velocity of $\mathbf{u}_2\cdot\mathbf{n}$, whereas the right state is a phase 1, with a velocity of $\mathbf{u}_1\cdot\mathbf{n}$.

$u^\star$ and $P^\star$ are defined as the velocity and pressure at the contact surface of the solution of this Riemann problem, and the nonconservative products containing $\mathbf{u}_I$ and P_I are equal to:

$$\begin{cases} \mathbf{u}_I\cdot\nabla\alpha_1 = u^\star\nabla\alpha_1\cdot\mathbf{n} \\ P_I\nabla\alpha_1 = P^\star\nabla\alpha_1 \\ P_I\mathbf{u}_I\cdot\nabla\alpha_1 = P^\star u^\star\nabla\alpha_1\cdot\mathbf{n} \end{cases}$$

Therefore, as $\mathbf{u}_k\cdot\nabla\alpha_k = 0$, and if we suppose that the pressures are locally equal, then $u^\star = 0$, and so the terms involving $\nabla\alpha_k$ are equal to zero. With this choice, the stationary equations on pressure, entropy and volume fraction of (21) are ensured, because the terms with $\nabla\alpha_k$ vanish and the velocities (colinear to $\mathbf{e}_\theta$) are orthogonal to the gradients of thermodynamic variables (which depend only on r).

Moreover, the solutions are supposed to be isentropic for having a regular solution. Therefore, the only constraints that remain are the equations on the velocities, and the equality of the pressures.

Since pressures are equal, and as the velocities are orthoradial, the equation on the velocity $\mathbf{u}_k$ of (21) becomes:

$$\alpha_k\rho_k(\mathbf{u}_k\cdot\nabla)\mathbf{u}_k+\alpha_k\nabla P_k = 0$$

This means that for $\mathbf{u}_k = u_r\mathbf{e}_r + u_\theta\mathbf{e}_\theta$, $P = P_k$ and $\rho = \rho_k$, the following equations hold:

$$\rho\left(\frac{\partial u_r}{\partial t}+u_r\frac{\partial u_r}{\partial r}+\frac{u_\theta}{r}\frac{\partial u_r}{\partial\theta}-\frac{u_\theta^2}{r}\right) = -\frac{\partial P}{\partial r}$$
$$\rho\left(\frac{\partial u_\theta}{\partial t}+u_r\frac{\partial u_\theta}{\partial r}+\frac{u_\theta}{r}\frac{\partial u_\theta}{\partial\theta}+\frac{u_r u_\theta}{r}\right) = -\frac{1}{r}\frac{\partial P}{\partial\theta}$$

Thermodynamic variables depending only on r and velocities being orthoradial, this set of equations reduces to:

$$\rho\frac{u_\theta^2}{r} = \frac{\mathrm{d}P}{\mathrm{d}r}$$

Thus, using the isentropic relation $P\rho_k^{-\gamma_k} = P^\infty(\rho_k^\infty)^{-\gamma_k}$ in each phase, we obtain:

$$\frac{u_\theta^2}{r} = \frac{(P^\infty)^{1/\gamma}}{\rho^\infty}P^{-\frac{1}{\gamma}}\frac{\mathrm{d}P}{\mathrm{d}r}$$

Integration of the right hand side leads to

$$\int_r^{+\infty}\frac{(P^\infty)^{1/\gamma}}{\rho^\infty}P^{-\frac{1}{\gamma}}\frac{\mathrm{d}P}{\mathrm{d}r} = \frac{\gamma}{\gamma-1}\frac{(P^\infty)^{1/\gamma}}{\rho^\infty}\left[P^{1-\frac{1}{\gamma}}\right]_r^\infty = \frac{\gamma(P^\infty)^{1/\gamma}}{(\gamma-1)\rho^\infty}\left[(P^\infty)^{1-\frac{1}{\gamma}}-P^{1-\frac{1}{\gamma}}\right] = \frac{\gamma P^\infty}{(\gamma-1)\rho^\infty}\left(1-\left(\frac{P}{P^\infty}\right)^{\frac{\gamma-1}{\gamma}}\right)$$

which induces:

$$P = P^\infty \left(1 - \frac{(\gamma-1)\rho^\infty}{\gamma P^\infty}\int_r^\infty \frac{u_\theta^2}{r'}\mathrm{d}r'\right)^{\frac{\gamma}{\gamma-1}}$$

Since the two pressures must be equal, we do have:

$$\left(1 - \frac{(\gamma_1-1)\rho_1^\infty}{\gamma_1 P^\infty}\int_r^\infty \frac{\left(u_1^\theta\right)^2}{r'}\mathrm{d}r'\right)^{\frac{\gamma_1}{\gamma_1-1}} = \left(1 - \frac{(\gamma_2-1)\rho_2^\infty}{\gamma_2 P^\infty}\int_r^\infty \frac{\left(u_2^\theta\right)^2}{r'}\mathrm{d}r'\right)^{\frac{\gamma_2}{\gamma_2-1}}$$

Here, if we put this last relation at the power $\frac{\gamma_2-1}{\gamma_2}$ and if we differentiate it with respect to r, we have:

$$\frac{\rho_2^\infty}{P^\infty}\frac{\left(u_2^\theta\right)^2}{r} = \frac{\rho_1^\infty}{P^\infty}\frac{\left(u_1^\theta\right)^2}{r}\left(1 - \frac{(\gamma_1-1)\rho_1^\infty}{\gamma_1 P^\infty}\int_r^\infty \frac{\left(u_1^\theta\right)^2}{r'}\mathrm{d}r'\right)^{\frac{\gamma_2-\gamma_1}{\gamma_2(\gamma_1-1)}}$$

and thus:

$$u_2^\theta = u_1^\theta\sqrt{\frac{\rho_1^\infty}{\rho_2^\infty}}\left(1 - \frac{(\gamma_1-1)\rho_1^\infty}{\gamma_1 P^\infty}\int_r^\infty \frac{\left(u_1^\theta\right)^2}{r'}\mathrm{d}r'\right)^{\frac{\gamma_2-\gamma_1}{2\gamma_2(\gamma_1-1)}}$$

The divergence-free velocity constraint for u_1^θ implies the existence of a stream function ψ such that $\mathbf{u}_1 = \nabla\times\begin{pmatrix}0\\0\\\psi\end{pmatrix}$. A classical choice [53] for ψ is:

$$\psi(r) = -\frac{\delta}{4\pi\phi}\mathrm{e}^{\phi(1-r^2)} \quad \text{so that } u_1^\theta = -\frac{r\delta}{2\pi}\mathrm{e}^{\phi(1-r^2)}$$

with this choice, we find:

$$\int_r^{+\infty}\frac{\left(u_1^\theta\right)^2}{r'}\mathrm{d}r' = \int_r^{+\infty}\frac{r'\delta^2}{4\pi^2}\mathrm{e}^{2\phi(1-r'^2)}\mathrm{d}r = \int_r^{+\infty}\frac{\delta^2}{-16\pi^2\phi}(-4r'\phi)\mathrm{e}^{2\phi(1-r'^2)}\mathrm{d}r = \frac{\delta^2}{16\pi^2\phi}\mathrm{e}^{2\phi(1-r^2)}$$

To conclude this section, we summarize the previous results. Thus, a stationary, radial-symmetric, isentropic and iso-mass fraction solution of the seven equations mode is given by:

$$\begin{cases} P = P^\infty\left(1 - \frac{\gamma_1-1}{\gamma_1}\frac{\rho_1^\infty}{P^\infty}\frac{\delta^2}{16\pi^2\phi}\mathrm{e}^{2\phi(1-r^2)}\right)^{\frac{\gamma_1}{\gamma_1-1}} \\ u_1^\theta = -\frac{r\delta}{2\pi}\mathrm{e}^{\phi(1-r^2)} \\ u_2^\theta = u_1^\theta\sqrt{\frac{\rho_1^\infty}{\rho_2^\infty}}\left(1 - \frac{\gamma_1-1}{\gamma_1}\frac{\rho_1^\infty}{P^\infty}\frac{\delta^2}{16\pi^2\phi}\mathrm{e}^{2\phi(1-r^2)}\right)^{\frac{\gamma_2-\gamma_1}{2\gamma_2(\gamma_1-1)}} \\ \rho_k = \rho_k^\infty\left(\frac{P}{P^\infty}\right)^{\frac{1}{\gamma_k}} \\ \rho = \left(\frac{Y_1^\infty}{\rho_1} + \frac{Y_2^\infty}{\rho_2}\right)^{-1} \\ \alpha_k = \frac{\rho Y_k^\infty}{\rho_k} \end{cases} \tag{22}$$

Appendix C. Derivation of a self similar regular solution associated to the eigenvalue u_I for the seven equations model

This section is devoted to finding regular solutions to the system of Baer and Nunziato, closed by arbitrary interfacial closures. For this, we start with the entropic formulation found by Murrone [28, p. 669]; the system can be written as

$$\partial_t\mathbf{U} + A(\mathbf{U})\partial_x\mathbf{U} = 0$$

with $\mathbf{U} = (s_1, s_2, u_1, u_2, p_1, p_2, \alpha_2)$

$$A(\mathbf{U}) = \begin{pmatrix} u_1 & 0 & 0 & 0 & 0 & 0 & \frac{(P_I-P_1)(u_I-u_1)}{\alpha_1\rho_1 T_1} \\ 0 & u_2 & 0 & 0 & 0 & 0 & -\frac{(P_I-P_2)(u_I-u_2)}{\alpha_2\rho_2 T_2} \\ 0 & 0 & u_1 & 0 & \frac{1}{\rho_1} & 0 & \frac{P_I-P_1}{\alpha_1\rho_1} \\ 0 & 0 & 0 & u_2 & 0 & \frac{1}{\rho_2} & -\frac{P_I-P_2}{\alpha_2\rho_2} \\ 0 & 0 & \rho_1 c_1^2 & 0 & u_1 & 0 & \frac{C_{1I}(u_I-u_1)}{\alpha_1} \\ 0 & 0 & 0 & \rho_1 c_2^2 & 0 & u_2 & -\frac{C_{2I}(u_I-u_2)}{\alpha_2} \\ 0 & 0 & 0 & 0 & 0 & 0 & u_I \end{pmatrix}$$

with $C_{kI} = \frac{1}{\left(\frac{\partial \varepsilon_k}{\partial P_k}\right)_{\rho_k}} \left(\frac{P_I}{\rho_k} - \rho_k \left(\frac{\partial \varepsilon_k}{\partial \rho_k}\right)_{P_k}\right)$. This matrix has u_I, u_1, u_2, $u_1 \pm c_1$ and $u_2 \pm c_2$ as eigenvalues, and if we suppose that these eigenvalues are not equal, the matrix A can be diagonalized.

We are interested in the regular solutions associated to the eigenvalue u_I. For such solutions

$$(A(\mathbf{U}) - u_I \mathrm{I})\mathbf{U}'(\xi) = 0$$

so that the equation on α_2' becomes $0 = 0$, which means that α_2 can be freely imposed, and the following equalities hold

$$\begin{cases} (u_1 - u_I)s_1' + \frac{(P_I - P_1)(u_I - u_1)}{\alpha_1 \rho_1 T_1}\alpha_2' = 0 \\ (u_2 - u_I)s_2' - \frac{(P_I - P_2)(u_I - u_2)}{\alpha_2 \rho_2 T_2}\alpha_2' = 0 \\ (u_1 - u_I)u_1' + \frac{1}{\rho_1}p_1' + \frac{P_I - P_1}{\alpha_1 \rho_1}\alpha_2' = 0 \\ \rho_1 c_1^2 u_1' + (u_1 - u_I)p_1' + \frac{C_{1I}(u_I - u_1)}{\alpha_1}\alpha_2' = 0 \\ (u_2 - u_I)u_2' + \frac{1}{\rho_2}p_2' - \frac{P_I - P_2}{\alpha_2 \rho_2}\alpha_2' = 0 \\ \rho_2 c_2^2 u_2' + (u_2 - u_I)p_2' - \frac{C_{2I}(u_I - u_2)}{\alpha_2}\alpha_2' = 0 \end{cases}$$

Considering α_2 as a parameter, we will try to compute the other variables with respect to it

$$\begin{cases} s_1' = \frac{P_I - P_1}{\alpha_1 \rho_1 T_1}\alpha_2' \\ s_2' = -\frac{P_I - P_2}{\alpha_2 \rho_2 T_2}\alpha_2' \\ (u_1 - u_I)u_1' + \frac{1}{\rho_1}p_1' = \frac{P_1 - P_I}{\alpha_1 \rho_1}\alpha_2' \\ \rho_1 c_1^2 u_1' + (u_1 - u_I)p_1' = \frac{C_{1I}(u_1 - u_I)}{\alpha_1}\alpha_2' \\ (u_2 - u_I)u_2' + \frac{1}{\rho_2}p_2' = -\frac{P_2 - P_I}{\alpha_2 \rho_2}\alpha_2' \\ \rho_2 c_2^2 u_2' + (u_2 - u_I)p_2' = -\frac{C_{2I}(u_2 - u_I)}{\alpha_2}\alpha_2' \end{cases}$$

p_1' and u_1' can be computed with respect to α_2' and to the other variables. For this, we use the Cramer formula. The determinant of the system is equal to

$$(u_1 - u_I)^2 - c_1^2$$

$$u_1' = \frac{1}{(u_1 - u_I)^2 - c_1^2}\begin{vmatrix} \frac{P_1 - P_I}{\alpha_1 \rho_1}\alpha_2' & \frac{1}{\rho_1} \\ \frac{C_{1I}(u_1 - u_I)}{\alpha_1}\alpha_2' & (u_1 - u_I) \end{vmatrix} = \frac{(u_1 - u_I)\alpha_2'}{\alpha_1 \rho_1 ((u_1 - u_I)^2 - c_1^2)}\begin{vmatrix} P_1 - P_I & 1 \\ C_{1I} & 1 \end{vmatrix} = \frac{(u_1 - u_I)(P_1 - P_I - C_{1I})\alpha_2'}{\alpha_1 \rho_1 \left((u_1 - u_I)^2 - c_1^2\right)}$$

$$p_1' = \frac{1}{(u_1 - u_I)^2 - c_1^2}\begin{vmatrix} (u_1 - u_I) & \frac{P_1 - P_I}{\alpha_1 \rho_1}\alpha_2' \\ \rho_1 c_1^2 & \frac{C_{1I}(u_1 - u_I)}{\alpha_1}\alpha_2' \end{vmatrix} = \frac{\alpha_2'}{\alpha_1\left((u_1 - u_I)^2 - c_1^2\right)}\begin{vmatrix} (u_1 - u_I) & \frac{P_1 - P_I}{\rho_1} \\ \rho_1 c_1^2 & C_{1I}(u_1 - u_I) \end{vmatrix} = \frac{\alpha_2'\left(C_{1I}(u_1 - u_I)^2 - c_1^2(P_1 - P_I)\right)}{\alpha_1\left((u_1 - u_I)^2 - c_1^2\right)}$$

In the case of a perfect gas, we compute the expression of C_{kI}

$$C_{kI} = \frac{1}{\left(\frac{\partial \varepsilon_k}{\partial P_k}\right)_{\rho_k}}\left(\frac{P_I}{\rho_k} - \rho_k\left(\frac{\partial \varepsilon_k}{\partial \rho_k}\right)_{P_k}\right) = (\gamma_k - 1)P_I + P_k = P_k - P_I + \gamma_k P_I$$

With this closure, we may find for the fluid 1

$$\begin{cases} u_1' = \frac{(u_1 - u_I)\gamma_k P_I \alpha_2'}{\alpha_1 \rho_1 \left(c_1^2 - (u_1 - u_I)^2\right)} \\ p_1' = \frac{\alpha_2'}{\alpha_1}(P_1 - P_I) + \frac{\gamma_1 P_I (u_1 - u_I)^2 \alpha_2'}{\alpha_1\left((u_1 - u_I)^2 - c_1^2\right)} \end{cases}$$

And for the variables of the fluid 2

$$\begin{cases} u_2' = -\frac{(u_2 - u_I)\gamma_k P_I \alpha_2'}{\alpha_2 \rho_2 \left(c_2^2 - (u_2 - u_I)^2\right)} \\ p_2' = -\frac{\alpha_2'}{\alpha_2}(P_2 - P_I) - \frac{\gamma_2 P_I (u_2 - u_I)^2 \alpha_2'}{\alpha_2\left((u_2 - u_I)^2 - c_2^2\right)} \end{cases}$$

Evolution of α_2 is imposed by an explicit function. The other variables through this wave are computed by numerically integrating the system of ODE. The exact solution at time t is computed by using the method of characteristics. This method is of course very easy to implement here, because all the variables are transported with velocity u_I. For the solution to be stable, we require that u_I increases through the wave when x increases, otherwise the characteristics would intersect.

Appendix D. Eigenvectors of the continuous multiphase model

Let us now deal with the case where we want to express system (1) under the following form:

$$\frac{\partial \mathbf{W}}{\partial t} + A(\mathbf{W}) \cdot \nabla(\mathbf{W}) = 0 \tag{23}$$

with $\mathbf{W} = (\alpha_1, \rho_1, \mathbf{u}_1, P_1, \rho_2, \mathbf{u}_2, P_2)^T$.

In such a case, we have in the one-dimensional case:

$$A(\mathbf{W}) = \begin{pmatrix} u_I & 0 & 0 & 0 & 0 & 0 & 0 & 0 \\ \frac{\rho_1(u_1-u_I)}{\alpha_1} & u_1 & \rho_1 & 0 & 0 & 0 & 0 & 0 \\ \frac{P_1-P_I}{\alpha_1\rho_1} & 0 & u_1 & \frac{1}{\rho_1} & 0 & 0 & 0 & 0 \\ \rho_1 c_{1,I}^2 \frac{u_1-u_I}{\alpha_1} & 0 & \rho_1 c_1^2 & u_1 & 0 & 0 & 0 & 0 \\ 0 & 0 & 0 & 0 & u_I & 0 & 0 & 0 \\ 0 & 0 & 0 & 0 & \frac{\rho_2(u_2-u_I)}{\alpha_2} & u_2 & \rho_2 & 0 \\ 0 & 0 & 0 & 0 & \frac{P_2-P_I}{\alpha_2\rho_2} & 0 & u_2 & \frac{1}{\rho_2} \\ 0 & 0 & 0 & 0 & \rho_2 c_{2,I}^2 \frac{u_2-u_I}{\alpha_2} & 0 & \rho_2 c_2^2 & u_2 \end{pmatrix} \tag{24}$$

Eigenvalues. They may be easily deduced from the matrix A and are now well known:

$$[u_I, u_1, u_2, u_1 - c_1, u_1 + c_1, u_2 - c_2, u_2 + c_2]$$

Eigenvectors. We first begin by the left eigenvectors, computed with SAGE:

$$L^1 = (1,0,0,0,0,0,0,0)^T \tag{25}$$

$$L^2 = (0,0,0,0,1,0,0,0)^T \tag{26}$$

$$L^3 = \left(1, \frac{\alpha_1 c_1^2}{\left(c_1^2 - c_{1,I}^2\right)\rho_1}, 0, -\frac{\alpha_1}{\left(c_1^2 - c_{1,I}^2\right)\rho_1}, 0,0,0,0\right)^T \tag{27}$$

$$L^4 = \left(0,0,0,0,1, \frac{\alpha_2 c_2^2}{\left(c_2^2 - c_{2,I}^2\right)\rho_2}, 0, -\frac{\alpha_2}{\left(c_2^2 - c_{2,I}^2\right)\rho_2}\right)^T \tag{28}$$

$$L^5 = \left(1,0, -\frac{\alpha_1\rho_1 c_1((u_1-c_1)-u_I)}{\rho_1 c_{1,I}^2(u_1-u_I) + (P_I - P_1)c_1}, \frac{\alpha_1((u_1-c_1)-u_I)}{\rho_1 c_{1,I}^2(u_1-u_I) + (P_I - P_1)c_1}, 0,0,0,0\right)^T \tag{29}$$

$$L^6 = \left(1,0, \frac{\alpha_1\rho_1 c_1((u_1+c_1)-u_I)}{\rho_1 c_{1,I}^2(u_1-u_I) + (P_1 - P_I)c_1}, \frac{\alpha_1((u_1+c_1)-u_I)}{\rho_1 c_{1,I}^2(u_1-u_I) + (P_1 - P_I)c_1}, 0,0,0,0\right)^T \tag{30}$$

$$L^7 = \left(0,0,0,0,0,1,0, -\frac{\alpha_2\rho_2 c_2((u_2-c_2)-u_I)}{\rho_2 c_{2,I}^2(u_2-u_I) + (P_I - P_2)c_2}, \frac{\alpha_2((u_2-c_2)-u_I)}{\rho_2 c_{2,I}^2(u_2-u_I) + (P_I - P_2)c_2}\right)^T \tag{31}$$

$$L^8 = \left(0,0,0,0,0,1,0, \frac{\alpha_2\rho_2 c_2((u_2+c_2)-u_I)}{\rho_2 c_{2,I}^2(u_2-u_I) + (P_2 - P_I)c_2}, \frac{\alpha_2((u_2+c_2)-u_I)}{\rho_2 c_{2,I}^2(u_2-u_I) + (P_2 - P_I)c_2}\right)^T \tag{32}$$

Let us now turn to the right eigenvectors:

$$R^1 = \left(1, \frac{\rho_1(u_1-u_I)^2 - \rho_1\left(c_1^2 - c_{1,I}^2\right) + P_I - P_1}{\alpha_1\left(c_1^2 - (u_1-u_I)^2\right)}, \frac{\left(\rho_1 c_{1,I}^2 + (P_I - P_1)\right)(u_I - u_1)}{\alpha_1\rho_1\left(c_1^2 - (u_1-u_I)^2\right)}, \frac{\rho_1 c_{1,I}^2(u_1-u_I)^2 + (P_I-P_1)c_1^2}{\alpha_1\left(c_1^2-(u_1-u_I)^2\right)}, 0,0,0,0\right) \tag{33}$$

$$R^2 = \left(0,0,0,0,1, \frac{\rho_2(u_2-u_I)^2 - \rho_2\left(c_2^2 - c_{2,I}^2\right) + P_I - P_2}{\alpha_2\left(c_2^2 - (u_2-u_I)^2\right)}, \frac{\left(\rho_2 c_{2,I}^2 + P_I - P_2\right)(u_I - u_2)}{\alpha_2\rho_2\left(c_2^2 - (u_2-u_I)^2\right)}, \frac{\rho_2 c_{2,I}^2(u_2-u_I)^2 + (P_I-P_2)c_2^2}{\alpha_2\left(c_2^2-(u_2-u_I)^2\right)}\right) \tag{34}$$

$$R^3 = (0,1,0,0,0,0,0,0) \tag{35}$$

$$R^4 = (0,0,0,0,0,1,0,0) \tag{36}$$

$$R^5 = \left(0,1,-\frac{c_1}{\rho_1}, c_1^2, 0,0,0,0\right) \tag{37}$$

$$R^6 = \left(0,1,\frac{c_1}{\rho_1}, c_1^2, 0,0,0,0\right) \tag{38}$$

$$R^7 = \left(0,0,0,0,0,1,-\frac{c_2}{\rho_2}, c_2^2\right) \tag{39}$$

$$R^8 = \left(0,0,0,0,0,1,\frac{c_2}{\rho_2}, c_2^2\right) \tag{40}$$

References

[1] R. Abgrall, How to prevent pressure oscillations in multicomponent flow calculations: a quasi-conservative approach, J. Comput. Phys. 125 (1996) 150–160.
[2] R. Abgrall, R. Saurel, Discrete equations for physical and numerical compressible multiphase mixtures, J. Comput. Phys. 186 (361–396) (2003).
[3] Nikolai Andrianov, Gerald Warnecke, The Riemann problem for the Baer–Nunziato two-phase flow model, J. Comput. Phys. 195 (2) (2004) 434–464.
[4] M.R. Baer, J.W. Nunziato, A two-phase mixture theory for the deflagration-to-detonation transition (ddt) in reactive granular materials, Int. J. Multiphase Flows 12 (12) (1986) 861–889.
[5] A. Chinnayya, E. Daniel, R. Saurel, Modelling detonation waves in heterogeneous energetic materials, J. Comput. Phys. 196 (2004) 490–538.
[6] Bernardo Cockburn, Suchung Hou, Chi-Wang Shu, The Runge–Kutta local projection discontinuous Galerkin finite element method for conservation laws. IV: The multidimensional case, Math. Comput. 54 (190) (1990) 545–581.
[7] Bernardo Cockburn, San Yih Lin, Chi-Wang Shu, TVB Runge–Kutta local projection discontinuous Galerkin finite element method for conservation laws. III: One-dimensional systems, J. Comput. Phys. 84 (1) (1989) 90–113.
[8] Bernardo Cockburn, Chi-Wang Shu, TVB Runge–Kutta local projection discontinuous Galerkin finite element method for conservation laws. II: General framework, Math. Comput. 52 (186) (1989) 411–435.
[9] Bernardo Cockburn, Chi-Wang Shu, The Runge–Kutta local projection P^1-discontinuous-Galerkin finite element method for scalar conservation laws. RAIRO Modél, Math. Anal. Numér. 25 (3) (1991) 337–361.
[10] Bernardo Cockburn, Chi-Wang Shu, The Runge–Kutta discontinuous Galerkin method for conservation laws. V: Multidimensional systems, J. Comput. Phys. 141 (2) (1998) 199–224.
[11] Bernardo Cockburn, Chi-Wang Shu, Runge–Kutta discontinuous Galerkin methods for convection-dominated problems, J. Sci. Comput. 16 (3) (2001) 173–261.
[12] F. Coquel, T. Gallouët, J.M. Hérard, N. Seguin, Closure laws for a two-fluid two-pressure model, C.R. Acad. Sci. Paris, I 334 (2002) 927–932.
[13] Gianni Dal Maso, Philippe G. Lefloch, François Murat, Definition and weak stability of nonconservative products, J. Math. Pure Appl. (9) 74 (6) (1995) 483–548.
[14] F. Davoudzadeh, H. McDonald, B.E. Thompson, Accuracy evaluation of unsteady CFD numerical schemes by vortex preservation, Comput. Fluids 24 (8) (1995) 883–895.
[15] Vincent Deledicque, Miltiadis V. Papalexandris, An exact Riemann solver for compressible two-phase flow models containing non-conservative products, J. Comput. Phys. 222 (1) (2007) 217–245.
[16] J.M. Delhaye, M. Giot, M.L. Riethmuller, Thermohydraulics of Two-Phase Systems for Industrial Design and Nuclear Engineering, vol. 5, A Von Karman linstitute Book, MC Graw Hill Book Company Edition, 1981.
[17] D.A. Drew, S.L. Passman, Theory of multicomponent fluids, Applied Mathematical Sciences, vol. 135, Springer-Verlag, New York, 1999.
[18] Michael Dumbser, Arturo Hidalgo, Manuel Castro, Carlos Parés, Eleuterio F. Toro, FORCE schemes on unstructured meshes. II: Non-conservative hyperbolic systems, Comput. Methods Appl. Mech. Eng. 199 (9–12) (2010) 625–647.
[19] Michael Dumbser, Eleuterio F. Toro, A simple extension of the Osher Riemann solver to non-conservative hyperbolic systems, J. Sci. Comput. 48 (1–3) (2011) 70–88.
[20] P. Embid, M. Baer, Mathematical analysis of a two-phase continuum mixture theory, Continuum Mech. Thermodyn. 4 (1992) 279–312, doi:10.1007/BF01129333.
[21] R.P. Fedkiw, T. Aslam, B. Merriman, S. Osher, A non-oscillatory Eulerian approach to interfaces in multimaterial flows (the ghost fluid method), J. Comput. Phys. 152 (2) (1999) 457–492.
[22] S. Gavrilyuk, R. Saurel, Mathematical and numerical modeling of two-phase compressible flows with micro-inertia, J. Comput. Phys. 175 (2002) 326–360.
[23] J. Glimm, J.W. Grove, X.L. Li, K.M. Shyue, Y. Zeng, Q. Zhang, Three-dimensional front tracking, SIAM J. Sci. Comput. 19 (3) (1998) 703–727.
[24] Sigal Gottlieb, Chi-Wang Shu, Eitan Tadmor, Strong stability-preserving high-order time discretization methods, SIAM Rev. 43 (1) (2001) 89–112 (electronic).
[25] J.-F. Haas, B. Sturtevant, Interactions of weak shock waves with cylindrical and spherical gas inhomogeneities, J. Fluid Mech. 181 (1987) 4l–76.
[26] S. Karni, Multicomponent flow calculations by a consistent primitive algorithm, J. Comput. Phys. 112 (1994) 31–43.
[27] Pierre-Henri Maire, Rémi Abgrall, Jérôme Breil, Jean Ovadia, A cell-centered Lagrangian scheme for two-dimensional compressible flow problems, SIAM J. Sci. Comput. 29 (4) (2007) 1781–1824. electronic.

[28] A. Murrone, H. Guillard, A five equation reduced model for compressible two phase flow problems, J. Comput. Phys. 202 (2005) 664–698.
[29] R.R. Nourgaliev, T.N. Dinh, T.G. Theofanous, Adaptive characteristics-based matching for compressible multifluid dynamics, J. Comput. Phys. 213 (2) (2006) 500–529.
[30] S. Osher, R.P. Fedkiw, Level Set Methods and Dynamic Implicit Surfaces, Springer-Verlag, 2002.
[31] S. Osher, J.A. Sethian, Fronts propagating with curvature de-pendent speed: algorithms based on Hamilton-Jacobi formulations, J. Comput. Phys. 79 (1988) 12–49.
[32] Carlos Parés, Numerical methods for nonconservative hyperbolic systems: a theoretical framework, SIAM J. Numer. Anal. 44 (1) (2006) 300–321.
[33] Richard B. Pember, John B. Bell, Phillip Colella, William Y. Crutchfield, Michael L. Welcome, An adaptive Cartesian grid method for unsteady compressible flow in irregular regions, J. Comput. Phys. 120 (2) (1995) 278–304.
[34] J.J. Quirk, S. Karni, On the dynamics of a shock-bubble interaction, J. Fluid Mech. 318 (1996) 129–163.
[35] W.H. Reed, T.R. Hill, Triangular Mesh Methods for the Neutron Transport Equation, Technical Report LA-UR-73-479, Los Alamos Scientific Laboratory, 1973.
[36] S. Rhebergen, O. Bokhove, J.J.W. van der Vegt, Discontinuous Galerkin finite element methods for hyperbolic nonconservative partial differential equations, J. Comput. Phys. 227 (3) (2008) 1887–1922.
[37] L. Sainsaulieu, Finite volume approximation of two phase fluids flows based on an approximate roe-type riemann solver, J. Comput. Phys. 121 (1995) 1–28.
[38] R. Saurel, R. Abgrall, A simple method for compressible multifluid flows, SIAM J. Sci. Comput. 21 (3) (1999) 1115–1145.
[39] R. Saurel, S. Gavrilyuk, F. Renaud, A multiphase model with internal degrees of freedom: application to shock–bubble interaction, J. Fluid Mech. 495 (2003) 283–321.
[40] Richard Saurel, Erwin Franquet, Eric Daniel, Olivier Le Metayer, A relaxation-projection method for compressible flows. I: The numerical equation of state for the Euler equations, J. Comput. Phys. 223 (2) (2007) 822–845.
[41] D.W. Schwendeman, C.W. Wahle, A.K. Kapila, The Riemann problem and a high-resolution Godunov method for a model of compressible two-phase flow, J. Comput. Phys. 212 (2) (2006) 490–526.
[42] J.A. Sethian, Level Set Methods and Fast Marching Methods: Evolving Interfaces in Computational Geometry, Fluid Mechanics, Computer Vision, and Materials Science, Cambridge University Press, 1999.
[43] K.M. Shyue, An efficient shock-capturing algorithm for compressible multicomponent problems, J. Comput. Phys. 142 (1998) 208–242.
[44] G.A. Sod, Survey of several finite difference methods for systems of nonlinear hyperbolic conservation laws, J. Comput. Phys. (1978).
[45] W.E.H. Sollie, O. Bokhove, J.J.W. van der Vegt, Space-time discontinuous Galerkin finite element method for two-fluid flows, J. Comput. Phys. 230 (3) (2011) 789–817.
[46] Mai Duc Thanh, Dietmar Kröner, Nguyen Thanh Nam, Numerical approximation for a Baer–Nunziato model of two-phase flows, Appl. Numer. Math. 61 (5) (2011) 702–721.
[47] S.A. Tokareva, E.F. Toro, HLLC-type Riemann solver for the Baer–Nunziato equations of compressible two-phase flow, J. Comput. Phys. 229 (10) (2010) 3573–3604.
[48] E.F. Toro, Riemann solvers and numerical methods for fluid dynamics. A practical introduction, second ed., Springer-Verlag, Berlin, 1999.
[49] I. Toumi, A. Kumbaro, An approximate linearized Riemann solver for a two-fluid model, J. Comput. Phys. 124 (2) (1996) 286–300.
[50] J. Von Neumann, R.D. Richtmyer, A method for the numerical calculation of hydrodynamic shocks, J. Appl. Phys. 21 (1950) 232–237.
[51] Chunwu Wang, Chi-Wang Shu, An interface treating technique for compressible multi-medium flow with Runge–Kutta discontinuous Galerkin method, J. Comput. Phys. 229 (23) (2010) 8823–8843.
[52] L. Wang, D.J. Mavriplis, Implicit solution of the unsteady euler equations for high-order accurate discontinuous Galerkin discretizations, J. Comput. Phys. 225 (2007) 1994–2015.
[53] H.C. Yee, M. Vinokur, M.J. Djomehri, Entropy splitting and numerical dissipation, J. Comput. Phys. 162 (1) (2000) 33–81.
[54] H.C. Yee, N.D. Sandham, M.J. Djomehri, Low-dissipative high-order shock-capturing methods using characteristic-based filters, J. Comput. Phys. 150 (1) (1999) 199–238.